UNIVERSITY OF CALIFORNIA
RIVERSIDE

Animals, Oxygen, and the Mid-Proterozoic Earth System

A Dissertation submitted in partial satisfaction
of the requirements for the degree of

Doctor of Philosophy

in

Geological Sciences

by

Charles Wilson Diamond

September 2021

Dissertation Committee:
Dr. Timothy W. Lyons, Chairperson
Dr. Mary L. Droser
Dr. Gordon D. Love

The Dissertation of Charles Wilson Diamond is approved:

_____

_____

_____

Committee Chairperson

University of California, Riverside

ACKNOWLEDGEMENTS

While the completion of a dissertation by anyone should obviously be viewed as a tremendous accomplishment, I think it is safe to say that throughout my teens and early twenties, most people who knew me would not have bet heavily in favor of this being in the cards for me. It has been a long, circuitous road to this point, and there have been high highs and low lows along the way. While this is neither the time nor place to acknowledge all the people that allowed me to grow at my own pace and figure out life on my own terms, those that played an instrumental role know who they are. I could not be more grateful for all your support along the way—I wouldn't be the person I am today without you, and I hope the way I have chosen to live my life makes you proud to be in my corner.

Over the course of my tenure as a UCR graduate student, there have been many people that I could not have done this without. I vividly remember one of my first days in the lab, someone asked me to pour out a small bottle of nitric acid and refill it, I didn't even really know what nitric acid was, let alone where to find it and how to refill this bottle. It truly does take a village, and for this I must thank the entire Lyons Lab family, extended to the countless collaborators that have shaped my thinking through long conversations at conferences and in the field. I would be remiss not to thank Steve Bates first and foremost; though we have not always been the best of friends, I have learned more about wet chemistry and mass spectrometry from you than words can describe. I also need to thank Leanne Hancock, Dalton Hardisty, Gordon Love, Noah Planavsky and Natascha Riedinger for teaching me everything else I know about lab work and most of what I know about historical biogeochemistry.

My time at UCR would not have been the same without the people I came to know and love along the way. There are many people in the department that made life bearable for me during the low points that come for many during grad school. In particular, and beyond several of the names already mentioned, I have to acknowledge my relationships with Scott E., Adam H., Caroline H., Carina L., Eddie S., and Alex Z. The past year, 2020-2021, has presented unusual challenges for many, me certainly included. I have grown significantly through my own personal struggles over this time, and my life would be much different without a handful people to whom I am deeply grateful. This list is long, but Dave B., Jenn D., S. Jon, Monica O., Michael P., Fran S, and Beach S. all deserve special mention.

Finally, I have to acknowledge the role that Tim Lyons has played in my development, both as a scientist and as a person. Thank you for being the person that you are Tim, you lead by example and speak your mind. Over the past seven years, you have put up with my wild ideas, antics, perfectionism, and complacency. In that time, I took on far too many projects, and few have been seen through to publication [in the unlikely event that a graduate student ever reads this, let that be a lesson]. Despite this apparently slow progress, you gave me space to develop and made sure I knew I was safe and supported. Without this freedom and support, I wouldn't have come to terms with my feelings about work, money, academia, family, or life writ large. I can honestly say that I am happy with who I am today—thank you Tim.

DEDICATION

There isn't any particular relationship between the messages, except that the author has chosen them carefully, so that, when seen all at once, they produce an image of life that is beautiful and surprising and deep. There is no beginning, no middle, no end, no suspense, no moral, no causes, no effects. What we love in our books are the depths of many marvelous moments seen all at one time.

– Tralfamadorian speaking to Billy Pilgrim (Kurt Vonnegut, *Slaughterhouse Five*)

For Jean Lynn Wilson (1951-present)

ABSTRACT OF THE DISSERTATION

Animals, Oxygen, and the Mid-Proterozoic Earth System: A Doctoral Dissertation

by

Charles Wilson Diamond

Doctor of Philosophy, Graduate Program in Geological Sciences
University of California, Riverside, September 2021
Dr. Timothy W. Lyons, Chairperson

Since life took its earliest footholds, organisms have been in a perpetual arms race. Evolutionary trial and error has produced increasingly complex organisms. All with a single purpose, to utilize available resources as efficiently as possible and reproduce. This progression has led to things like photosynthesis and respiration, phagocytosis, multicellularity, differentiated cell types, neural networks, and apparently consciousness. This dissertation presents one account of the history of the push-and-pull relationship between life and the environment as both evolved together, centered around two case studies that contributed to the knowledgebase on which the larger argument is founded.

Because the net outcome of biological activity is the concentration of reduced material, the net outcome is also environmental oxidation, so long as some of that material still exists. Oxygenic photosynthesis was not necessarily the path of least resistance to ecological success, but once the machinery was assembled, the substrates were nearly limitless in many environments. This intuitively leads to the utilization of O_2 in

respiration—it is by far the best candidate for the job, assuming it is ambiently present. That statement suggests implicitly that evolution will continually exploit its environment to gain a competitive advantage.

This effectively frames one side of a long-standing debate concerning the role that environmental O_2 concentrations played the evolution of the eukaryotic clade. The chapters herein elaborate on this argument. It begins with a case study of the 1.4-billion-year-old Xiamaling Formation, presenting iron speciation, sulfur isotope, trace metal, and molybdenum isotope data; concluding that while the Xiamaling Formation was likely deposited in a restricted setting, it still holds geochemical indications that global oceans could have been more well oxygenated at the time than many previously thought. The middle chapters explore these ideas further. The dissertation closes with another case study, Meiklejohn Peak. This study presents paired carbon isotope, sulfur isotope, and iodine concentration data, along with detailed sedimentology. The formation explored in this chapter was deposited during one of the largest pulses of diversification in the history of animal life, and multiple independent geochemical proxies suggest rising environmental O_2 concentrations accompanied this event.

TABLE OF CONTENTS

TABLE OF FIGURES

Exordium

Earth's history is the most interesting story ever told, at least among humans—every other story we can tell is inherently a part of it. For thousands of years people have been telling tales about why the world is the way it is or why we are here in the first place. The pursuit of answers to these questions has led directly to wars, religion, great works of art, diplomacy, and scientific discovery. As time has progressed, the story of Earth's past has become significantly more detailed and significantly more grounded in empirical data. The questions at the heart of the subject, however, have not really changed: why does the world look the way that it does? and why are we here? The answers to these questions, as science has taught us, are inextricably linked.

Earth's surface has been evolving continuously over the past 4.5 billion years, and life has been evolving along with it for most of that time. Evidence for early microbial life can be ambiguous, but multiple studies independently point to its presence for at least 3.5 billion years. Since then, Earth's surface, in particular its chemistry, has been in a push-and-pull between the effects of solid Earth processes and those of biological activity. The impacts each of these has on the other have been, and continue to be, attenuated through a complex network of feedbacks, many of which are linked to one another through physical or chemical processes. The study of these feedback networks essentially is geobiology.

There are many obvious, macroscopic examples of how the Earth and life can affect one another. Tree roots can break up rocks or stabilize soil, and volcanic eruptions can decimate an entire landscape. These processes, like many, can have system-wide effects as well. The impact that vascular plants have on the global weathering flux, for example, is

by no means trivial. Nor is the global warming or cooling that can result from massive volcanism. Far more fundamental than these, however, (and far more profound in its bidirectional impact on life and the environment) are the natural redox gradients that exist on Earth's surface and how life utilizes these, steepening them at a range of scales in consequence. This sounds jargony and complicated, and on some levels it is, but at its core it is relatively straight forward.

A chasm of understanding exists between specialists in most fields and the laypeople outside of it. It is my firm opinion that in most instances this is entirely superficial, and most subjects can be broken down into a logical series of intelligible pieces for nearly anybody. The topics of this dissertation certainly fit that criteria, and while I am aware of the unlikelihood that anyone outside academia (or my committee for that matter) will ever read this, I would like it to be interesting and informative should they. With that said, I have included a forward at the beginning of each chapter. These are intended to summarize the salient points laid out with rigor in the chapter, as well as give context and, at times, my opinions. I hope that you, the reader, will allow me this indulgence—if you find them redundant or unhelpful, please skip them.

Chapter 1

Introduction

Returning to the statement made in the exordium, that the most profound relationship between life and the Earth concerns redox gradients, this should seem like a tautology, because both life and the Earth are, at their essence, redox gradient machines. By that I mean that through their mere existence, they create redox gradients. The Earth does so naturally, through (primarily) mineralogical changes associated with temperature and pressure gradients between the surface and the core, and essentially everything about life revolves around redox reactions. Whether bacterial, archaeal, or eukaryotic, to the best of my knowledge most life is using glucose, and everything is using ATP or a very similar energy carrying molecule. The earliest life almost certainly relied on a form of chemoautotrophy, whereby a naturally occurring redox gradient was exploited to harvest electrons to form ATP or a more primitive energy carrier. In the time since, metabolisms have evolved to take advantage of available resources more efficiently, and complexity has increased correspondingly.

Given the observation that life exists to exploit redox gradients in its environment, one might intuitively expect that the net result of this activity would be the dissipation of these gradients. However, in this instance, one would be wrong. The net effect of life, whether on the cellular, organismal, or ecosystem scale, is the concentration of reduced material. This concentration of reduced material steepens the redox gradient, rather than flattening it, in the area surrounding it.

Life is a redox gradient machine. This fact has had enormous implications for the evolution of Earth's surface environments. The Earth's atmosphere is 21% molecular oxygen, a highly oxidizing gas. This oxygen is maintained dynamically through the presence of a standing biosphere and ancient biomass that was buried in sediments—both made up of concentrated, reduced carbon. The existence of this oxygen in the atmosphere fundamentally changes the cycling of many elements in surface environments. Beyond oxygen, metabolic processes collectively have the net effect of concentrating reduced carbon and releasing an oxidized species back to the environment. Oxygen just happens to be the end of the road and where we find ourselves on the modern Earth.

It is not by happenstance that the most abundant metabolic biproduct in the environment is oxygen. Nor is it by chance that in oxygen rich environments, the dominant heterotrophic metabolism is aerobic respiration. These are both the outcome one would predict based on thermodynamics and a rudimentary knowledge of environmental chemistry. The most potent oxidant readily available in most environments today is molecular oxygen, and hence, the respiratory pathways that utilize it are the highest yielding in terms of energy per unit of reduced material oxidized. Life uses redox reactions as an energy source to perform cellular functions, ultimately division. The energy advantage that oxygen provides over other oxidants (nitrate, sulfate, etc.) has resulted in the effective obsolescence of other respiratory pathways in environments where it is present, even at low levels.

Environments that contain free molecular oxygen were not always a common feature of the Earth's surface, though. The presence of oxygen in the ocean and atmosphere

is almost exclusively the result of oxygenic photosynthesis (photosynthesis that uses light energy to take an electron away from a water molecule, oxidizing it into molecular oxygen), which is a complex process that did not evolve until at least three billion years ago (Planavsky et al., 2014; Cardona et al., 2019). Other photoautotrophic metabolisms existed prior to the evolution of oxygenic photosynthesis, using light to oxidize things like hydrogen sulfide and ferrous iron. Today, organisms using these primitive photosynthetic pathways are confined to environments containing both light and abundant reduced species, uncommon outside of anoxic springs, acid mine drainage, and a handful of microenvironments. By any account, though, these anoxygenic photosynthetic pathways represented the base of the food chain for several hundred million years before the advent of oxygenic photosynthesis.

The reason for the shift to oxygenic photosynthesis; water is much more abundant in well-lit environments than the further-reduced alternatives. The reason for the delay in assembling the machinery required for carrying out oxygenic photosynthesis; it is incredibly complicated to oxidize water and the resultant molecular oxygen is highly reactive and hence, potentially hazardous to the cell itself. The details of photosynthetic evolution are still areas of significant research, but by approximately twenty-four hundred million years ago, molecular oxygen began to accumulate in the atmosphere, and its concentrations have remained above trace levels ever since (e.g., Farquhar et al., 2000; the initial rise in oxygen is generally referred to as the Great Oxidation Event or GOE and is well summarized in Lyons et al., 2014). Bear in mind that this is purely microbial

photosynthesis, eukaryotic photosynthesis (algae, plants, etc.) did not appear until much later, likely closer to a billion years ago.

It stands to reason that once molecular oxygen began to accumulate in the environment, aerobic respiration would rapidly come to dominate heterotrophic metabolisms in oxic environments (those that contain free molecular oxygen). By all accounts, this seems to have been the case. However, significant evidence exists that the biosphere remained dominated by bacteria and archaea until at least eight hundred million years ago. This suggests that eukaryotes, while having evolved some billion years earlier, remained a minor constituent of most ecosystems until that time (Macdonald and Cohen, 2015; Isson et al., 2018). Given the direct correlation between eukaryotic diversity and environmental oxygen concentrations that exists in many environments today, this result may seem counterintuitive.

In fact, this conundrum has been at the heart of a now decades long debate that brings us to the topic of this dissertation, the true exordium as Cicero would have it. It is this author's opinion that environmental oxygen concentrations, although rising to appreciable levels at the time of the GOE, probably remained quite low for a long time after, until around eight hundred million years ago. Further to the point, I am of the opinion that this either directly, or through a variety of feedbacks, led to a general lack of ecological success for eukaryotes during the billion or so years between their initial evolution and later rise to ecological relevance. This argument will, of course, be laid out in significant detail in the chapters that follow, however, I will briefly outline the salient points of both this and the counter argument now.

The use of molecular oxygen is ubiquitous in eukaryotes. It is used in a variety of processes, sterol synthesis is one that is often mentioned (e.g., Mills and Canfield, 2014). Seemingly more importantly, though, all modern eukaryotes are either obligate aerobes or possess specialized mitochondria, the latter of which is restricted to specialized protozoa that inhabit persistently anoxic environments. Further, modern well oxygenated environments are generally either nutrient deprived to the point that little photosynthetic production is occurring, or they are dominated by macroscopic animals (a branch of the eukaryotic tree that is filled with large, complex, multicellular organisms). Now, it is clearly a large evolutionary jump from the earliest, single-celled eukaryotes to swordfish, but a chasm of evolutionary progress exists between sponges and trilobites as well. That amount of evolutionary progress required for the latter took a little over a hundred million years, and within twenty-five million years of that, the marine realm looked a lot like it does today in terms of animal dominance and trophic tiering. This bears relevance because the argument against environmental oxygenation pacing the ecological expansion and diversification of eukaryotes, animals in particular, is that evolution is a random process that takes time and sufficient oxygen to fuel early animal metabolisms was likely present in the surface ocean throughout the billion years between the first eukaryotes and the first animals (e.g., Butterfield, 2009; Mills et al., 2014).

The argument in favor of oxygen as a controlling factor finds support in evidence for still extremely low environmental oxygen concentrations throughout these above mentioned billion years (colloquially referred to as the mid-Proterozoic), and in an apparent coincidence between increasing oxygen and the significant evolutionary steps that

eukaryotes took in the hundred million years leading up to the appearance of animals (e.g., Cole et al., 2016; Hardisty et al., 2017). It is also supported by the relationship that animals and oxygen have had since their appearance; as environmental oxygen concentrations decrease, animals become smaller, less diverse, and less abundant, until eventually, they are no longer present. This is true today and it is demonstrated countless times throughout the geological record. Afterall, it takes a lot of energy to be a large, complex heterotrophic organism. Mammals are only able to sustain their respiratory requirements using lungs, which in humans, have a surface area that is roughly equivalent to the square footage of a one-bedroom apartment—while breathing an atmosphere of 0.2 bar oxygen!

The argument against low mid-Proterozoic atmospheric oxygen concentrations delaying the rise of animals is essentially that evolution took its course independently from environmental oxygen concentrations or associated implications for oceanic nutrient inventories. The timing, instead, reflects factors intrinsic to evolutionary process, and the rapid escalation in eukaryotic (and subsequently animal) evolution following the end of the mid-Proterozoic reflects mainly a predator-prey type of arms race. This argument also seems entirely plausible, though it does leave out an explanation for the roughly coincident timing of increasing oxygenation of the environment. It could be that both are tied to larger Earth system changes that were ongoing (this was one of the most inexplicably chaotic times in Earth history), or, as some authors have suggested, perhaps the evolution of animals led to oxygenation of the environment (e.g., Butterfield, 2009; 2018).

Neither of these explanations is fully satisfying, partly because we do not have enough geochemical or paleontological data to fully understand the nuanced progression

of Earth's surface environments or that of biological evolution. Nor are either of these explanations likely to be the answer on their own anyway. The true account of the co-evolution of life and the environment is much more likely to have existed on a spectrum somewhere between these two endmembers, and at different times in the past, the balance point between them may have shifted. In any event, it seems short sighted to this author to imagine that either intrinsic or extrinsic factors played no role at all.

Through the work captured in this dissertation, I have tried to both add meaningfully to the detailed records that we as a community have assembled, and to go beyond that by compiling published work and making several arguments about the nature of the mid-Proterozoic environment and its implications for evolution. Throughout the progression of my doctoral work, a competing group of authors published frequently on the formation that takes a lead role in most of this story, the Xiamaling Formation. As the reader will find, our interpretations of the data, which was reproduced independently by both groups, could not have been more different.

In Chapter 2, the first manuscript that we published on the Xiamaling Formation is presented. This manuscript represents a wholistic, independent exploration of the data that we produced. The conclusions that were drawn, as I hope is made clear in Chapter 2, were ones of necessity. They were the unique solution that accounted for the observed trends. All the trends, both stratigraphically within individual proxy data and as one proxy correlates with others. The conclusions that we came to were not influenced by preconceived ideas about the mid-Proterozoic or the Xiamaling Formation. In fact, they run contrary to what we might have expected (or hoped) to find. Rather than seeking an

explanation for the data that fit the rest of our presumptions about the mid-Proterozoic, however, we let the data guide our interpretation and then tried to fit these observations into our preexisting ideas about Earth's history.

In Chapter 3, a manuscript is presented which compiles published data from throughout Earth's history and forms an argument for an alternative interpretation of atmospheric oxygen dynamics throughout the mid-Proterozoic; namely, that things were dynamic. This argument stems logically from the information gleaned from the Xiamaling Formation, and the publication of this manuscript represented a statement that the authorship fully endorses the implications for the bigger picture. It is my hope that Chapter 3 makes that case effectively.

As mentioned above, a second group was publishing on the Xiamaling Formation at the same time as we were. Our interpretations of very similar data were in conflict, and this came to a proverbial head in early 2019. The other group, led by Don Canfield, published a manuscript in response to Chapter 2. They did so in the same journal, *Geobiology*, using a title that was very similar ours—it was a direct response in the form of an original article. The authors left no ambiguity about the point-counter point nature of the piece with respect to the paper we had published a year earlier. I quote,

> *In what follows, we will compare the data from Diamond et al. (2018) to* [our] *previously published results from the Xiahuayuan region, and will discuss each of the points raised by Diamond et al. (2018) in turn.*
>
> Zhang et al., 2019, *Geobiology*

In Chapter 4, an editorial response to Zhang et al. (2019) is presented. I wrote this response with the intent to submit it, but like so many things, it has been left open ended. The writing

and opinions are solely my own. The Forward to Chapter 4 gives more context to the actual content of the manuscripts and the finer points of the debate, though much of this is explored logically and at length in the main text.

Following the brief digression of Chapter 4, a manuscript is presented in Chapter 5 that was published this year (2021) as part of an AGU Books special project. It serves as a follow-up to Chapter 3, further refining the (still very incomplete) geochemical record compilation and offering an additional argument that the driving force behind environmental dynamics in the mid-Proterozoic was plate tectonics. This contribution acts as both a buttress for Chapter 3 and as a natural extension. Chapter 5 represents the end of my published work on the mid-Proterozoic to date. It is worth adding that over the course of my doctoral studies, I produced a significant amount of data for the slightly older Hongshuizhuang and Tieling formations that will be published in the near future.

Chapter 6 takes a leap almost a billion years into the future from the debate framed in the preceding chapters. While this may seem like a stretch for one dissertation, it is more natural a step than one might expect. The focus of Chapter 6 is the Middle Ordovician Period, specifically a time during which the most rapid and sustained diversification among marine animals in all Earth history took place. This event, known as the Great Ordovician Biodiversification Event (GOBE), occurred during a time when significant global cooling was taking place, geochemical records indicate dramatic changes in weathering were occurring, and the carbon cycle was beginning to experience perturbations of increasing magnitude, potentially driving environmental oxygenation.

Given the greater context of my interest in the mid-Proterozoic, studying the GOBE seems like a perfect place to further test the hypothesis that changes in environmental oxygen concentrations shaped the course of eukaryotic evolution. In fact, it was my initial interest in the GOBE that led me deeper into geological history, not the other way around. The manuscript presented in Chapter 6 is an extension of work I began as an undergraduate at Ohio State. It uses a combined sedimentological and geochemical approach to characterize a portion of an expansive, shallow carbonate platform that existed on the western Laurentian margin for much of the Lower Paleozoic. A significant amount of my time at UCR was spent thinking about and testing methods for the measurement of carbonate-associated-iodine. Over the past few years, I have identified several problems with conventional methods for making this analysis. Leading into 2020, I was producing data on a regular basis to test the long-term reproducibility of my techniques, chapter 6 is a good showcase of the method.

Chapter 7 concludes the dissertation. The arguments presented in the preceding chapters are briefly summarized and some concluding remarks are made. It has truly been a pleasure working on this over the years, thank you to the many that contributed and thank you to you, the reader.

References:

Butterfield, N.J., 2009. Oxygen, animals and oceanic ventilation: an alternative view.

Butterfield, N. J. (2018). Oxygen, animals and aquatic bioturbation: An updated account. Geobiology, 16(1), 3-16.

Cardona, T., Sánchez-Baracaldo, P., Rutherford, A. W., & Larkum, A. W. (2019). Early Archean origin of photosystem II. *Geobiology*, *17*(2), 127-150.

Cohen, P. A., & Macdonald, F. A. (2015). The Proterozoic record of eukaryotes. *Paleobiology*, *41*(4), 610-632.

Cole, D. B., Reinhard, C. T., Wang, X., Gueguen, B., Halverson, G. P., Gibson, T., et al. (2016). A shale-hosted Cr isotope record of low atmospheric oxygen during the Proterozoic. Geology, 44(7), 555-558.

Diamond, C. W., Planavsky, N. J., Wang, C., & Lyons, T. W. (2018). What the~ 1.4 Ga Xiamaling Formation can and cannot tell us about the mid-Proterozoic ocean. Geobiology.

Farquhar, J., Bao, H., & Thiemens, M. (2000). Atmospheric influence of Earth's earliest sulfur cycle. Science, 289(5480), 756-758.

Hardisty, D. S., Lu, Z., Bekker, A., Diamond, C. W., Gill, B. C., Jiang, G., et al. (2017). Perspectives on Proterozoic surface ocean redox from iodine contents in ancient and recent carbonate. Earth and Planetary Science Letters, 463, 159-170.

Isson, T. T., Love, G. D., Dupont, C. L., Reinhard, C. T., Zumberge, A. J., Asael, D., ... & Planavsky, N. J. (2018). Tracking the rise of eukaryotes to ecological dominance with zinc isotopes. *Geobiology*, *16*(4), 341-352.

Lyons, T. W., Reinhard, C. T., & Planavsky, N. J. (2014). The rise of oxygen in Earth's early ocean and atmosphere. Nature, 506(7488), 307.

Mills, D. B., & Canfield, D. E. (2014). Oxygen and animal evolution: Did a rise of atmospheric oxygen "trigger" the origin of animals? BioEssays, 36(12), 1145-1155.

Mills, D. B., Ward, L. M., Jones, C., Sweeten, B., Forth, M., Treusch, A. H., & Canfield, D. E. (2014). Oxygen requirements of the earliest animals. *Proceedings of the National Academy of Sciences*, *111*(11), 4168-4172.

Planavsky, N. J., Asael, D., Hofmann, A., Reinhard, C. T., Lalonde, S. V., Knudsen, A., ... & Rouxel, O. J. (2014). Evidence for oxygenic photosynthesis half a billion years before the Great Oxidation Event. *Nature Geoscience*, *7*(4), 283-286.

Zhang, S., Wang, X., Wang, H., Bjerrum, C. J., Hammarlund, E. U., Costa, M. M., et al. (2016). Sufficient oxygen for animal respiration 1,400 million years ago. Proceedings of the National Academy of Sciences, 113(7), 1731-1736.

Chapter 2

What the ~1.4 Ga Xiamaling Formation can and cannot tell us about the mid-Proterozoic ocean

Preface:

The contents of this chapter, less the Forward, have been published in a modified form as:

> Diamond, C.W., Planavsky, N.J., Wang, C. and Lyons, T.W., 2018. What the~ 1.4 Ga Xiamaling Formation can and cannot tell us about the mid-Proterozoic ocean. Geobiology, 16(3), pp.219-236.

Forward

The first major project I worked on when I came to UCR was on a suite of black shales (and some associated carbonates) from the Mesoproterozoic of north China. The goal at the outset was to use routine geochemical techniques, along with some novel newer ones, to characterize the local redox landscape of a long-lived passive margin. Then, if applicable, extend these interpretations to the global ocean-atmosphere system. The targets of this work were the Xiamaling and Hongshuizhuang formations, which are both around 1.4 billion years old. This held promise to add significantly more information to our understanding of this time period, as the only other shale of roughly equivalent age that has been extensively studied is the Velkerri Formation of Australia. This work was made possible through a collaboration with Professor Chunjiang Wang at the China University of Petroleum.

Shortly after collecting drill core samples with Chunjiang and colleagues, a series of papers began being published by another group of authors on samples of the Xiamaling Formation from a core drilled not far from our own. To our surprise, the authors produced a suite of data that looked almost identical to ours, but they came up with an entirely different interpretation. A few key differences existed between the two data sets, in particular, sulfur concentration and isotope measurements were left out of the initial Zhang et al. (2016) publication. As the reader will find in this chapter, sulfur concentrations and isotopes play a key role in determining the unique solution to this system.

Much of the data presented in this chapter was produced and interpretations well in the works before Zhang et al. (2016) was published. Accordingly, this paper is mostly written as a first principles exploration of the formation—little rhetoric is devoted to refuting the claims made by Zhang and others, though the discrepancies between interpretations are addressed. The general conclusion of this work is that while many hundred million years of passive margin deposition are preserved on the northern margin of the North China Craton, the Xiamaling Formation was not part of it. It was instead deposited some time after the carbonate platform was uplifted and exposed above sea level. The sedimentology and geochemistry of the whole formation reflect this. It was likely deposited in a large, inland coastal basin that was frequently, and at times completely, restricted from exchanging water with the open ocean. The geochemical consequences of this are profound and can be seen in the data presented.

Despite this severe isolation, or arguably because of it, we were able to uniquely identify times when a demonstrably strong connection to the open ocean existed. Anyone

who has worked in the Precambrian knows that it can be a challenge to even establish that you are looking at ocean sediments in the first place. Through the use of molybdenum isotope data in conjunction with several complementary data types, we were able to investigate the broader redox landscape of the global oceans at times when the basin was connected with the ocean. Unexpectedly, these data turned out to be higher than had been observed previously in the mid-Proterozoic. Our interpretation of the data was that these heavy values most likely reflect a minimum for contemporaneous seawater composition, and this indicates a more oxic world than we had previously envisaged. This idea is developed in this Chapter and expanded upon in Chapters 3 and 5.

Abstract

Despite a surge of recent work, the evolution of mid-Proterozoic oceanic-atmospheric redox remains heavily debated. Constraining the dynamics of Proterozoic redox evolution is essential to determining the role, if any, that anoxia played in protracting the development of eukaryotic diversity. We present a multi-proxy suite of high-resolution geochemical measurements from a drill core capturing the ~1.4 Ga Xiamaling Formation, North China Craton. Specifically, we analyzed major and trace element concentrations, sulfur and molybdenum isotopes, and iron-speciation to better understand not only the local redox conditions but also to establish how relevant our data are to understanding the contemporaneous global ocean. Our results suggest that throughout deposition of the Xiamaling Formation the basin experienced varying degrees of isolation from the global ocean. During deposition of the lower organic-rich shales (130-85 meters depth), the basin

was extremely restricted, and the reservoirs of sulfate and trace metals were drawn down almost completely. Above a depth of 85 m, shales were deposited in dominantly euxinic waters that more closely resembled a marine system and thus potentially bear signatures of coeval seawater. In the most highly enriched sample from this upper interval, the concentration of molybdenum is 51 ppm with a δ^{98}Mo value of +1.7‰. Concentrations of Mo and other redox-sensitive elements in our samples are consistent with a deep ocean that was largely anoxic on a global scale. Our maximum δ^{98}Mo value, in contrast, is high compared to published mid-Proterozoic data. This high value raises the possibility that Earth's surface environments were transiently more oxygenated at ~1.4 Ga compared to preceding or postdating times. More broadly, this study demonstrates the importance of integrating all available data when attempting to reconstruct surface O_2 dynamics based on rocks of any age.

Introduction

Despite a growing number of studies, the mid-Proterozoic Era, 1.8 – 0.8 billion-years-ago (Ga), remains among the least understood periods of Earth's history (e.g., Arnold et al., 2004; Kah et al., 2004; Slack et al., 2007; Kendall et al., 2009; Lyons et al., 2009; Planavsky et al., 2011; Cumming et al., 2013; Reinhard et al., 2013; Planavsky et al., 2014; Sperling et al., 2014; Li et al., 2015; Gilleaudeau and Kah, 2015; Kendall et al., 2015; Luo et al., 2015a, 2015b; Cole et al., 2016; Cox et al., 2016; Gilleaudeau et al., 2016; Zhang et al., 2016). The scarcity of well-preserved rocks of this age amenable to fossil preservation or geochemical environmental reconstruction has hindered progress. At the same time, though, several studies have presented seemingly contradictory lines of evidence concerning environmental conditions in this key middle chapter of our planet's history (Canfield et al., 2005; Parnell et al., 2010; Planavsky et al., 2011; Cumming et al., 2013; Cole et al., 2016; Zhang et al., 2016).

One of the most spirited ongoing disputes in the Precambrian research community pertains specifically to the magnitude and stability of oxygenation of Earth's surface environments throughout the Proterozoic. The presence of O_2 and its persistence are thought by many to have profound implications for the suitability of environments to eukaryotic life (e.g., Knoll, 2014). Sterol synthesis, as well as other processes ubiquitous in eukaryotes, requires the presence of free O_2 (e.g., Stolper et al., 2010; Waldbauer et al., 2011), while motility, large size, and predation have even higher respiratory demands (e.g., Williams et al., 2004). These facts have led many to hypothesize that low O_2 levels in the mid-Proterozoic could have delayed the emergence of metazoans and potentially even led

to the protracted diversification and late rise to ecological significance of all eukaryotes (Anbar and Knoll, 2002; Knoll, 2014; Planavsky et al., 2014; Reinhard et al., 2016; Brocks et al., 2017). The oldest demonstrably eukaryotic microfossils have been observed in the Changzhougou Formation and Ruyang Group of north China (~1.65 Ga; Yin et al., 2005; Lamb et al., 2009; Agić et al., 2017). As a group, however, eukaryotes remain at low abundance and diversity until a period of rapid diversification beginning around 800 Ma (Knoll et al., 2006; Cohen and Macdonald, 2015; Brocks et al., 2017)—coincident with a long envisaged early Neoproterozoic rise in atmospheric oxygen (e.g., Och and Shields, 2012).

Traditional estimates placed atmospheric O_2 during the Mesoproterozoic between 1% and 40% of present atmospheric levels (PAL) (Kump et al., 2008). The upper and lower bounds on this estimate are based on the presence of anoxic deep oceans and predictions specific to oxidative weathering on land, respectively (Canfield et al., 2005; Kump, 2008), though the upper bound of 40% has largely been dismissed, and recent discussions have focused on a lower maximum bound of ~10% (e.g., Dianes et al., 2017). However, the best preserved mid-Proterozoic paleosols are characterized by loss of iron (Fe) and manganese (Mn), similar to Archean paleosols and in contrast to Paleoproterozoic and Phanerozoic records, which suggests low (<1% PAL) pO_2 (Zbinden et al., 1988; Mitchell and Sheldon, 2009; Lyons et al., 2014). More recently, chromium (Cr) isotope data and Zn/Fe ratios in carbonates have also been used to suggest lower atmospheric oxygen levels (<0.1% to <1% PAL) for most of the mid-Proterozoic (Planavsky et al., 2014; Cole et al., 2016; Liu et al., 2016). Such low atmospheric pO_2 levels would likely have produced a surface ocean with

low but highly variable O_2 levels that could have stifled eukaryotic diversification and perhaps the origins of animal life—or at least their earliest proliferation (Reinhard et al., 2016). A weakly oxic surface ocean carries the implication of a shallow and unstable chemocline as well, which has been previously proposed for much of the mid-Proterozoic (e.g., Gilleaudeau and Kah, 2015; Reinhard et al., 2016; Hardisty et al., 2017). Frequent shoaling of anoxic and, at times, sulfidic waters into productive shelf environments could have been the defining characteristic that held eukaryotes back from rising to ecological significance (Johnston et al., 2012; Hardisty et al., 2017).

However, previously published literature has challenged the causal link between O_2 concentrations and eukaryotic evolution, and others have argued directly against the notion of low Proterozoic O_2 (e.g., Butterfield, 2009; Daines et al., 2017). A recent study by Zhang et al. (2016) applied a carbon export and oxidation model to quantify mid-Proterozoic atmospheric pO_2. The authors used data collected from the ~1.4 Ga Xiamaling Formation, North China Craton, as input parameters for their model and concluded that the minimum atmospheric pO_2 was 4 to 6% PAL at the time of its deposition. Central to the validity of their conclusion, however, the authors argued that a high total organic carbon (TOC) interval of the lower Xiamaling Formation was deposited under oxic bottom waters (Zhang et al., 2016). The model constructed by Zhang et al. (2016) prescribed an organic matter oxidation rate defined by a set of assumptions (sinking velocity, water depth, sedimentation rate, compaction, etc.) and then, based on the measured TOC contents, calculated the oxygen consumption from overlying water during the settling and deposition of that organic matter. Assuming the water at depth was being sourced from the surface ocean

along isopycnal surfaces and that surface waters were in equilibrium with the overlying atmosphere, the authors then arrive at a minimum atmospheric pO_2.

At the most fundamental level, the model relies on the assumption that if there was excess O_2 in the bottom water at the time of deposition, then the amount of O_2 consumed during oxic degradation of organic matter can be calculated—and specifically that the calculated O⁻2 would be a minimum as the model cannot account for excess O_2. It follows, however, that if bottom water O_2 was exhausted while contemporaneous organic matter was being deposited, then remineralization would have progressed using terminal electron acceptors other than O_2 and/or organic matter preservation would have been favored. Either scenario would result in model outputs antithetical to those mentioned above—that is, the model would calculate a maximum O_2 concentration, though no minimum could be determined because the timing of O_2 exhaustion and transition to anaerobic remineralization cannot be constrained. To justify the model's validity and downplay the role of other electron acceptors, Zhang et al. (2016) suggested that the lack of enrichment in redox-sensitive trace metals in their lower, TOC-rich horizons is an indication of oxic depositional conditions. However, other confounding possibilities exist and must be considered.

This study presents a comprehensive suite of new geochemical measurements from drill core material capturing ~120 m of the lower and middle Xiamaling Formation. A combination of carbon/sulfur relationships, sulfur isotopes, and major and trace element chemistry is used to interpret basin hydrography and connectedness to the open ocean, and Fe-speciation is used as an indicator of local anoxia at the time of deposition. Finally, we

present molybdenum isotope measurements for a suite of samples including those identified as the best candidates for preserving a seawater isotopic composition.

Geologic Setting

Exposed today in outcrops stretching through the mountains north of Beijing (Figure 2.1), the Xiamaling Formation sits unconformably atop a multiple km-thick, well-studied succession of Paleo-Mesoproterozoic sediments (Figure 2.2; Qu et al., 2014). Many authors have interpreted the thick package of strata underlying the Xiamaling Formation to represent the initial rifting and subsequent transformation to a passive margin following the breakup of the Paleoproterozoic 'supercontinent' Nuna (e.g., Meng et al., 2011).

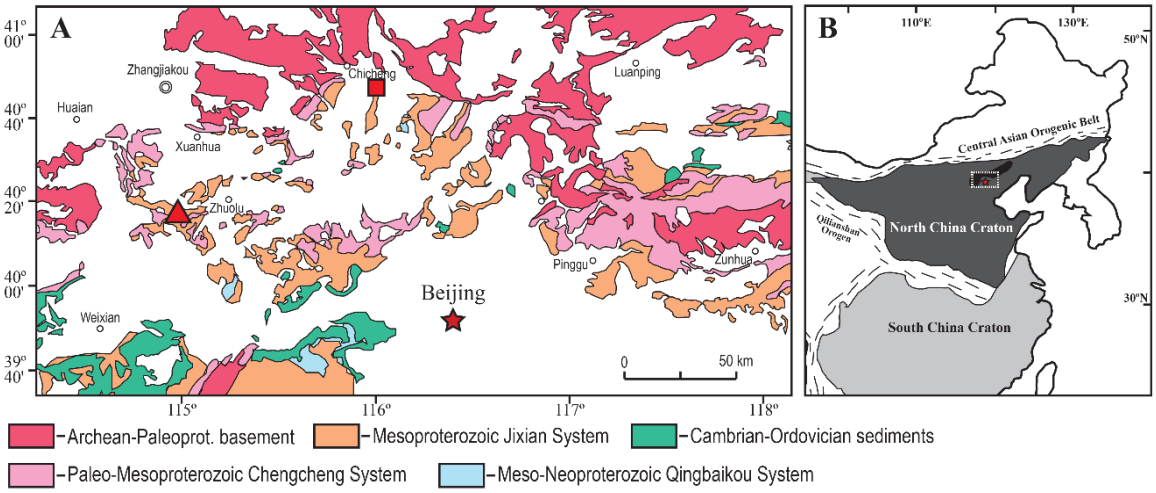

Figure 2.1. Panel A: geologic map showing the distribution of Proterozoic to Paleozoic strata on the northern margin of the North China craton. Red triangle indicates approximate location of drill core material used in both this study and by Zhang et al., 2018 (modified from Zhang et al., 2009). Panel B: regional map showing location of study area.

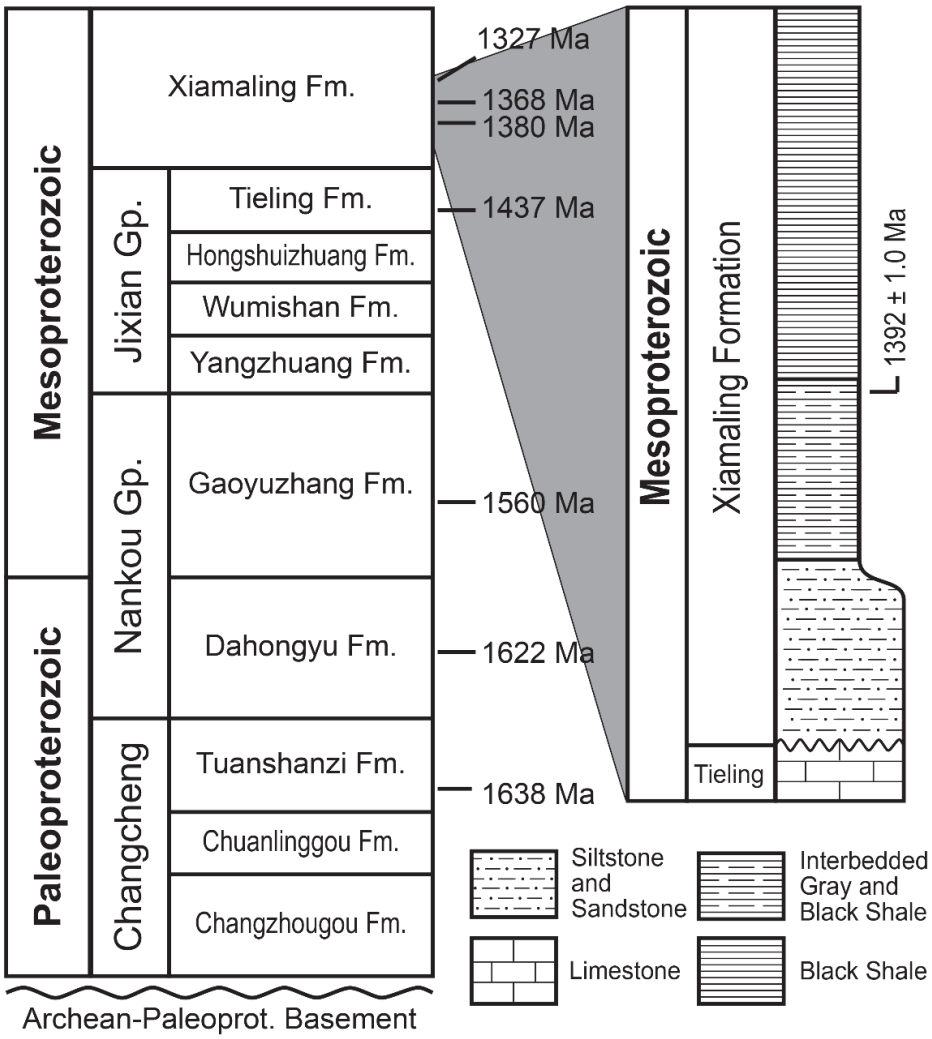

Figure 2.2. Generalized Proterozoic stratigraphy of the northern margin of North China craton and Xiamaling Formation with associated radiometric ages (Gao et al., 2007; Lu et al., 2008; Li et al., 2010; Su et al., 2010; Zhang et al., 2016).

The carbonate-dominated Jixian system directly underlies the Xiamaling Formation and has been interpreted to reflect deposition on the shelf of a passive continental margin (Qu et al., 2014, and references therein). After deposition of several hundred meters of shallow-water carbonates that make up the stromatolite-rich Tieling Formation but before accumulation of the Xiamaling Formation commenced, the local Qinyu uplift event led to

extended subaerial exposure (Qiao, 1976; Qu et al., 2014). The duration of this exposure is not well constrained, although it was sufficiently long to develop thick weathered crusts and laterites over much of the Tieling's areal extent (Qiao, 1976; Mei et al., 1998; Qu et al., 2014). Additionally, the Xiamaling Formation does not extend laterally to the same extent as the Tieling Formation. In some locations, presumably beyond the Xiamaling's depositional basin, the Neoproterozoic Longshan Formation was deposited directly on top of the Tieling Formation or even older strata.

Qu et al. (2014) linked the Qinyu uplift to the initiation of subduction along the long-lived passive margin and possibly some associated collisional event. Shallow initial subduction may have led to the uplift. As the slab began to roll back, extensional forces dominated the more proximal settings—a notion that is supported by the presence of diabase dikes within the Xiamaling Formation (Wang and Simoneit, 1995; Hou et al., 2005; Qu et al., 2014). Some researchers have viewed the presence of bentonites within the Xiamaling as additional evidence for a possible back-arc extensional setting (Qiao et al., 2007). These ash layers have also provided good depositional age constraints (Gao et al., 2007; Su et al., 2008; Zhang et al., 2016).

The Xiamaling Formation is composed almost exclusively of siliciclastic facies. Specifically, immediately overlying the Tieling Formation is a coarse clastic interval composed of conglomerates and coarse sandstones, fining upward into finer sandstones and siltstones. The lower contact of the Xiamaling Formation is characterized at many localities by Fe-rich sandstones, limonite, or bauxite beds—likely products of the initial filling of the basin after prolonged subaerial exposure and development of deeply

weathered soils that were in some cases Fe-rich (Qu et al., 2014, and references therein). Moving upward through the formation, sandstones and siltstones transition into relatively homogenous, interbedded black and gray shales.

This study focuses on the XQ-1 drill core, taken ~110 km north-northwest of Beijing, near Xiahuayuan (Figure 2.1). The bottom of the sampled interval begins in the uppermost coarse clastics of the basal Xiamaling Formation and continues up through ~130 meters of shales. In most locations, the coarser basal unit transitions upward into an interval of rhythmically interbedded gray and black shales. This sequence then gives way to an interval of predominantly black shale. In some reports, these three intervals—the coarse basal unit, rhythmically interbedded gray and black shale, and predominantly black shale—are referred to as separate members. Although we have chosen not to use these informal divisions here and instead refer directly to stratigraphic drill core depths to avoid confusion, the interbedded gray/black shales immediately overlying the transition from coarser grained clastics to shale are correlative with 'unit 3' of Zhang et al. (2016), and the upper black shale interval that overlies this correlates with their 'unit 2'.

Materials and Methods

Carbon and Sulfur

The XQ-1 drill core was sampled at ~2 m intervals where possible, beginning with the first occurrence of shale in the lower Xiamaling and continuing through the top of the core. The outer portions of samples and any veins or macroscopic pyrite were removed, and the remaining sample was cleaned with ultra-pure water. Samples were then powdered

using a clean silicon nitride ball mill, and all subsequent geochemical measurements were carried out on these homogenized powders.

Total carbon (C), sulfur (S), and inorganic carbon (TIC) were measured using an ELTRA carbon and sulfur analyzer. Total C and S were determined through combustion of samples at 1350°C, with quantification of evolved gasses by infrared absorption. TIC was measured by online acidification and quantification of liberated CO_2 by infrared absorption. Total organic carbon (TOC) was calculated as the difference between total carbon and TIC.

All reduced sulfur present in sulfide-bound species (predominantly pyrite in this case) was extracted by a 2-hr hot chromous chloride/HCl distillation and quantitatively captured as Ag_2S using a basic $AgNO_3$ trap solution (Canfield et al., 1986). Ag_2S was filtered, and the concentration of S present was determined gravimetrically. The concentration of Fe present in each sample as pyrite (Fep) was calculated assuming all chromium reducible sulfide was present as FeS_2.

Sulfur isotope analyses were performed using a Costech Elemental Analyzer (EA) coupled to a Thermo Finnegan Delta V Plus gas-source isotope-ratio mass-spectrometer (IRMS) via a ConFlo III open-split interface. The $^{34}S/^{32}S$ ratios of samples were calibrated using three international reference standards (IAEA-S1, IAEA-S2, and IAEA-S3), which were measured at the beginning of the run, after each block of 15 samples, and at the end of the run. Standard deviations of all repeat sample analyses were better than 0.2‰. Results are reported in standard per-mil notation relative to Vienna-Canyon Diablo Troilite (V-CDT). All C and S analyses were performed at the University of California, Riverside.

Iron Speciation

Iron-speciation analyses were undertaken to delineate pools of Fe that would have been reactive to hydrogen sulfide (H_2S^-) on early diagenetic timescales (Poulton et al., 2004; Poulton and Canfield 2005). This fraction of the total Fe contained within the sample is operationally defined as 'highly-reactive' Fe and is denoted Fe_{HR}. We adopted a three-step sequential extraction. First, sample powder was treated with a buffered sodium acetate solution for 48 hours to extract Fe bearing carbonate phases (e.g., siderite or ankerite). The Fe measured in this extract solution is referred to here as Fe_{carb}. Following this first step, the samples were treated with a buffered sodium dithionite solution for two hours to extract labile Fe-oxides (Fe_{ox}). The final treatment was a buffered ammonium oxalate solution for six hours to extract Fe present as mixed valence or highly crystalline oxides (e.g., magnetite), a pool termed Fe_{mag}. Following extraction, concentrations of Fe in resulting solutions were determined via inductively coupled plasma-mass spectrometry (ICP-MS) on an Agilent 7500ce ICP-MS. Multiple samples were replicated through all steps of the procedure (n=12). Among these replicates, average reproducibility of each was ±7%. As mentioned above, Fe present as pyrite was calculated by chromium reduction and is referred to here as Fe_P. The operationally defined 'highly reactive' pool of Fe is then given as $Fe_{HR} = Fe_{carb} + Fe_{ox} + Fe_{mag} + Fe_p$.

Major and Trace Elements

We performed standard HF-HNO_3-HCl total digests to determine the concentrations of major and trace elements in our samples. In this process, 100 to 200 mg of sample powders were first ashed at 750°C for 10-16 hours, then transferred to PTFE screw top vials, followed by a two-step high temperature digestion procedure. During the digestion, samples were first heated to 150°C in a solution of four parts concentrated HNO_3 and one part concentrated HF and kept at this temperature overnight. After heating overnight, digest solutions were allowed to evaporate to near completion at a lower temperature (65°C). Aqua regia was then added to the vials, and they were heated to 130°C and kept overnight. After again allowing the digest solutions to evaporate to near completion at a lower temperature, residues were dissolved in dilute nitric acid in preparation for analysis and to facilitate short-term storage. Concentrations of all major and trace elements in these solutions were determined using an Agilent 7500ce ICP-MS at the University of California, Riverside. A minimum of one USGS reference material, two sample repeats, and a procedural blank were included in each batch of 25 digested samples to monitor for accuracy, reproducibility, and contamination. The results of these repeat analyses suggest 1σ reproducibility of less than 2% for major elements and 5% for trace elements. The Fe concentrations from total digest analyses were used in conjunction with sequential Fe extraction data and are referred to as total Fe or Fe_T.

Molybdenum Isotopes

Molybdenum (Mo) isotope ratios were measured in all sample digest solutions that contained enough Mo to meet minimum analyte requirements. Aliquots of each digest solution were treated with a Mo^{97}/Mo^{100} double spike to achieve a sample/spike Mo ratio of 1:1. The Mo was then purified using a two-stage column chromatographic procedure described by Asael et al. (2013) and Planavsky et al. (2014). The first step of the separation involved columns loaded with 2 ml of AG MP-1M anion exchange resin to isolate Mo and Fe from the remainder of matrix elements. Then, AG 50W-X8 cation exchange resin (2 ml) was used to separate Mo from Fe. The isotopic compositions of Mo and Fe in these purified solutions were measured using a Thermo Neptune Plus MC-ICP-MS with an ESI Apex without membrane desolvation. The cup configuration and interference monitoring were identical to those outlined in Asael et al. (2013). The internal 2-sigma error of the measurements was less than 0.1‰, and errors on full protocol duplicates were less than 0.15‰. Accuracy and precision were monitored through repeated measurements of processed USGS standard NOD-A-1, and all measurements were within 0.1‰ of accepted values (Li et al., 2016). The Mo isotope data are reported following the protocol outlined in Nägler et al. (2014).

Results

Carbon, Sulfur, and Iron

Stratigraphic trends for carbon and sulfur concentrations are shown in Figure 2.3 (next page). In the lower portion of our sampled interval, from a depth of 130 to 85 meters,

TOC is strongly enriched in some samples, while others are very organic-lean, ranging from 0.05 to 13.4 wt% (mean 4.5 wt% 1σ=4.2 wt%). In this same interval, total sulfur is uniformly low, ranging from undetectable to 0.63 wt% (mean 0.2 wt% 1σ=0.2 wt%). The sulfur isotope composition of pyrite ($\delta^{34}S_{pyr}$) in this interval ranged from +3.4 to +11.5‰ (mean of +4.7‰ 1σ=4.2‰). Above this interval, from 85 meters to the top of the core, TOC is more uniformly enriched, with all but one sample preserving between 2.2 to 7.6 wt% (mean of 4.3 wt% 1σ=1.8 wt%). Total sulfur in this interval shows some variability, ranging from 0.2 to 3.5 wt% (mean of 1.8 wt% 1σ=0.8 wt%). Although this upper interval does contain some samples with low total sulfur, the strong enrichments present in most samples stand in stark contrast to their absence in the interval below. The $\delta^{34}S_{pyr}$ in the

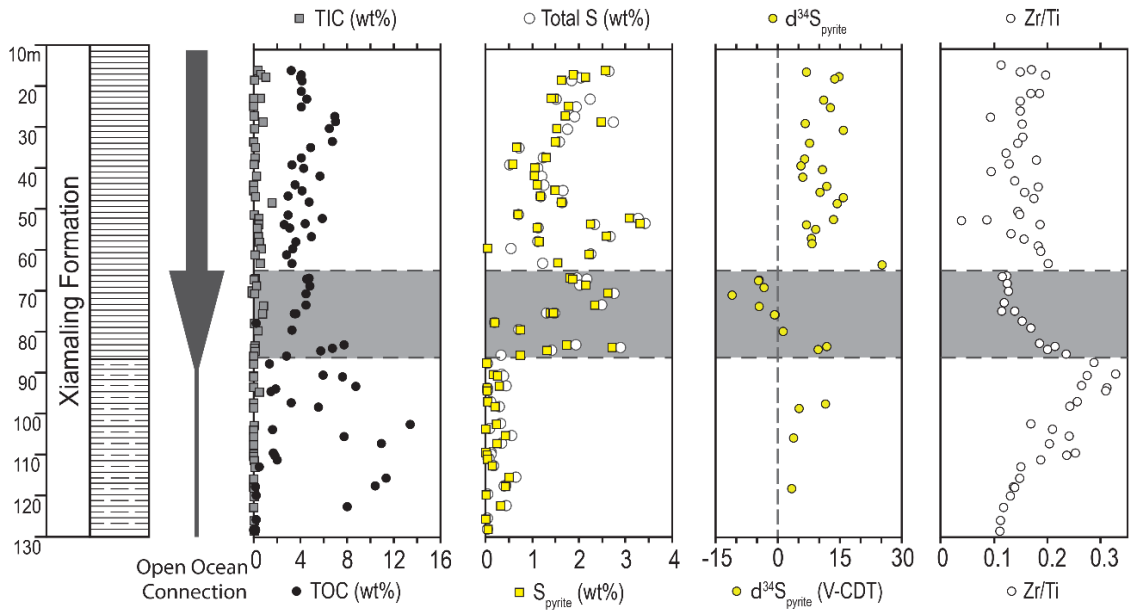

Figure 2.3. Stratigraphic geochemical profiles of the Xiamaling Formation from the XQ-1 drill core. From left to right: total organic carbon (closed circles) and total inorganic carbon (gray squares) both measured in wt%. Concentration of pyrite sulfur (open squares) measured in wt%; sulfur isotopic composition of pyrite (open circles) ‰ relative to V-CDT; zirconium to titanium ratio calculated as ppm/ppm (open circles); and schematic representation of interpreted degree of connection to open ocean.

upper interval ranges from -11.1 to +25.2‰ (mean of 7.1‰ 1σ=7.4‰), though two separate systematic trends are present. From 85 to 65 m, $\delta^{34}S_{pyr}$ trends negatively up core, beginning at +10‰ and decreasing to -11.1‰. At a depth of 65 m, $\delta^{34}S_{pyr}$ increases abruptly to +25.2‰ before decreasing to a range from 5.6 to 15.8‰ for the remainder of the sampled interval.

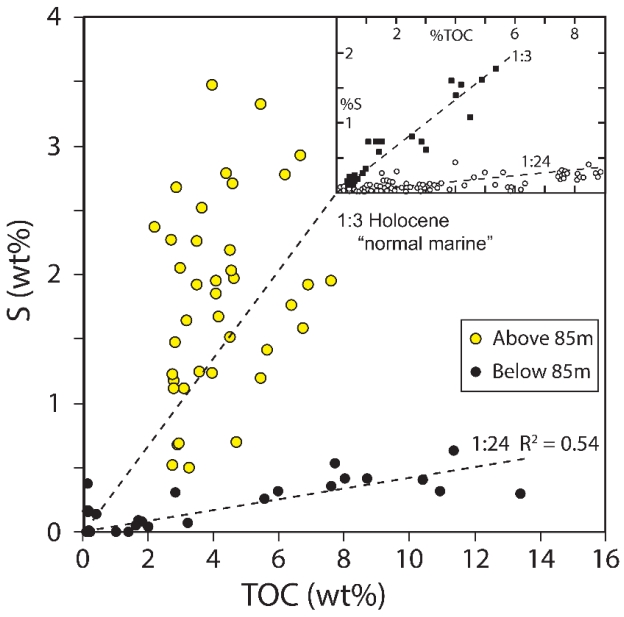

Figure 2.4. Cross-plot of total sulfur concentration and TOC for all samples from the XQ-1 core, both measured as wt%. Samples above depth of 85 m in open circles and below 85 m in closed circles. Inset: cross-plot of data from Berner and Raiswell (1983) showing sulfur concentration plotted against TOC from normal marine sediments (closed squares) and freshwater lacustrine sediments (open circles). 1:3 and 1:24 lines are shown for comparison.

Taken together, the TOC and total S results outlined above produce systematically different C/S ratios in the two intervals discussed (from the base of the sampled interval to 85 m and from 85 m to the top of the core). Figure 2.4 shows a cross-plot of wt% TOC against wt% total sulfur. The lower interval (closed symbols) has very high C/S ratios (maximum C/S > 50), with an average C/S ratio of 23.3 (1σ=13.7); a linear regression of these C-S data yields a best fit line with a slope of 19.2 and an R^2=0.58. The upper interval (open symbols), conversely, has an average C/S of 2.7 (1σ=1.1); due to the strong enrichments in S in this interval, the C-S correlation is much weaker, with a slope of 5.0 for the best fit line and an R^2=0.15.

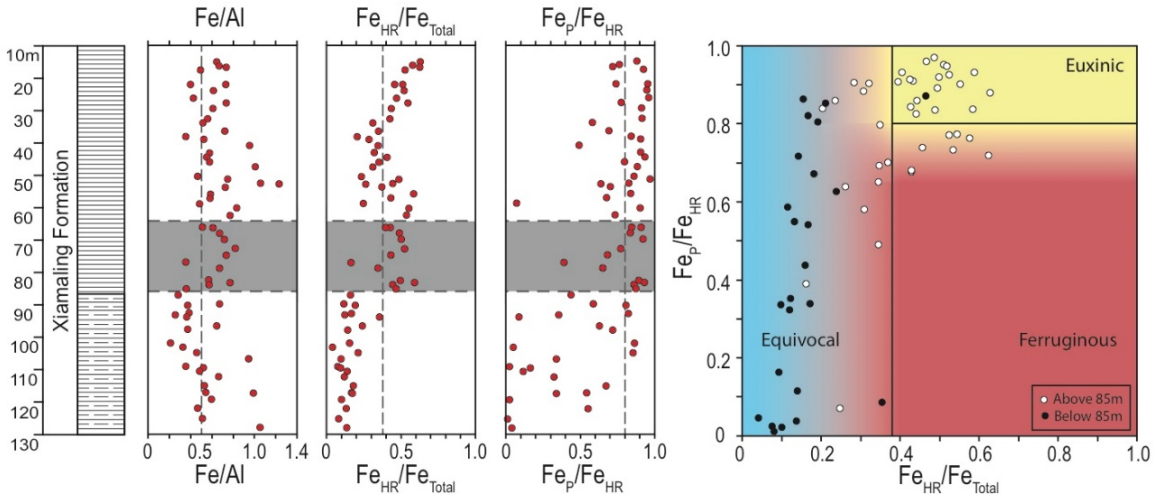

Figure 2.5. Iron-speciation data from the XQ-1 core. From left to right panels show: Fe/Al ratio; highly reactive Fe to total Fe ratio (Fe_{HR}/Fe_{total}); ratio of pyrite Fe to highly reactive Fe (Fe_P/Fe_{HR}) expressed in wt%/wt%; cross-plot of all Fe_P/Fe_{HR} data against Fe_{HR}/Fe_{total} data.

Figure 2.5 shows a compilation of Fe-speciation results from the studied interval. Consistent with the TOC and S data described above, our Fe results show that samples from below 85 m are chemically distinct from those collected above that horizon. Below 85 m, Fe_{HR}-/Fe_T is uniformly low, with an average value of 0.16 (1σ=0.09). Fe_P/Fe_{HR} ratios in this interval are variable, although most samples are well below 0.8 (average of 0.43 1σ=0.31) and contain appreciable Fe_{carb} and Fe_{mag}. In the interval above 85 m, the ratio of Fe_{HR}/Fe_T is significantly higher, with an average of 0.41 (1σ=0.15). The majority of highly reactive Fe in the upper interval is pyritized as well, with an average Fe_P/Fe_{HR} of 0.75 (1σ=0.24).

Major and Trace Elements

Redox-sensitive metals also show differing behavior in the two intervals delineated above. In the lower interval (below 85 m), vanadium (V), uranium (U), and molybdenum

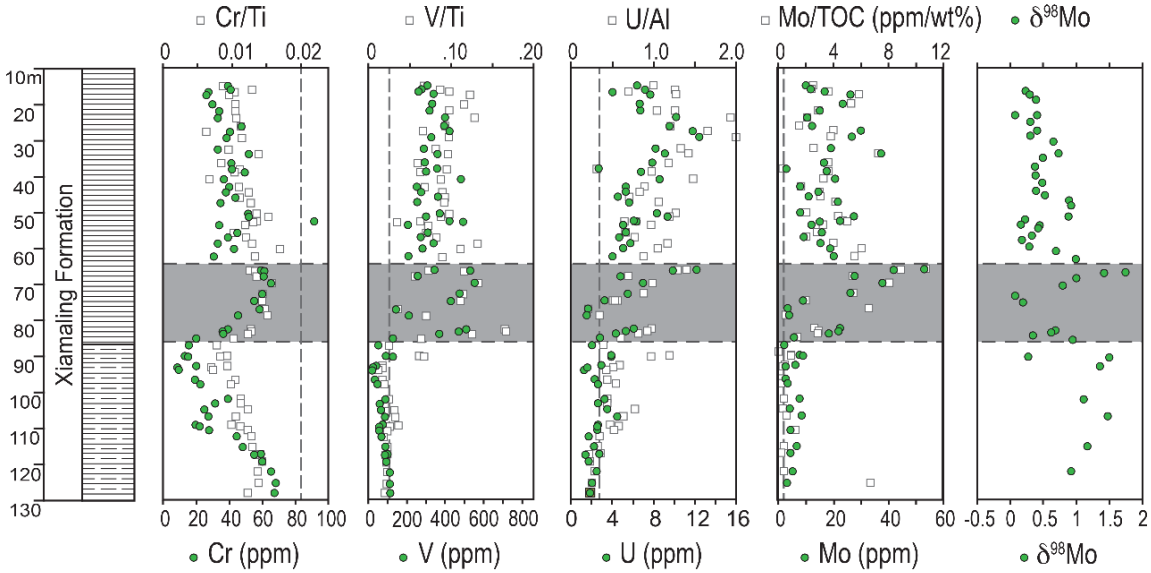

Figure 2.6. Stratigraphic profiles of redox sensitive trace metal concentrations and molybdenum isotopes from the XQ-1 drill core. Filled circles show absolute concentrations, vertical dashed lines indicate the average crustal concentration, and open squares show normalized values, Cr/Ti and V/Ti are reported as ppm/ppm and U/Al is reported as ppm/wt%. Mo is normalized to TOC. The rightmost panel shows Mo isotopes, values are reported as ‰ deviations in accordance with Nägler et al. (2014).

(Mo) fluctuate around crustal levels, while chromium (Cr) remains well below the crustal average throughout the sampled interval (Figure 2.6, next page). At ~85 m, however, V increases sharply to a maximum greater than 500 ppm. Concentrations of Mo and U are also enriched relative to crustal values for the first time at this depth and continue to trend positively up core until reaching their maximum observed concentrations (51 ppm and 12 ppm, respectively) just before 65 m. At ~65 m, both Mo and U decrease sharply, though both elements remain enriched well beyond crustal levels up core, and a subtle increasing trend was observed in the uppermost portion. Although Cr consistently remains below crustal levels, it too shows a change in behavior at ~85 m (Figure 2.6), trending negatively

up core below this horizon and increasing sharply at 85 m before returning to a similar decreasing trend.

A stratigraphic plot of Zr/Ti ratios is shown in Figure 2.3. Both Zr and Ti are highly insoluble elements, and as such, this ratio should reflect the bulk composition of local detrital sediment with a high degree of fidelity. The data show gradual stratigraphic changes through the lower portion of our core, first increasing steadily and then decreasing. At ~65 m, however, there is a significant stepwise change, and above this depth there is more scatter in this ratio compared to the lower interval. Although this stepwise change in bulk composition is well expressed in the ratio of Zr/Ti, a similar feature is also present in other major and minor elements, including traditional provenance tracers (e.g., Ni, Pb, K, P; see Supplementary Information for additional elemental data). We conclude that this stepwise shift in Zr/Ti reflects a change in depositional conditions that warrants additional attention and explore potential causes in the Discussion. For the purposes of this study, we will treat these three intervals (bottom of sampled interval to 85 m, 85 m to 65 m, and 65 m to top of core) as having been deposited in distinct geochemical environments.

Molybdenum Isotopes

Molybdenum isotope data, while variable, show only minor differences in the three intervals differentiated above, though a systematic trend is only present from 85 to 65 m (Figure 2.6). From the bottom of the core to 85 m, δ^{98}Mo values are consistently positive, ranging from 0.3 to 1.5‰ (average +1.1 1σ=0.4). Above 85 m, values begin by trending lighter up core, reaching a low of +0.1‰ before rebounding and trending positively up

core, reaching the maximum value of +1.7‰ just below 65 m. Above 65 m, δ^{98}Mo decreases stepwise to less positive values, ranging from 0.2 to 1.0‰; no systematic trend is present from 65 m to the top of the core; the average value for this interval is +0.46‰ (1σ=0.25).

Discussion

The Significance of the 85 m Horizon

There is a clear geochemical difference between samples from below 85 m in the XQ-1 drill core and those above. In particular, there are several features in the lower interval that are anomalous relative to typical marine sediments; samples from above 85 m lack such anomalies. Rocks of the lower interval are characterized by very high C/S ratios, which could reflect a freshwater depositional setting or one with very limited marine input (e.g., Berner and Raiswell, 1983; 1984). Furthermore, there is a rather sharp stratigraphic change in C/S ratios without any indication of a depositional hiatus or erosional feature, which is inconsistent with a gradual change in global marine conditions—such as the sulfate concentration of seawater. Samples in the lower interval also have low concentrations of redox-sensitive trace metals despite highly variable—and in some cases highly enriched—TOC contents. This too could be a sign of a highly restricted water mass (Algeo and Lyons, 2006).

The absence of diagnostic marine fossils in the Proterozoic makes distinguishing between marine and freshwater settings a challenge. One of the hallmarks of modern normal (oxic) marine sediment chemistry, however, are modest C/S ratios that arises from

the key role sulfate plays in anaerobic organic matter remineralization and the sulfate-replete conditions of the modern ocean (Berner and Raiswell, 1983, 1984). Despite estimates of low sulfate in the mid-Proterozoic ocean (e.g., Kah et al., 2004; Gellatly and Lyons, 2005), pyrite is a common constituent in marine shales of this age (e.g., Cox et al., 2016), and C/S ratios similar to those in modern marine settings are common even in Archean black shales, despite unambiguous evidence for very low Archean marine sulfate concentrations (e.g., Raiswell et al., 2011; Habicht et al., 2002; Crowe et al., 2014). Exceptionally high Precambrian C/S ratios should thus be viewed as a potential fingerprint of environments with limited or no marine input.

The formation of pyrite requires three things: (1) excess organic matter that is remineralized through microbial sulfate reduction (MSR), (2) available sulfate used as an electron acceptor in MSR, and (3) Fe to react with the resultant hydrogen sulfide (H_2S^-). In oxic marine systems, where pyrite formation is exclusively diagenetic (i.e., forms only within the sediments) and typically C-limited, C and S should covary with a linear regression on a carbon-sulfur cross-plot that intercepts both the S and C axes at zero. In other words, early diagenetic pyrite should not form in the absence of excess organic matter (Raiswell and Berner, 1985). The slope of this regression line reflects many factors, including sulfate concentration in overlying waters, sedimentation rate, depth of the sulfate-reduction zone, and selective loss of C through time—to name a few. Despite the many confounding influences, however, an empirical average C/S ratio of 2.8 emerges from Holocene normal (oxic) marine sediments (inset on Figure 2.4; Berner and Raiswell, 1983). In contrast, freshwater systems are characterized by very low sulfate concentrations,

which allows for deposition of large quantities of organic matter without concomitant MSR and subsequent pyrite formation. Hence, the severe S-limitation of freshwaters, or marginal marine settings that are episodically cut off from the oceans, can result in significantly higher sedimentary C/S ratios compared to normal marine systems (Berner and Raiswell, 1983).

Euxinic systems, with a ubiquity of appreciable free hydrogen sulfide (H_2S^-) in their water columns, are Fe-limited by definition. As such, most pyrite formation occurs in the water column as reactive Fe encounters H_2S^- below the chemocline (e.g., Lyons and Severmann, 2006). This pyrite, as it settles to the sediment-water interface, provides a mechanism of S delivery to sediments that is independent from the local organic C flux. Consequently, and in contrast to oxic marine settings, C and S accumulation are decoupled, and the C-independent, syngenetic pyrite flux can lead to samples with C/S ratios that are much lower than those typical of normal marine conditions. In the extreme, appreciable syngenetic pyrite can be present in euxinic samples containing very little or no TOC (Raiswell and Berner, 1985).

In a similar way, Fe-limitation can also result in higher than expected C/S ratios in euxinic sediments. High productivity in surface waters can lead to high local organic matter loading and vigorous MSR and associated H_2S^- production, but because pyrite formation is limited by the local delivery of reactive Fe, much of the H_2S^- produced in the sediments or water column goes unreacted. The most recent sediments of the modern Black Sea (Unit 1), for example, have C/S ratios noticeably greater than 2.8 because of high TOC contents

combined with limited Fe supplies (Lyons and Berner, 1992). Importantly, though, these ratios are still substantially lower than those observed in freshwater settings.

We must also consider that primary C/S ratios can shift over time with selective loss of organic C during burial and the changing nature of organic matter through time, among other controls (e.g., Raiswell and Berner, 1986, 1987). Such relationships, however, are not a concern in our case, as the upper and lower intervals of the Xiamaling Formation were deposited relatively continuously. In such a light, it is clear that basinal C-S dynamics were very different during the deposition of the two intervals.

The average C/S ratio in samples from below 85 m is greater than 23. We have presented two mechanisms by which such high ratios can result in the presence of abundant organic matter, namely extreme sulfate-limitation or extreme Fe-limitation. In the case of the latter, we would expect all reactive Fe to have been converted to pyrite. In samples from below 85 m, however, near-quantitative pyritization of reactive Fe is rare (average FeP/FeHR=0.43), suggesting that sulfate availability, rather than Fe, limited pyrite formation during deposition. It is worth repeating that while C/S ratios can be elevated in the Fe-limited, modern Black Sea, they are substantially lower than those we report from the lower interval of our core (Lyons and Berner, 1992; Lyons, 1997).

Above 85 m in our core, TOC is dramatically less variable compared to below (Figure 2.3), though average TOC contents of the upper and lower intervals are similar. Despite this similarity, the average pyrite concentration in the upper samples is nearly an order of magnitude higher. Consequently, the average C/S ratio for samples above 85 m is 2.7 (1σ=1.1)—much more typical of a marine setting. This result alone suggests that sulfate

concentrations were dramatically higher during the deposition of the upper interval. Extensive pyritization of reactive Fe in samples above 85 m supports this interpretation, indicating that pyrite formation was limited by supply of reactive Fe during deposition rather than the inadequate sulfate availability that characterized the lower interval.

The increase in pyrite concentrations across the horizon at 85 m happens abruptly, with no sedimentological evidence for depositional hiatus, suggesting that conditions changed rapidly from those of severe sulfate-limitation to an environment relatively replete with sulfate. If we allow for the possibility that basinal waters were restricted from the global ocean to the point of near-quantitative drawdown of sulfate during the deposition of the lower interval, then the horizon at 85 m can be explained without invoking changes in the composition of global seawater. Instead, a local or global change in sea level could have created (more likely strengthened) a connection to the open ocean, facilitating increasing basinal sulfate availability along with all other ions that would have been present in mid-Proterozoic seawater.

Following deposition of the underlying Tieling Formation, there is evidence that the shallow seaway was exposed subaerially, and our data suggest that the lower portions of the overlying Xiamaling Formation were deposited before a stable connection to the open ocean was once again established. The lower contact of the Xiamaling Formation, with thick weathering rinds below and extensively weathered coarse clastics above, marks this exposure, and freshwater or weakly marine conditions would have followed. The wide spatial extent of the Xiamaling Formation argues for a very large restricted watermass, but such a situation is not unique—the Baltic and Black seas, for example, both teeter on the

edge between lacustrine and marine deposition, with eustatic sea level change and crustal isostasy controlling the balance. The interpretation of the horizon at 85 m as a marine incursion into an otherwise restricted setting is the only explanation that is wholly consistent with the data for the intervals above and below. Additionally, while it is possible that the observed data are confined to an area very proximal to the drill site (as in a sub-basin or otherwise), the striking similarities between the data presented here and those of Zhang et al. (2016; sampling location >100 km west of XQ-1) suggest otherwise. To further develop the relationships delineated by C-S systematics, we follow with a discussion of the comprehensive geochemical properties of the samples below and above this horizon.

The Interval Below 85 Meters

As discussed above, the C/S ratios in samples from below 85 m in core XQ-1 are abnormally high for a fully marine system, suggesting that sulfate levels in the overlying waters at the time of deposition were extremely low, near the point of complete consumption. The isotopic composition of pyrite sulfur ($\delta^{34}S_{pyr}$) supports this notion. The use of sulfate as a terminal electron acceptor during anaerobic remineralization of organic carbon through MSR can impart an isotopic fractionation as large as 70‰, favoring the lighter ^{32}S in the H_2S^- product (e.g., Sim et al., 2011; Wing and Halevy, 2014). Although the difference between the $\delta^{34}S$ of early diagenetic pyrite—formed from H_2S^- produced through MSR—and coeval seawater sulfate is rarely as high as 70‰ in the geologic record, a substantial fractionation is often preserved. One important exception to this relationship

is in environments where the resupply of sulfate is insufficient to keep pace with the rate of MSR (Gomes and Hurtgen, 2015). In such a system, as the fraction of sulfate consumed by MSR increases, the net isotopic offset between the integrated H_2S^- product and the initial sulfate pool decreases (e.g., Crowe et al., 2014). In the extreme case, where sulfate is quantitatively converted to H_2S^- and captured as pyrite, there is no isotopic expression preserved in bulk samples.

Although the amount of pyrite-S required for routine isotope measurements was recovered from only a few samples in the interval below 85 m, which itself speaks to low sulfate availability, those values are all slightly positive (Figure 2.3). This observation suggests quantitative uptake of sulfate into pyrite under low sulfate conditions—consistent with low rates of resupply relative to consumption via MSR. Importantly, these slightly positive values are broadly consistent with estimates for middle Mesoproterozoic seawater sulfate (Gellatly and Lyons, 2005), suggesting that the Xiamaling's depositional basin shared only a weak and/or intermittent connection with the open ocean.

The Fe-speciation data from the interval below 85 m also support the notion of extremely low basinal sulfate concentrations at the time of deposition. Below 85 m, Fe_P/Fe_{HR} values are generally low, while Fe_{HR}/Fe_T ratios in this same interval are also low (average Fe_{HR}/Fe_T=0.16). Combined, these two observations demonstrate incomplete pyritization of a very small reservoir of reactive Fe. In concert with TOC greater than 10 wt%, these data are very difficult to explain by anything other than low sulfate concentrations in overlying waters (recall that these are fresh drill core samples, so pyrite weathering is not an issue). Although Fe_{HR}/Fe_T ratios of less than 0.38 are often suggested

as evidence for oxic depositional conditions, we would caution against such an interpretation in every case. A substantial enrichment in Fe_{HR} ($Fe_{HR}/Fe_T > 0.38$) provides a robust indicator of an anoxic depositional environment because elevated levels require mobilization of Fe as Fe (II) in the absence of v (e.g., Anderson and Raiswell, 2004; Lyons and Severmann, 2006; Severmann et al., 2008). However, lower ratios do not necessarily imply oxic depositional conditions. In anoxic settings, mobilized Fe (II) must be available and deposited to achieve elevated Fe_{HR}, which typically occurs through precipitation of authigenic Fe minerals (siderite, ankerite, pyrite, etc.). In an anoxic system lacking a sufficient external source of readily reducible Fe, however, aqueous Fe (II) concentrations may not reach the levels necessary to induce authigenic Fe enrichment in sediments. While this aspect of the Fe-speciation proxy has not been adequately studied, an investigation of Fe chemistry within the water column and upper sediments of the Salton Sea, California, provides some insight (de Koff et al., 2008).

The Salton Sea is a large, hypersaline, hypereutrophic lacustrine basin receiving inflow primarily from agricultural runoff and washouts of ephemeral streams during storm events. The lake is stably stratified throughout the majority of the year, with abundant H_2S^- accumulating seasonally in the water column and persisting in portions of the basin interannually. The study by de Koff et al. (2008) found that on average Salton Sea sediments have Fe_{HR}/Fe_T ratios ~ 0.2, including data from the anoxic portions of the basin. While the Salton Sea and the samples from the lower interval of the Xiamaling Formation differ fundamentally in that the former is a sulfidic basin where Fe availability limits Fe-sulfide production and all indications suggest extreme sulfate-limitation during the

deposition of the latter, the study by de Koff et al. (2008) does highlight potential for local Fe fluxes to modulate Fe_{HR}/Fe_T ratios, independent of water column redox. In some instances, rapid detrital sedimentation can also mute Fe enrichments in anoxic settings that would otherwise delineate anoxia/euxinia (reviewed in Lyons and Severmann, 2006). For these reasons, we caution against the use of Fe_{HR}/Fe_T data alone in determination of oxic conditions.

Enrichments in redox sensitive trace metals are also often used to delineate bottom water redox conditions (e.g., Scott and Lyons, 2012). This utility arises from the fact that several trace metals are actively scavenged and form authigenic mineralization in and beneath anoxic or sulfidic waters (e.g., V, Mo, U). Under the degree of restriction that we envisage for the lower Xiamaling, however, basinal inventories could have been depleted to the point of precluding enrichment, particularly in those elements sensitive to anoxic but non-sulfidic conditions, such as V. Redox sensitive metals are all near crustal levels in samples below 85 m despite highly variable TOC. This observation implies that either there was no change in bottom water redox between deposition of samples containing <0.2 and >13 wt% TOC (and that both were deposited in fully oxic conditions), or that trace metal reservoir sizes were exerting a stronger control on enrichment patterns than redox conditions—specifically, that reservoirs were diminished to the point that little or no authigenic enrichment was possible regardless of the redox state of overlying waters. Because our C/S, Fe-speciation, and $\delta^{34}S$ results all speak to quantitative drawdown of the basinal sulfate reservoir, it is most parsimonious to interpret the lack of trace metal

enrichments in the high TOC portions of the lower Xiamaling Formation as also reflecting reservoir drawdown, rather than oxic depositional conditions.

The data from the lower interval of our core are, in many ways, unlike those from rocks deposited in open marine or even moderately restricted settings across geologic time. Evidence for extreme restriction becomes even more compelling when viewed in light of the overlying portion of the core, which shows signs of a stronger marine connection (discussed below). While this depositional reconstruction does not fully preclude the possibility that the high TOC intervals of the lower Xiamaling Formation were deposited in oxic conditions as interpreted by Zhang et al. (2016), it does give an alternative and perhaps more parsimonious explanation for the near crustal metal concentrations cited by Zhang et al. (2016) as evidence of oxic deposition. Additionally, a large basin with weak, likely intermittent marine inputs, as we have interpreted for the lower Xiamaling Formation, would be conducive to the development of stratification, much like the modern Black Sea. It seems unlikely that high TOC shales—up to ~13.5 wt% in this study and ~20 wt% in Zhang et al. (2016)—accumulating in an isolated system would maintain persistently oxic conditions.

The Interval Above 85 m

At a depth of 85 m in our core, the bulk chemistry of samples changes abruptly—a feature that we attribute to a dramatic increase in the amount of seawater entering the basin, perhaps for the first time with any temporal consistency during Xiamaling deposition. Above this horizon, the ranges and variability of nearly all measurements change

dramatically—an observation illustrated most intensely by our sulfur concentration data. If this interpretation is correct, it implies that unlike samples from the lower interval, the samples above 85 m do have the potential to preserve signatures of contemporaneous ocean chemistry. The degree to which this is true, however, is dependent on many factors—principal among them is how strong and persistent the connection to the open ocean was and how persistent.

Once again, careful examination of stratigraphic trends in multiple geochemical tracers is essential. Moving up core from 85 m, the $\delta^{34}S_{pyr}$ data trend negatively from 85-65 m (Figure 2.3). At 65 m, however, there is a positive, stepwise change of ~30‰, and above 65 m the $\delta^{34}S_{pyr}$ data remain positive for the remainder of the core. Within our interpretive framework, the negative trend between 85 and 65 m likely reflects a shift away from sulfate-limited MSR rather than a change in the isotopic composition of the sulfate input. Specifically, the $\delta^{34}S_{pyr}$ data decreased as the fraction of available sulfate consumed by MSR also decreased. In this respect, the $\delta^{34}S_{pyr}$ data can serve in at least a qualitative way as a proxy for the strength of the marine input above 85 m. Within this interpretive framework, the stepwise increase in $\delta^{34}S_{pyr}$ data to positive values at 65 m suggests a return to near-quantitative utilization of sulfate. Interestingly, the positive $\delta^{34}S_{pyr}$ data from above 65 m fall in a similar range to those from the lowermost portion of the core, suggesting that they could have shared a similar source (i.e., seawater).

The horizon at 65 m is also marked by stepwise changes in several other major and trace elements. The Zr/Ti ratio preserved in sediments should reflect the ratio of the local detrital flux (felsic and mafic sources are richer in Zr and Ti, respectively) integrated across

the watershed, with negligible authigenic or diagenetic addition or loss of either element. Given this, one might expect the ratio to change relatively gradually under constant sedimentation. Accordingly, any large stepwise changes could be signaling the presence of unconformities or very condensed intervals. From the base of our core to 65 m, the ratio mostly changes gradually; however, the data become significantly more scattered above a stepwise change at 65 m.

One interpretation of these data is that the changes at 65 m reflect a weakening of the marine connection and return to more restricted conditions. This transition could reflect a local or global decrease in sea level—events commonly associated in the rock record with condensed intervals or unconformable surfaces. Iron-speciation data for the interval above 65 m (Figure 2.4) indicate mostly persistent euxinia. This observation suggests that while restriction above 65 m could have led to basinal water chemistries modified from seawater, sulfate concentrations never returned to levels as low as they were before the marine connection was firmly established (below 85 m). The possibility for restriction in the uppermost interval limits the potential for these samples to inform our understanding of the global ocean.

We are left with the samples from 85 to 65 m as the archive most likely to have been deposited during a time of strong connection to the open ocean. Within this interval, $\delta^{34}S_{pyr}$ trends negatively up core, which we interpret as a progressive strengthening of marine connectivity—specifically reflecting the increasing sulfate concentrations that would have accompanied it. Iron-speciation data within this interval indicate that local depositional conditions were persistently euxinic, with the exception of one low TOC

sample at 77 m. However, despite the indication of persistent euxinia during the deposition of this interval, redox-sensitive metal concentrations show gradually increasing up-section trends (Figure 2.6). Because redox-sensitive metals like U and Mo are scavenged so efficiently under anoxic and sulfidic conditions, respectively, their local and global reservoir sizes exert first-order controls on enrichment patterns (e.g., Scott et al., 2008; Partin et al., 2013). The decreasing trend in $\delta^{34}S_{pyr}$ mirrored by increasing trends in U and Mo, through an interval that Fe-speciation indicates was persistently euxinic, reinforces the possibility that the interval from 85-65 m was characterized by a progressive strengthening of marine inputs.

Across the horizon at 65 m, there are precipitous decreases in U and Mo concentrations. Given that Fe-speciation data indicate a persistence of euxinia through this interval, we can infer a significant depletion in trace-metal inventories, again consistent with a return to more restricted conditions allowing for reservoir drawdown—albeit a level of restriction far less extreme than that captured in the interval below 85 m. In sum, the interval above 85 m should be viewed as representative of two distinctly different depositional conditions, one from 65-85 m that was deposited during a time of progressively increasing connectivity to the ocean and one above 65 m that was deposited in a setting sufficiently restricted to compromise its utility in paleoceanographic interpretations.

Implications for the Global Redox Landscape

Through a careful examination of the multi-proxy dataset presented here, we have established a nuanced hydrographic depositional history for the Xiamaling Formation that implicates the interval between 85 and 65 m depth as perhaps the only window to global conditions. Even within this interval, there are strong up-section trends expressed in multiple proxies that suggest a progressive increase in the influence of seawater on basinal water chemistry. In the uppermost reaches of the interval, we observed the maximum concentrations of U (12 ppm) and Mo (51 ppm). Maximum concentrations of these and other redox-sensitive elements in anoxic and euxinic black shales can be used to infer minimum seawater reservoir sizes for the global ocean and, by extension, the global balance of oxic to suboxic and anoxic/euxinic depositional settings (e.g., Reinhard et al., 2013). The mid-Proterozoic, as a whole, is characterized by low enrichments in redox-sensitive metals, with typical maxima for U and Mo in shales independently constrained to represent the global ocean in the ranges of 10-20 ppm and 50-60 ppm, respectively (by comparison, Phanerozoic U and Mo values are frequently in excess of 50 and 200 ppm, respectively; Scott et al., 2008; Partin et al., 2013). Hence, the trace metal concentration data presented here are in full agreement with previous arguments made for widespread anoxia and euxinia in the mid-Proterozoic ocean (see Lyons et al., 2014, for a review).

While similarities between the maximum concentrations observed in this study and those from other mid-Proterozoic work are encouraging, there is no way to be certain that the maxima from the middle interval of the Xiamaling Formation are wholly representative of the global ocean's trace metal inventory. The possibility remains that even at its most

connected to the ocean, the basin was still somewhat isolated. Work on the similarly aged Velkerri Formation of northern Australia has shown Mo concentrations in excess of 100 ppm, though it remains the only example of such high values for the mid-Proterozoic, and U concentrations from the same samples are relatively low, ranging from 10-14 ppm (Kendall et al., 2009; Cox et al., 2016). Nevertheless, the observation that concentrations of U and Mo increase in the middle Xiamaling Formation in proportions that mimic those observed in other, more demonstrably marine mid-Proterozoic successions reinforces our interpretation of strong marine inputs of sulfate and trace metals at that time.

Molybdenum isotope data provide an additional means of tracking mid-Proterozoic trace metal cycling. Even if basinal waters were only weakly marine, there is still potential for sediments to have captured the oceanic Mo isotope (δ^{98}Mo) value, in part because riverine delivery is very small, and a lower inventory would favor quantitative behavior. This possibility is validated by the modern Black Sea, where surface waters contain a Mo concentration ~60% lower than the open ocean, yet recent sediments capture a δ^{98}Mo value very close to that of modern seawater (Emerson and Huestad, 1991; Barling et al., 2001). This relationship arises from the redox-dependent behavior of Mo in solution. In non-sulfidic seawater, Mo is primarily present as the relatively unreactive molybdate oxyanion (MoO_4^{2-}), though recent work has drawn attention to the potential importance of complexation with organic ligands (Wagner et al., 2017). In the presence of H_2S^-, however, the molybdate ion can undergo a series of progressive sulfurization steps, producing intermediate thiomolybdates species ($MoO_xS_{4-x}^{2-}$), with the reaction running to completion at concentrations of greater than ~11 μM $H_2S_{(aq)}$. At this point, nearly all Mo in solution

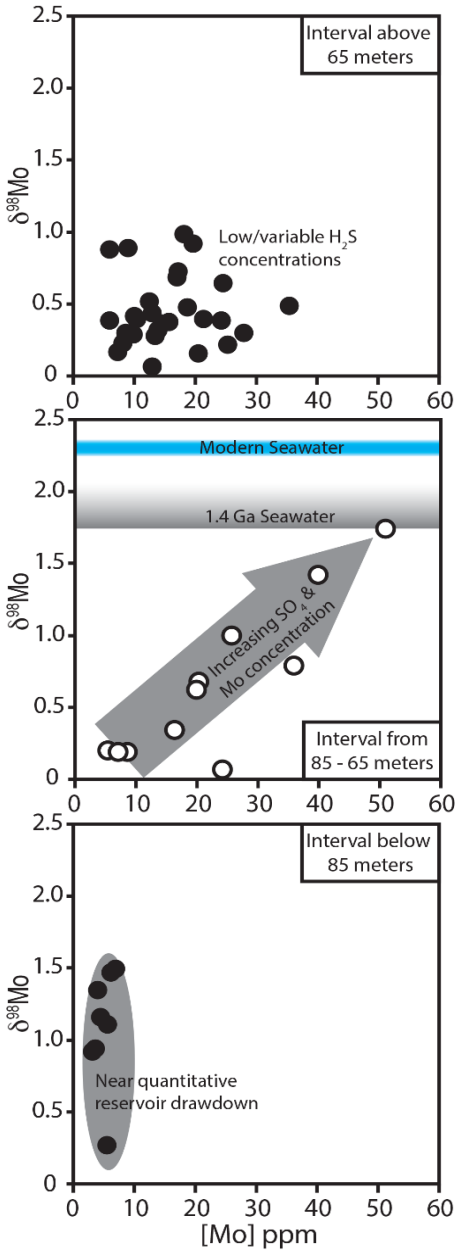

Figure 2.7. δ^{98}Mo values plotted against Mo concentration for the three intervals. The lower panel shows the interval below 85 m. Middle panel shows samples from 65-85 m, the interval that is interpreted to have been deposited when the connection to the open ocean was strongest. The uppermost panel shows samples taken above 85 m.

will be present as tetrathiomolybdate (MoS_4^{2-}; Helz et al., 1996; Erickson and Helz, 2000). Importantly, these reactive species are scavenged efficiently by Fe-sulfides and organic matter (Helz et al., 1996, 2004; Tribovillard et al., 2004; Chappaz et al., 2014) or precipitated directly as Fe-molybdenum sulfides (Helz et al., 2011). These removal pathways are efficient, so that in strongly euxinic environments (high, persistent H_2S^-) Mo removal can be near-quantitative, and such uptake translates to little or no isotopic expression of the multiple processes involved. At least some of these steps are known to fractionate Mo; for example, under conditions of non-quantitative uptake, even complete sulfurization of molybdate will lead to small fractionations between MoS_4^{2-} and authigenic Mo, where the lighter 95Mo is favored in the solid phase by ~0.5‰ (±0.3‰; Nägler et al., 2011). It is commonly suggested, therefore,

that sediments deposited under Mo-depleted euxinic conditions can capture a bulk Mo isotope value close or equal to that of seawater.

This relationship contrasts with Mo deposition in oxic environments where it is primarily delivered to sediments adsorbed onto Mn-oxides, carrying a fractionation of ~3‰ toward the lighter ^{95}Mo (Barling et al., 2001; Siebert et al., 2003; Barling and Anbar, 2004; Poulson Brucker et al., 2009). An additional and potentially significant sink for oceanic Mo exists in suboxic and anoxic waters where sulfide is restricted to porewaters. In such cases, authigenic Mo is typically ~1‰ lighter than the associated seawater (Barling et al., 2001; Arnold et al., 2004; Poulson et al., 2006; Siebert et al., 2006; Neubert et al., 2008; Poulson Brucker et al., 2009). In the modern ocean, the isotopic composition of Mo is about +2.3‰ (Barling et al., 2001; Siebert et al., 2003; Nakagawa et al., 2012; Nägler et al., 2014), which is significantly heavier than the riverine input of +0.7‰ (Archer and Vance, 2008). This disparity is maintained through dominance by the Mn-oxide sink in today's well-ventilated oceans, exporting large amounts of the lighter ^{95}Mo. With a residence time on the order of ~440 kyr (Miller et al., 2011), this value is relatively homogenous.

Given the Mo isotope systematics outlined above, previous work has attempted to model the redox landscape of the global oceans based on δ^{98}Mo data from euxinic black shales (e.g., Arnold et al., 2004; Dahl et al., 2011). While our understanding of Mo sinks in the modern and ancient ocean has advanced significantly over the past decade, there are still many unanswered questions. Further, even with a thorough understanding of these processes, quantitative mass balance modeling of δ^{98}Mo—in terms of oxic, suboxic, and

euxinic deposition—will produce non-unique solutions without the incorporation of additional constraints. Nevertheless, given our current understanding of the system, heavier oceanic values qualitatively indicate a greater proportion of Mo going into oxic and suboxic marine settings compared to euxinic sites and thus less reducing oceans.

Like the concentration data for Mo, the δ^{98}Mo data presented here capture three distinct behaviors in the intervals below 85 m, from 85-65 m, and from 65 m to the top of the sampled interval (Figure 2.6). In the interval below 85 m, δ^{98}Mo is consistently positive, with several samples clustering around +1.5‰. We have interpreted the interval below 85 m as having been deposited in an extremely restricted environment with nearly quantitatively depleted reservoirs of sulfate and trace metals. Iron-speciation analyses indicate that despite there being very little reactive Fe in sediments, H_2S^- production was insufficient to achieve high conversion to pyrite. Given this interpretation—specifically that any H_2S^- accumulation was likely restricted to porewaters and even there, likely intermittent and at very low concentrations—it is possible that the heavy δ^{98}Mo values observed are the result of a very small basinal Mo reservoir derived sparingly from the weak marine connection. Under these conditions near-quantitative capture in even intermittently sulfidic porewaters could have been achieved fairly easily.

While there are uncertainties as to why such heavy δ^{98}Mo values were captured in the lower interval, their presence provides an independent line of reasoning that could argue against oxic depositional conditions. If low trace metal concentrations despite high TOC contents in the lowermost shales of the Xiamaling (below 85 m in our core) reflect oxic depositional conditions, as interpreted by Zhang et al. (2016), rather than restriction

and reservoir drawdown as we suggest, then the δ^{98}Mo value of bulk samples should be significantly fractionated toward lighter values as a result of Mo uptake onto oxide phases. Like the discussion of the lower interval as a whole, however, the observation of heavy δ^{98}Mo values cannot unequivocally demonstrate anoxic depositional conditions. With a strongly depleted reservoir, uptake could be quantitative even through adsorption to oxides and thus capture a δ^{98}Mo value close to seawater with little fractionation preserved in the bulk Mo of the sediments.

We have presented multiple lines of evidence that point to extreme restriction during the deposition of the lower Xiamaling Formation. In light of the proposed restricted depositional setting, which are often vulnerable to water column stratification, it is most likely that bottom waters were anoxic during the deposition of the high-TOC portions of the lower Xiamaling. More generally, given the unusual chemistry of these samples when compared with marine rocks of any age, we would urge caution in using the lower Xiamaling to infer global conditions in any way. The overlying interval, however, appears to have been deposited in a setting ideal for capturing global seawater signatures.

From 85-65 m, δ^{98}Mo data decrease up section initially before increasing to +1.7‰. This trend can be reconciled within the established framework of Mo isotope systematics. With initial strengthening of the marine connection, water column $H_2S_{(aq)}$ accumulation would have initiated as pyrite formation shifted from S-limited to Fe-limited. Under weakly sulfidic conditions, thiomolybdate intermediates can be present, and there are significant negative fractionations associated with each step of the progressive sulfurization of MoO_4^{2-}. As observed in modern settings, sediments deposited under a weakly sulfidic water

column can have δ^{98}Mo values up to 3‰ lighter than seawater because of these fractionations (Arnold et al., 2004, 2012; Neubert et al., 2008; Nägler et al., 2011). As $H_2S_{(aq)}$ increased in the water column, effectively starting at zero, there would have been a temporal window when $H_2S_{(aq)}$ was less than the critical 11 μM required to induce quantitative conversion to tetrathiomolybdate. At the same time, increasing Mo concentrations in sediments suggest that dissolved Mo was also increasing, potentially reaching concentrations sufficient to preclude quantitative uptake of intermediate species. The increasing trend in δ^{98}Mo that follows could reflect the progression to complete conversion to tetrathiomolybdate and its effective (quantitative) uptake under high $H_2S_{(aq)}$ concentrations. A persistently euxinic basin with a strong connection to an ocean containing a relatively small seawater Mo inventory would be ideal for capturing the oceanic δ^{98}Mo. It is perhaps not surprising, then, that our reported +1.7‰ is the highest mid-Proterozoic value to date—given that processes disfavoring capture of the seawater value consistently fractionate toward lighter values. The similarly aged Velkerri Formation, which has unusually high Mo concentrations for the mid-Proterozoic (>100 ppm), has a maximum δ^{98}Mo value of +1.1‰ (Kendall et al., 2009). It is unclear why the Velkerri Formation would be fractionated from seawater to such a degree, while at the same time enriching sediments to a uniquely high level for the time. We also note, however, that these units, while similarly aged, could have been deposited millions of years apart.

Within the simplistic Mo isotope framework of an ocean with three sink terms, each with a distinctive fractionation factor, a value of +1.7‰ for seawater suggests that the global balance of oxic, suboxic, and euxinic settings was shifted more toward oxic and/or

suboxic settings relative to the more dominantly anoxic/euxinic conditions suggested by previous data for the mid-Proterozoic. As mentioned, δ^{98}Mo alone is underdetermined with respect to whether oxic or suboxic settings leveraged the global isotope mass-balance. Nevertheless, it raises the possibility that Earth's surface environments were more oxygenated at ~1.4 Ga compared to other times in the mid-Proterozoic. Molybdenum isotope data are few and far between for the mid-Proterozoic, and a more continuous record is needed to determine whether this heavy δ^{98}Mo value for seawater is a transient signal or a more permanent feature of the Proterozoic oceans. We also note that heavy Mo isotopes values are found in Archean shales (e.g., Duan et al., 2010), potentially highlighting the uncertainty that ferruginous environments add to the global Mo isotope mass balance. Iron-rich deep waters were a common feature during the mid-Proterozoic (Planavsky et al., 2011; Poulton and Canfield, 2011).

Generally low oxygen conditions for the mid-Proterozoic ocean are supported by numerous past studies (e.g., Canfield, 1998; Kah et al., 2004; Scott et al., 2008; Mitchell and Sheldon, 2009; Planavsky et al., 2011; Cumming et al., 2013; Partin et al., 2013; Planavsky et al., 2014; Gilleaudeau and Kah, 2015; Cole et al., 2016; Liu et al., 2016; Hardisty et al., 2017). However, inherent limitations in the resolution of these studies allow for ample temporal gaps and thus for the possibility that transient oxygenation events may be more important than previously imagined. For example, other recently published geochemical data also suggest a transient episode of heightened surface v at ~1.4 Ga. While the maximum δ^{98}Mo of the Velkerri Formation is lower than our value for the Xiamaling Formation, the U isotope composition (δ^{238}U) of samples from the same interval were

recently measured and modeled to be consistent with <25% of the seafloor situated beneath anoxic waters (Yang et al., 2017). Interestingly, samples from a lower interval of euxinic black shale in the Velkerri were examined in the same study, and the mass-balance model suggested widespread seafloor anoxia at the time of their deposition (Yang et al., 2017). This difference is consistent with the possibility of transient oxygenation and highly variable redox conditions.

In a recent compilation of iodine concentrations in shallow marine carbonates through Earth's history, the mid-Proterozoic is characterized by dominantly very low, non-zero I/(Ca+Mg) ratios (Hardisty et al., 2017). This observation suggests that while surface waters were oxic, the chemocline was likely shallow and unstable and, through mixing, frequently introduced anoxic waters to the surface layer (Hardisty et al., 2017). One exception to this pattern is the Tieling Formation, which directly underlies the Xiamaling. Among all the mid-Proterozoic I/(Ca+Mg) data presented by Hardisty et al. (2017), the Tieling is the only formation that stands out as having consistently higher than baseline ratios, again suggesting the possibility of a transient episode (or episodes) of expanded surface ocean O_2 at ~1.4 Ga.

In addition to the δ^{98}Mo data from our study, other recent studies using diverse proxies provide tantalizing hints at the potential for redox conditions that were significantly more dynamic in the mid-Proterozoic than previously thought. Given the myriad of feedbacks that operate on Earth's oxygen cycle, both positive and negative, it stands to reason that stabilization of atmospheric pO_2 at the very low levels suggested by Cr isotope record (Planavsky et al., 2014; Cole et al., 2016) would lead to oscillations around the

baseline value. Confirming the validity, duration, amplitude, and other qualities of the potential transient increases will require significant additional work.

Conclusions

By carefully reconstructing the depositional history of the Xiamaling Formation through a high-resolution, multi-proxy approach, we have revealed three distinct depositional environments, each with distinct water column properties. The lowermost interval (below 85 m) was deposited during a time when the basin was almost completely isolated from the global ocean, likely beneath anoxic waters during times of high export productivity. While carbon-sulfur relationships speak to the extreme isolation, the sulfur and molybdenum isotope data suggest some, likely weak and intermittent, connection to the ocean. Similarly, the uppermost interval in our core (above 65 m) may have been restricted enough to have compromised its potential to record signatures of coeval seawater. The interval from 85-65 m, however, was deposited during a time when connectedness with the open ocean grew increasingly stronger as deposition progressed.

Within the interval from 85-65 m, Fe-speciation data indicate that local depositional conditions were dominantly euxinic, and Mo, V, and U all reach maximum concentrations typical of mid-Proterozoic marine black shales (Scott et al., 2008; Partin et al., 2013). High molybdenum isotope values (maximum δ^{98}Mo of +1.7‰)—the highest to date from the mid-Proterozoic—raise the possibility that environmental conditions at the time of Xiamaling deposition were less reducing than before or after, carrying potentially important biological implications. We suggest that additional work will further expose the

texture of mid-Proterozoic redox evolution, and other such events are likely. Nevertheless, robust first-order trends for multiple geochemical tracers do exist throughout the mid-Proterozoic, and, while allowing for the possibility of dynamic redox, they expose an ocean/atmosphere system that was mostly O_2 lean. Additional data throughout the mid-Proterozoic will be needed to identify, confirm, and adequately model the dynamics of such oscillations, which may be the key to understanding their significance in the trajectory of early eukaryotic evolution. This study adds confidence to the assertion that even very old materials can retain stories rich in detail with high fidelity.

References

Agić, H., Moczydłowska, M. and Yin, L. (2017). Diversity of organic-walled microfossils from the early Mesoproterozoic Ruyang Group, North China Craton-a window into the early eukaryote evolution. Precambrian Research, 297, 101-130.

Algeo, T.J. and Lyons, T.W. (2006). Mo–total organic carbon covariation in modern anoxic marine environments: Implications for analysis of paleoredox and paleohydrographic conditions. Paleoceanography, 21, PA1016.

Anbar, A. D., and Knoll, A. H. (2002). Proterozoic Ocean Chemistry and Evolution: A Bioinorganic Bridge? Science, 297, 1137-1142.

Anderson, T.F., and Raiswell, R. (2004). Sources and mechanisms for the enrichment of highly reactive iron in euxinic Black Sea sediments. American Journal of Science, 304, 203-233.

Archer, C., and Vance, D. (2008). The isotopic signature of the global riverine molybdenum flux and anoxia in the ancient oceans. Nature Geoscience, 1, 597-600.

Arnold, G. L., Anbar, A. D., Barling, J., and Lyons, T. W. (2004). Molybdenum isotope evidence for widespread anoxia in mid-Proterozoic oceans. Science, 304, 87-90.

Arnold, G. L., Lyons, T. W., Gordon, G. W., and Anbar, A. D. (2012). Extreme change in sulfide concentrations in the Black Sea during the Little Ice Age reconstructed using molybdenum isotopes. Geology, 40, 595-598.

Asael, D., Tissot, F. L. H., Reinhard, C. T., Rouxel, O., Dauphas, N., Lyons, T. W., Ponzevera, E., Liorzou, C., and Chéron, S. (2013). Coupled molybdenum, iron and uranium stable isotopes as oceanic paleoredox proxies during the Paleoproterozoic Shunga Event. Chemical Geology, 362, 193-210.

Barling, J., and Anbar, A. D. (2004). Molybdenum isotope fractionation during adsorption by manganese oxides. Earth & Planetary Science Letters, 217, 315-329.

Barling, J., Arnold, G. L., and Anbar, A. D. (2001). Natural mass-dependent variations in the isotopic composition of molybdenum. Earth & Planetary Science Letters, 193, 447-457.

Berner, R. A., and Raiswell, R. (1983). Burial of organic carbon and pyrite sulfur in sediments over Phanerozoic time: a new theory. Geochimica et Cosmochimica Acta, 47, 855-862.

Berner, R. A., and Raiswell, R. (1984). C/S method for distinguishing freshwater from marine sedimentary rocks. Chemical Geology, 12, 365-368.

Brocks, J.J., Jarrett, A.J., Sirantoine, E., Hallmann, C., Hoshino, Y. and Liyanage, T. (2017). The rise of algae in Cryogenian oceans and the emergence of animals. Nature, 548, 578.

Butterfield, N. J. (2009). Oxygen, animals and oceanic ventilation: an alternative view. Geobiology, 7, 1-7.

Canfield, D. E. (1998). A new model for Proterozoic ocean chemistry. Nature, 396, 450.

Canfield, D. E., Raiswell, R., Westrich, J. T., Reaves, C. M., and Berner, R. A. (1986). The use of chromium reduction in the analysis of reduced inorganic sulfur in sediments and shales. Chemical Geology, 54, 149-155.

Canfield, D. E. (2005). The early history of atmospheric oxygen: homage to Robert M. Garrels. Annual Reviews in Earth and Planetary Sciences, 33, 1-36.

Chappaz, A., Lyons, T. W., Gregory, D. D., Reinhard, C. T., Gill, B. C., Li, C., and Large, R. (2014). Does pyrite act as an important host for molybdenum in modern and ancient euxinic sediments? Geochimica et Cosmochimica Acta, 126, 112-122.

Cohen, P.A. and Macdonald, F.A. (2015). The Proterozoic record of eukaryotes. Paleobiology, 41, 610-632.

Cole, D. B., Reinhard, C. T., Wang, X., Gueguen, B., Halverson, G. P., Gibson, T., Hodgskiss, M. S. W., McKenzie, N. R., Lyons, T. W., and Planavsky, N. J. (2016). A shale-hosted Cr isotope record of low atmospheric oxygen during the Proterozoic. Geology, 44, 555-558.

Cox, G. M., Jarrett, A. J. M., Edwards, D., Crockford, P. W., Halverson, G. P., Collins, A. S., Poirier, A., and Li, Z-X. (2016). Basin redox and primary productivity within the Mesoproterozoic Roper Seaway. Chemical Geology, 440, 101-114.

Crowe, S. A., Paris, G., Katsev, S., Jones, C., Kim, S. T., Zerkle, A. L., Sulung, N., Fowle, D. A., Adkins, J. F., Sessions, A. L., Farquhar, J., and Canfield, D. E. (2014). Sulfate was a trace constituent of Archean seawater. Science, 346, 735-739.

Cumming, V. M., Poulton, S. W., Rooney, A. D., and Selby, D. (2013). Anoxia in the terrestrial environment during the late Mesoproterozoic. Geology, 41, 583-586.

Dahl, T. W., Canfield, D. E., Rosing, M. T., Frei, R. E., Gordon, G. W., Knoll, A. H., & Anbar, A. D. (2011). Molybdenum evidence for expansive sulfidic water masses in ~750 Ma oceans. Earth and Planetary Science Letters, 311, 264-274.

Daines, S. J., Mills, B. J. W., and Lenton, T. M. (2017). Atmospheric oxygen regulation at low Proterozoic levels by incomplete oxidative weathering of sedimentary organic carbon. Nature Communications, 8, 14379

Duan, Y., Anbar, A. D., Arnold, G. L., Lyons, T. W., Gordon, G. W. and Kendall, B. (2010). Molybdenum isotope evidence for mild environmental oxygenation before the Great Oxidation Event. Geochimica et Cosmochimica Acta, 74,6655-6668.

Emerson, S. R. and Huested, S. S. (1991). Ocean anoxia and the concentrations of molybdenum and vanadium in seawater. Marine Chemistry, 34,177-196.

Erickson, B. E. and Helz, G. R. (2000). Molybdenum (VI) speciation in sulfidic waters: stability and lability of thiomolybdates. Geochimica et Cosmochimica Acta, 64,1149-1158.

Gao, L. Z., Zhang, C. H., Shi, X. Y., Zhou, H. R., and Wang, Z. Q. (2007). Zircon SHRIMP U-Pb dating of the tuff bed in the Xiamaling formation of the Qingbaikouan system in North China. Geological Bulletin of China, 26, 249-255.

Gomes, M. L., and Hurtgen, M. T. (2015). Sulfur isotope fractionation in modern euxinic systems: Implications for paleoenvironmental reconstructions of paired sulfate-sulfide isotope records. Geochimica et Cosmochimica Acta, 157, 39-55.

Gellatly, A. M., and Lyons, T. W. (2005). Trace sulfate in mid-Proterozoic carbonates and the sulfur isotope record of biospheric evolution. Geochimica et Cosmochimica Acta, 69, 3813-3829.

Gilleaudeau, G. J., and Kah, L. C. (2015). Heterogeneous redox conditions and a shallow chemocline in the Mesoproterozoic ocean: Evidence from carbon–sulfur–iron relationships: Precambrian Research, 257, 94-108.

Gilleaudeau, G. J., Frei, R., Kaufman, A. J., Kah, L. C., Azmy, K., Bartley, J. K., Chernyavskiy, P., and Knoll, A. H. (2016). Oxygenation of the mid-Proterozoic atmosphere: clues from chromium isotopes in carbonates. Geochemical Perspectives Letters, 2, 178-187.

Habicht, K. S., Gade, M., Thamdrup, B., Berg, P., and Canfield, D. E. (2002). Calibration of sulfate levels in the Archean ocean. Science, 298, 2372-2374.

Hardisty, D. S., Lu, Z., Bekker, A., Diamond, C. W., Gill, B. C., Jiang, G., Kah, L. C., Knoll, A. H., Loyd, S., Osburn, M. R., Planavsky, N. J., Wang, C., Zhou, X., and Lyons, T. W. (2017). Perspectives on Proterozoic surface ocean redox from iodine contents in ancient and recent carbonate. Earth and Planetary Science Letters, 463, 159-170.

Helz, G. R., Miller, C. V., Charnock, J. M., Mosselmans, J. F. W., Pattrick, R. A. D., Garner, C. D., and Vaughan, D. J. (1996). Mechanism of molybdenum removal from the sea and its concentration in black shales: EXAFS evidence. Geochimica et Cosmochimica Acta, 60, 3631-3642.

Helz, G. R., Bura-Nakić, E., Mikac, N., and Ciglenečki, I. (2011). New model for molybdenum behavior in euxinic waters. Chemical Geology, 284, 323-332.

Hou, G. T., Li, J. H., Liu, Y. L., and Qian, X. L. (2005). Late Paleo-proterozoic extension events in North China Craton: aulacogens and dyke swarms. Progress in Natural Science, 15, 1366-1373 (in Chinese with English abstract).

Johnston, D., Poulton, S., Goldberg, T., Sergeev, V., Podkovyrov, V., Vorob'eva, N., Bekker, A., Knoll, A. (2012). Late Ediacaran redox stability and metazoan evolution. Earth and Planetary Science Letters, 335, 25-35.

Kah, L. C., Lyons, T. W., and Frank, T. D. (2004). Low marine sulphate and protracted oxygenation of the Proterozoic biosphere. Nature, 431, 834-838.

Kendall, B., Creaser, R. A., Gordon, G. W., and Anbar, A. D. (2009). Re–Os and Mo isotope systematics of black shales from the Middle Proterozoic Velkerri and Wollogorang formations, McArthur Basin, northern Australia. Geochimica et Cosmochimica Acta, 73, 2534-2558.

Kendall, B., Komiya, T., Lyons, T. W., Bates, S. M., Gordon, G. W., Romaniello, S. J., Jiang, G., Creaser, R. A., Xiao, S., McFadden, K., Sawaki, Y., Tahata, M., Shu, D., Han, J., Li, Y., Chu, X., and Anbar, A. D. (2015). Uranium and molybdenum isotope evidence for an episode of widespread ocean oxygenation during the late Ediacaran Period. Geochimica et Cosmochimica Acta, 156, 173-193.

Knoll, A. H., Javaux, E. J., Hewitt, D., and Cohen, P. (2006). Eukaryotic organisms in Proterozoic oceans. Philosophical Transactions of the Royal Society B: Biological Sciences, 361, 1023-1038.

Knoll, A. H. (2014). Paleobiological perspectives on early eukaryotic evolution: Cold Spring Harbor perspectives in biology, 6, a016121.

Kump, L. R. (2008). The rise of atmospheric oxygen. Nature, 451, 277-278.

Lamb, D.M., Awramik, S.M., Chapman, D.J. and Zhu, S. (2009). Evidence for eukaryotic diversification in the∼ 1800 million-year-old Changzhougou Formation, North China. Precambrian Research, 173, 93-104.

Lenton, T. M., Boyle, R. A., Poulton, S. W., Shields-Zhou, G. A., and Butterfield, N. J. (2014). Co-evolution of eukaryotes and ocean oxygenation in the Neoproterozoic era. Nature Geoscience, 7, 257-265.

Li, H.K., Lu, S.N., Li, H.M., Sun, L.X., Xiang, Z.Q., Geng, J.Z., Zhou, H.Y. (2009) Zircon and beddeleyite U-Pb precision dating of basic rock sills intruding Xiamaling Formation, North China. Geological Bulletin China, 28, 1396-1404

Li, C., Planavsky, N. J., Love, G. D., Reinhard, C. T., Hardisty, D., Feng, L., Bates, S. M., Huang, J., Zhang, Q., Chu, X., and Lyons, T. W. (2015). Marine redox conditions in the middle Proterozoic ocean and isotopic constraints on authigenic carbonate formation:

Insights from the Chuanlinggou Formation, Yanshan Basin, North China. Geochimica et Cosmochimica Acta, 150, 90-105.

Li, J., Zhu, X-K., Tang, S-H., and Zhang, K. (2016). High-precision measurement of molybdenum isotopic compositions of selected geochemical reference materials. Geostandards and Geoanalytical Research, 40, 405-415.

Liu, X., Kah, L., Knoll, A., Cui, H., Kaufman, A., Shahar, A., and Hazen, R. (2016). Tracing Earth's O_2 evolution using Zn/Fe ratios in marine carbonates. Geochemical Perspectives Letters, 2, 24-34.

Lu, S. N., Zhao, G. C., Wang, H. C., and Hao, G. J. (2008). Precambrian metamorphic basement and sedimentary cover of the North China craton: A review. Precambrian Research, 160, 77-93.

Luo, G., Hallmann, C., Xie, S., Ruan, X., and Summons, R. E. (2015a). Comparative microbial diversity and redox environments of black shale and stromatolite facies in the Mesoproterozoic Xiamaling Formation. Geochimica et Cosmochimica Acta, 151, 150-167.

Luo, G., Ono, S., Huang, J., Algeo, T. J., Li, C., Zhou, L., Robinson, A., Lyons, T. W., and Xie, S. (2015b). Decline in oceanic sulfate levels during the early Mesoproterozoic. Precambrian Research, 258, 36-47.

Lyons, T. W. (1997). Sulfur isotopic trends and pathways of iron sulfide formation in upper Holocene sediments of the anoxic Black Sea. Geochimica et Cosmochimica Acta, 61, 3367-3382.

Lyons, T. W., and Berner, R. A. (1992). Carbon-sulfur-iron systematics of the Holocene sediments of the anoxic Black Sea. Chemical Geology, 99, 1-27.

Lyons, T. W., and Severmann, S. (2006). A critical look at iron paleoredox proxies: New insights from modern euxinic marine basins. Geochimica et Cosmochimica Acta, 70, 5698-5722.

Lyons, T. W., Anbar, A. D., Severmann, S., Scott, C., and Gill, B. C. (2009). Tracking euxinia in the ancient ocean: a multiproxy perspective and Proterozoic case study. Annual Review of Earth and Planetary Sciences, 37, 507-534.

Lyons, T. W., Reinhard, C. T., and Planavsky, N. J. (2014). The rise of oxygen in Earth's early ocean and atmosphere. Nature, 506, 307-315.

Mei, M. X., Li, Z. Z., Bai, Z. D., and Xu, D. B. (1998). Preliminary study on the middle and upper Proterozoic cyclic-sequences in Xinlong County, Hebei. Journal of Stratigraphy, 22, 102-108 (in Chinese with English abstract).

Meng, Q.-R., Wei, H.-H., Qu, Y.-Q., and Ma, S.-X. (2011). Stratigraphic and sedimentary records of the rift to drift evolution of the northern North China craton at the Paleo- to Mesoproterozoic transition. Gondwana Research, 20, 205-218.

Miller, C. A., Peucker-Ehrenbrink, B., Walker, B. D., Marcantonio, F. (2011). Re-assessing the surface cycling of molybdenum and rhenium. Geochimica et Cosmochimica Acta,75, 7146-7179.

Mitchell, R. L., and Sheldon, N. (2009). Weathering and paleosol formation in the 1.1 Ga Keweenawan Rift. Precambrian Research, 168, 271-283.

Nägler, T. F., Neubert, N., Böttcher, M. E., Dellwig, O. and Schnetger, B. (2011). Molybdenum isotope fractionation in pelagic euxinia: evidence from the modern Black and Baltic Seas. Chemical Geology, 289, 1-11.

Nägler, T. F., Anbar, A. D., Archer, C., Goldberg, T., Gordon, G. W., Greber, N. D., Siebert, C., Sohrin, Y., and Vance, D. (2014). Proposal for an international molybdenum isotope measurement standard and data representation. Geostandards and Geoanalytical Research, 38, 149-151.

Nakagawa, Y., Takano, S., Firdaus, M. L., Norisuye, K., Hirata, T., Vance, D., and Sohrin, Y. (2012). The molybdenum isotopic composition of the modern ocean. Geochemical Journal, 46, 131-141.

Neubert, N., Nägler, T. F., and Böttcher, M. E. (2008). Sulfidity controls molybdenum isotope fractionation onto euxinic sediments: Evidence from the modern Black Sea. Geology, 36, 775-778.

Och, L.M. and Shields-Zhou, G.A., 2012. The Neoproterozoic oxygenation event: Environmental perturbations and biogeochemical cycling. Earth-Science Reviews, 110, 26-57.

Parnell, J., Boyce, A. J., Mark, D., Bowden, S., and Spinks, S. (2010). Early oxygenation of the terrestrial environment during the Mesoproterozoic. Nature, 468, 290-293.

Partin, C. A., Bekker, A., Planavsky, N. J., Scott, C. T., Gill, B. C., Li, C., Podkovyrov, V., Maslov, A., Konhauser, K. O., Lalonde, S. V., Love, G. D., Poulton, S. W., and Lyons, T. W. (2013). Large-scale fluctuations in Precambrian atmospheric and oceanic oxygen levels from the record of U in shales. Earth and Planetary Science Letters, 369–370, 284-293.

Planavsky, N. J., McGoldrick, P., Scott, C. T., Li, C., Reinhard, C. T., Kelly, A. E., Chu, X., Bekker, A., Love, G. D., and Lyons, T. W. (2011). Widespread iron-rich conditions in the mid-Proterozoic ocean. Nature, 477, 448-451.

Planavsky, N. J., Reinhard, C. T., Wang, X., Thomson, D., McGoldrick, P., Rainbird, R. H., Johnson, T., Fischer, W. W., and Lyons, T. W. (2014). Low Mid-Proterozoic atmospheric oxygen levels and the delayed rise of animals. Science, 346, 635-638.

Poulson, R. L., Siebert, C., McManus, J., and Berelson, W. M. (2006). Authigenic molybdenum isotope signatures in marine sediments. Geology, 34, 617-620.

Poulson Brucker, R. L., McManus, J., Severmann, S., and Berelson, W. M. (2009). Molybdenum behavior during early diagenesis: Insights from Mo isotopes. Geochemistry, Geophysics, Geosystems, 10, Q06010.

Poulton, S. W., Fralick, P. W., and Canfield, D. E. (2004). The transition to a sulfidic ocean ~1.84 billion years ago. Nature, 431, 173-177.

Poulton, S. W., and Canfield, D. E. (2005). Development of a sequential extraction procedure for iron: Implications for iron partitioning in continentally-derived particulates. Chemical Geology, 214, 209-221.

Qiao, X., (1976). Investigation on stratigraphy of the Qingbaikou Group of the Yenshan Mountains, North China. Scientia Geologica Sinica, 3, 246-265. (in chinese with English abstract)

Qiao, X. F., Gao, L. Z., and Zhang, C. H. (2007). New idea of the Meso- and Neoproterozoic chronostratigraphic chart and tectonic environment in Sino-Korean Plate. Geological Bulletin of China, 26, 503-509 (in Chinese with English abstract).

Qu, Y., Pan, J., Ma, S., Lei, Z., Li, L., and Wu, G. (2014). Geological characteristics and tectonic significance of unconformities in Mesoproterozoic successions in the northern margin of the North China Block. Geoscience Frontiers, 5, 127-138.

Raiswell, R., and Berner, R. A. (1985). Pyrite formation in euxinic and semi-euxinic sediments. American Journal of Science, 285, 710-724.

Raiswell, R., and Berner, R. A. (1986). Pyrite and organic matter in Phanerozoic normal marine shales. Geochimica et Cosmochimica Acta, 50, 1967-1976.

Raiswell, R., and Berner, R. A. (1987). Organic carbon losses during burial and thermal maturation of normal marine shales. Geology, 15, 853-856.

Raiswell, R., Reinhard, C. T., Derkowski, A., Owens, J. D., Bottrell, S. H., Anbar, A. D., and Lyons, T. W. (2011). Formation of syngenetic and early diagenetic iron minerals in the late Archean Mt. McRae Shale, Hamersley Basin, Australia: New insights on the patterns, controls and paleoenvironmental implications of authigenic mineral formation. Geochimica et Cosmochimica Acta, 75, 1072-1087.

Reinhard, C. T., Planavsky, N. J., Robbins, L. J., Partin, C. A., Gill, B. C., Lalonde, S. V., Bekker, A., Konhauser, K. O., and Lyons, T. W. (2013). Proterozoic ocean redox and biogeochemical stasis. Proceedings of the National Academy of Sciences of the United States of America, 110, 5357-5362.

Reinhard, C. T., Planavsky, N. J., Olson, S. L., Lyons, T. W., and Erwin, D. H. (2016). Earth's oxygen cycle and the evolution of animal life. Proceedings of the National Academy of Sciences of the United States of America, 113, 8933-8938.

Scott, C., Lyons, T. W., Bekker, A., Shen, Y., Poulton, S. W., Chu, X., and Anbar, A. D. (2008). Tracing the stepwise oxygenation of the Proterozoic ocean. Nature, 452, 456-459.

Scott, C., and Lyons, T. W. (2012). Contrasting molybdenum cycling and isotopic properties in euxinic versus non-euxinic sediments and sedimentary rocks: Redefining the paleoproxies. Chemical Geology, 324-325, 19-27.

Severmann, S., Lyons, T. W., Anbar, A., McManus, J., and Gordon, G. (2008). Modern iron isotope perspective on the benthic iron shuttle and the redox evolution of ancient oceans. Geology, 36, 487-490.

Siebert, C., Nägler, T.F., von Blanckenburg, F., and Kramers, J.D. (2003). Molybdenum isotope records as a potential new proxy for paleoceanography. Earth and Planetary Science Letters, 211, 159-171.

Siebert, C., McManus, J., Bice, A., Poulson, R., and Berelson, W. M. (2006). Molybdenum isotope signatures in continental margin sediments. Earth and Planetary Science Letters, 241, 723-733.

Sim, M. S., Bosak, T. and Ono, S. (2011). Large sulfur isotope fractionation does not require disproportionation. Science, 333,74-77.

Slack, J. F., Grenne, T., Bekker, A., Rouxel, O. J., and Lindberg, P. A. (2007). Suboxic deep seawater in the late Paleoproterozoic: evidence from hematitic chert and iron formation related to seafloor-hydrothermal sulfide deposits, central Arizona, USA. Earth and Planetary Science Letters, 255, 243-256.

Sperling, E., Rooney, A., Hays, L., Sergeev, V., Vorob'eva, N., Sergeeva, N., Selby, D., Johnston, D., and Knoll, A. (2014). Redox heterogeneity of subsurface waters in the Mesoproterozoic ocean. Geobiology, 12, 373-386.

Stolper, D. A., Revsbech, N. P. and Canfield, D. E. (2010). Aerobic growth at nanomolar oxygen concentrations. Proceedings of the National Academy of Sciences of the United States of America, 10718755-18760.

Su, W. B., Zhang, S. H., Huff, W. D., Li, H. K., Ettensohn, F. R., Chen, X. Y., Yang, H. M., Han, Y. G., Song, B., and Santosh, M. (2008). SHRIMP U-Pb ages of K-bentonite beds in the Xiamaling Formation: Implications for revised subdivision of the Meso- to Neoproterozoic history of the North China craton. Gondwana Research, 14, 543-553.

Su, W. B., Li, H. K., Huff, W. D., Ettensohn, F. R., Zhang, S. H., Zhou, H. Y., and Wan, Y. S. (2010). SHRIMP U-Pb dating for a K-bentonite bed in the Tieling Formation, North China. Chinese Science Bulletin, 55, 2197-2206.

Tribovillard, N., Riboulleau, A., Lyons, T. W., and Baudin, F. (2004). Enhanced trapping of molybdenum by sulfurized organic matter of marine origin as recorded by various Mesozoic formations. Chemical Geology, 213, 385-401.

Wagner, W., Chappaz, A., and Lyons, T. W. (2017). Molybdenum speciation and burial pathway in weakly sulfidic environments: Insights from XAFS. Geochimica et Cosmochimica Acta, 206, 18-29.

Waldbauer, J. R., Newman, D. K. and Summons, R. E. (2011). Microaerobic steroid biosynthesis and the molecular fossil record of Archean life. Proceedings of the National Academy of Sciences of the United States of America, 108, 13409-13414.

Wang, T. G., and Simoneit, B. R. T. (1995). Tricyclic terpanes in Precambrian bituminous sandstone from the eastern Yanshan region, North China. Chemical Geology, 120, 155-170.

Williams, T.M., Estes, J.A., Doak, D.F. and Springer, A.M. (2004). Killer appetites: assessing the role of predators in ecological communities. Ecology, 85, 3373-3384.

Wing, B. A. and Halevy, I. (2014). Intracellular metabolite levels shape sulfur isotope fractionation during microbial sulfate respiration. Proceedings of the National Academy of Sciences of the United States of America of the United States of America, 111, 18116-18125.

Yang, S., Kendall, B., Lu, X., Zhang, F., and Zheng, W. (2017). Uranium Isotope Compositions of Mid-Proterozoic Black Shales: Evidence for an Episode of Increased Ocean Oxygenation at 1.36 Ga and Evaluation of the Effect of Post-Depositional Hydrothermal Fluid Flow. Precambrian Research, 298, 187-201.

Yin, L., Yuan, X., Meng, F., Hu, J. (2005). Protists of the Upper Mesoproterozoic Ruyang Group in Shanxi Province, China. Precambrian Research, 141, 49-66

Zbinden, E. A., Holland, H. D., Feakes, C. R. and Dobos, S. K. (1988). The Sturgeon Falls paleosol and the composition of the atmosphere 1.1 Ga BP. Precambrian Research, 42, 141-163.

Zhang, S.-H., Zhao, Y., Yang, Z.-Y., He, Z.-F., and Wu, H. (2009). The 1.35 Ga diabase sills from the northern North China Craton: implications for breakup of the Columbia (Nuna) supercontinent. Earth and Planetary Science Letters, 288, 588-600.

Zhang, S., Wang, X., Wang, H., Bjerrum, C. J., Hammarlund, E. U., Mafalda Costa, M., Connelly, J. N., Zhang, B., Su, J., and Canfield, D. E. (2016). Sufficient oxygen for animal respiration 1,400 million years ago. Proceedings of the National Academy of Sciences of the United States of America of the United States of America, 113, 1731-1736.

Chapter 3

Mid-Proterozoic redox evolution and the possibility of transient oxygenation events

Preface:

The contents of this chapter, less the forward, have been published in a modified form as:

> Diamond, C.W. and Lyons, T.W., 2018. Mid-Proterozoic redox evolution and the possibility of transient oxygenation events. Emerging topics in life sciences, 2(2), pp.235-245.

Forward

This chapter presents a manuscript that was published as part of a special issue of *Emerging Topics in Life Sciences*. It represented the evolution of our thinking as we grappled with the ideas of chromium isotope data remaining low while indications of higher oceanic O_2 at times during the mid-Proterozoic continued to appear. The conclusion that we came to, which is alluded to in the previous chapter, was that the mid-Proterozoic world was likely dominated by a stable steady state with low atmospheric O_2, but that some transient oxygenation events, perhaps many, punctuated the long, relatively stable baseline. This seemed to be where the data were pointing, and this chapter builds that case using what are, in my opinion, the most compelling data available.

Abstract

It is often assumed that rising environmental oxygen concentrations played a significant role in the timing of the first appearance of animals and the trajectory of their early proliferation and diversification. The inherent large size and complexity of animals come with large energy requirements—levels of energy that can best, if not only, be acquired through aerobic respiration. There is also abundant geochemical evidence for an increase in ocean-atmosphere O_2 concentrations in temporal proximity with the emergence of the group. To adequately test this hypothesis, however, a thorough understanding of the history of environmental oxygenation in the time between the first appearance of eukaryotes and the eventual appearance of animals is necessary. In this review, we summarize the evidence for the prevailing long-term conditions of the Proterozoic Eon prior to the emergence of Metazoa and go on to highlight multiple independent geochemical proxy records that suggest at least two transient oxygenation events—at ~1.4 and ~1.1 billion years ago (Ga)—during this time. These emerging datasets open the door to an important possibility: while prevailing conditions during much of this time would likely have presented challenges for early animals, there were intervals when oxygenated conditions were more widespread and could have favored yet undetermined advances in eukaryotic innovation, including critical early steps toward animal evolution.

Introduction

The general association between environmental change in the late Proterozoic, 0.8-0.54 Ga, and the emergence and proliferation of the metazoan lineage is a topic that has attracted interest for decades. There is a striking temporal coincidence between the first evidence of Metazoa (Love et al., 2009; Love et al., 2015) and eukaryote-dominated ecosystems (3) in the geological record and apparent first order changes in biologically relevant environmental conditions (Och and Shields-Zhou, 2012; Planavsky et al., 2014; Cole et al., 2016; Reinhard et al., 2017). This relationship is perhaps most true with respect to oxygen concentrations in the surface oceans and, for that reason, much discussion has focused on a possible connection between rising oxygen concentrations in the ocean-atmosphere system and the suitability of habitats for animal life (Och and Shields-Zhou, 2012; Sperling et al., 2013; Planavsky et al., 2014; Catling et al., 2015; Sperling et al., 2015; Cole et al., 2016; Reinhard et al., 2016). Multiple processes found throughout the eukaryotic domain require the presence of free molecular oxygen (e.g., Towe, 1970; Summons et al., 2006; Waldbauer et al., 2011;), and on the modern Earth, oxygen concentrations and metazoan diversity in marine ecosystems scale directly (Levin and Gage, 1998). While it is true that some modern animals are adapted to very low oxygen environments (Levin, 2003), this is an exception to the rule.

Correlation, however, is not causation, and despite geochemical records that indicate environmental O_2 concentrations rose just prior to the emergence of the first animals (Love et al., 2009; Planavsky et al., 2014; Cole et al., 2016), this coincidence alone does not require that the former drove the latter. Indeed, while the argument for a

connection between these two observations has been made many times over the past 70 years (e.g., Nursall, 1959), others have argued that there is no connection (Mills and Canfield, 2014) or even that the emergence of Metazoa drove environmental oxygenation (Butterfield, 2009; 2018). Any attempt to reconcile this open question must not only integrate all available geochemical and paleontological data during the interval over which animals first appeared and radiated, but it must also specifically take into account the history of environmental oxygenation in the time preceding these critical evolutionary advances—that is, the mid-Proterozoic (1.8-0.8 Ga).

Although it is not possible to turn to the geological record and measure the oxygen concentration of ancient oceans or atmospheres directly, a number of diverse and independent proxies have been developed to indirectly assess this quantity. Among those that have been applied to Precambrian strata (older than about 0.5 Ga), robust first-order trends have emerged, generally in good agreement with one another, revealing a mid-Proterozoic world characterized by dominantly low ocean-atmosphere O_2 concentrations (Scott et al., 2008; Partin et al., 2013; Planavsky et al., 2014; Liu et al., 2015; Cole et al., 2016; Mukherjee and Large, 2016; Hardisty et al., 2017; Sheen et al., 2018). Studies of individual formations, however, have hinted at periods within the mid-Proterozoic when oceanic-atmospheric O_2 concentrations rose (e.g., Yang et al., 2017; Diamond et al., 2018). Given the diverse evidence for generally low O_2 during the mid-Proterozoic, these episodes were likely transient. Such variability is entirely consistent with models that favor generally low O_2 conditions. While only speculation at this stage, a growing body of evidence points to the possibility of such events (Cox et al., 2016; Gilleaudeau et al., 2016; Mukherjee and

Large, 2016; Hardisty et al., 2017; Sheen et al., 2018; Diamond et al., 2018; Kendall et al., 2009). In this review, we will summarize the geochemical proxy evidence for two such transient events with an eye toward their potential implications for the evolution of complex life.

A backdrop of low mid-Proterozoic atmospheric O_2

Among the available proxy records, few provide a more straightforward or compelling argument for the prevailing conditions of the mid-Proterozoic than the combined records of mass-independent fractionation of sulfur isotopes ($\Delta^{33}S$) and chromium isotopic data ($\delta^{53}Cr$) from marine shales and ironstones (Figure 3.1; Reinhard et al., 2013; Cole et al., 2016, and references therein). As initially presented by Farquhar et al. (2000) and further refined by Luo et al. (2016), among many others, the record of Δ33S data shows a preservation of strong $\Delta^{33}S$ anomalies prior to ~2.33 Ga, after which these anomalies are not observed gain for the remainder of Earth history. The permanent loss of this signal from the geological record has been called the 'smoking gun' for the Great Oxidation Event (GOE; see ref. 35 for GOE review). Generation of the signal is attributed to photochemical dissociation of sulfur compounds in the upper atmosphere, a process that fractionates isotopes independent of their masses (Pavlov and Kasting, 2002). While this

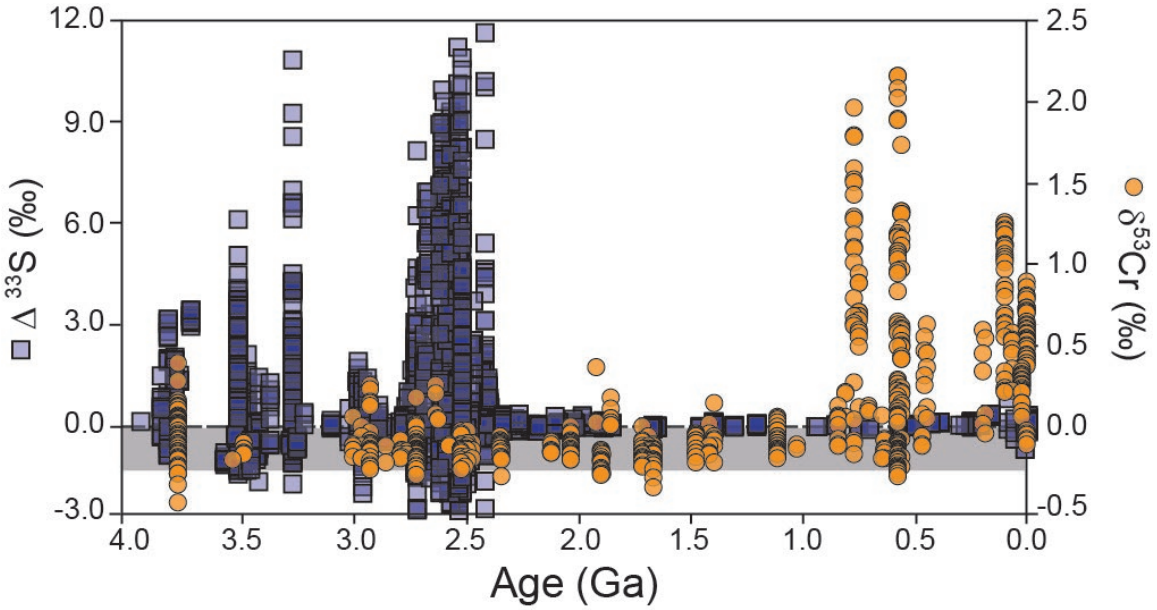

Figure 3.1. Record of mass-independent fractionation of sulfur isotopes in sedimentary pyrite ($\Delta^{33}S$) and chromium isotope data ($\delta^{53}Cr$) from marine ironstones and shales over the past four billion years. Blue squares show $\Delta^{33}S$ data as compiled in Reinhard et al., 2013. Orange circles show the δ53Cr record from iron-rich chemical sediments (i.e., iron formations and ironstones) and organic-rich shales as presented in Cole et al., 2016. Gray region denotes the crustal range of $\delta^{53}Cr$ values. Note that fractionations in $\Delta^{33}S$ data are not present after ~2.33 Ga but large fractionations in $\delta^{53}Cr$ data do not begin until ~0.8 Ga.

process continued to operate after the GOE, the loss of the signal from the record is attributed to reoxidation of dissociation products and their homogenization prior to deposition (Pavlov and Kasting, 2002). Prevention of this oxidation, and therefore retention of the signal, is thought to require atmospheric partial pressure of O_2 (pO_2) less than 10-5 times the present atmospheric levels (PAL; Pavlov and Kasting, 2002). Hence, it is generally agreed that the GOE represents a permanent shift in atmospheric pO_2 from below 10-5 PAL, likely far below, to values above—placing a lower limit on mid-Proterozoic pO_2.

Like preservation of the $\Delta^{33}S$ signal, the chromium isotope paleoredox proxy is also thought to exhibit a threshold response to atmospheric pO_2 (Crowe et al., 2013; Frei et al., 2014; Planavsky et al., 2014). Chromium is present in igneous rocks in the reduced and poorly soluble Cr(III) valence state, while the oxidized Cr(VI) species is highly soluble and mobile in the environment. The high redox potential required to induce this oxidation, however, limits the settings in which it can take place. Even on the modern Earth, few oxidizing agents in the natural environment are capable of oxidizing Cr(III) to Cr(VI), and oxidation by dissolved O_2 alone has been shown to be negligible, if present at all (Eary and Rai, 1987). Instead, nearly all observable Cr(III) oxidation is mediated by manganese-(Mn) oxides in the subaerial weathering environment (Kotaś and Stasicka, 2000). During transport, mobile Cr(VI) can be re-reduced to immobile Cr(III) through interactions with organic matter or other reduced compounds ubiquitous in natural systems, with a strong preference for the lighter Cr isotope (^{52}Cr; Zink et al., 2010). The net result is a residual, mobile Cr(VI) pool that is enriched in ^{53}Cr.

Importantly, the formation of Mn-oxides requires the presence of significant O_2. In a global system with sufficient atmospheric pO_2 to form Mn-oxides in the weathering environment, some portion of the mobilized Cr(VI) will be delivered to the oceans. Upon encountering anoxic conditions in the oceans, the Cr will be reduced and sequestered into sediments, preserving an isotopic fingerprint of Mn-oxide-dependent redox transformations (Reinhard et al., 2014). Estimates on atmospheric pO_2 levels required to 'turn on' the oxidative Cr cycle vary. Crowe et al. (2013) argued that the presence of abundant Fe(II) would reduce any Cr(VI) that was produced in the weathering environment

and calculated the minimum pO_2 required to quantitatively oxidize Fe in the system to be on the order of ~10^{-4} PAL. Planavsky et al. (2014) took a different approach, modeling instead the range of pO_2 required to stimulate extensive Mn oxidation, also finding a low threshold—in this case, ~10^{-3} PAL. Hence, regardless of the method, the estimated threshold pO_2 level for inducing and preserving large fractionations in Cr isotopes should be significantly less than 1% PAL.

Multiple studies have reported $\delta^{53}Cr$ data from iron- and organic-rich marine sediments throughout Earth's history (Frei et al., 2014; Planavsky et al., 2014; Cole et al., 2016). Among the most recent of those investigations, Cole et al. (2016) presented a record of $\delta^{53}Cr$ data from marine shales deposited under anoxic conditions (Figure 3.1). Importantly, all of these studies showed a lack of fractionated $\delta^{53}Cr$ data prior to ~0.8 Ga, suggesting that oxidative Cr cycling was not active until that time. Thus, these data present an upper limit on long-term mid-Proterozoic pO_2 of less than 1% PAL, potentially much less. When viewed in combination with the $\Delta^{33}S$ record, a picture emerges in which intermediate but still low pO_2 levels likely persisted for the majority of the mid-Proterozoic. However, given the incomplete nature of the Precambrian rock record, as well as other inherent limitations in generating multi-billion-year compilations of geochemical data, there are temporal gaps in the $\delta^{53}Cr$ datasets that would allow for transient oxygenation events to have gone undetected.

A possible transient event at ~1.4 Ga

In recent years, mounting evidence has suggested the possibility of a transient period of more oxic conditions at ~1.4 Ga (Kendall et al., 2009; Cox et al., 2016; Zhang et al., 2016; Hardisty et al., 2017; Yang et al., 2017; Diamond et al., 2018; Sheen et al., 2018). Diverse types of geochemical data are available that independently support this conclusion, including trace metal concentration and isotopic data from organic-rich shales of the ~1.4 Ga Velkerri and Xiamaling formations of northern Australia and the North China Craton, respectively, as well as iodine concentrations in the Tieling Formation, which directly underlies the Xiamaling Formation (Kendall et al., 2009; Cox et al., 2016; Hardisty et al., 2017; Yang et al., 2017; Sheen et al., 2018; Diamond et al., 2018). The first piece of evidence that suggested this possibility was heightened molybdenum (Mo) concentrations in organic-rich shales of the Velkerri Formation (Kendall et al., 2009).

Through oxidative weathering of the continents, Mo is delivered to the oceans as poorly reactive molybdate (MoO_4^{2-}). Molybdate removal from oxic waters is slow, the primary sink being sorption onto iron- and manganese-oxide crusts (Bertine and Turekian, 1973; Kashiwabara et al., 2009). In euxinic waters (those devoid of O_2 and with free H_2S^-), molybdate can react with available $H_2S_{(aq)}$ to progressively form thiomolybdate species (taking the form MoO_xS_{4-x}) and tetrathiomolybdate (MoS_4^{2-}) when $H_2S_{(aq)}$ is sufficiently abundant (Helz et al., 1996; Erickson and Helz, 2000; Helz et al., 2011). These thiomolybdates are highly reactive, such that reaction with the charged surfaces of sinking particles makes Mo deposition rates in euxinic systems orders of magnitude higher than those in oxic settings (Bertine and Turekian, 1973; Vorlicek et al., 2004; Tribovillard et

al., 2004; Scott et al., 2008; Scitt and Lyons 2012). Importantly, the accumulation rate of Mo in sediments underlying euxinic waters scales proportionally with the concentration of Mo in overlying waters (Algeo and Lyons 2006). Thus, the concentration of Mo in a marine shale deposited beneath euxinic waters can be used to gauge the concentration of Mo in seawater (e.g., Reinhard et al., 2013). The rapid removal of Mo from euxinic waters also makes the size of the oceanic Mo reservoir highly sensitive to the prevalence of euxinia in the broader ocean (i.e., when more of the oceans are euxinic, the concentration of Mo in seawater, and thus within individual euxinic shales, will diminish). By examining the Mo concentration in organic-rich shales deposited beneath euxinic waters throughout Earth's history, it is possible to observe the waxing and waning of euxinia on a global scale (e.g., Scott et al., 2008; Scott and Lyons 2012).

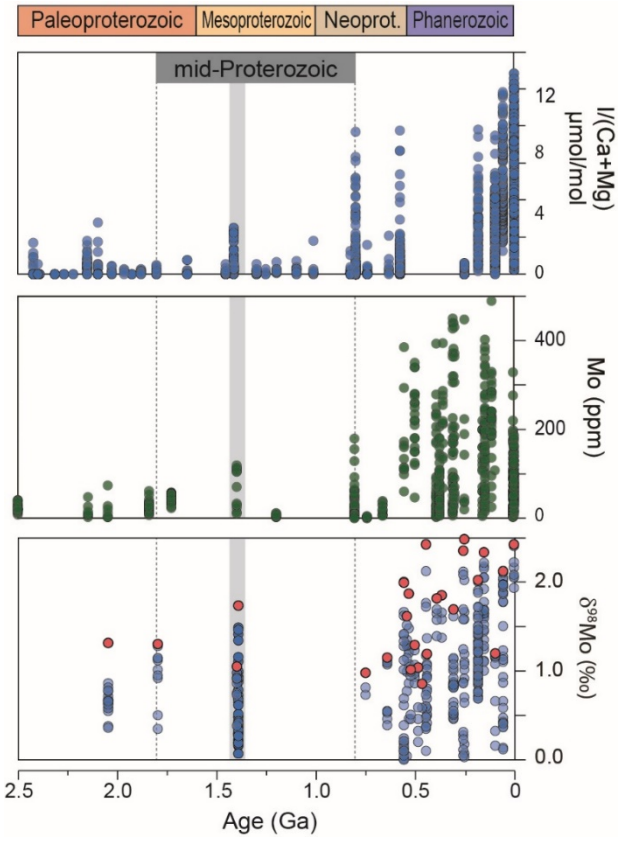

Figure 3.2. Compilation of select geochemical redox-proxy data indicating a transient event at ~1.4 Ga. Top panel shows the concentration of iodine, normalized to carbonate content, in shallow marine carbonates (updated from ref. 25). Lower two panels show molybdenum concentrations (middle) and isotopic data (lower) from marine shales independently constrained to have been deposited in euxinic conditions (updated from refs. 53,61). Red filled circles in lower panel indicate maximum δ^{98}Mo value for each formation. Gray bar denotes putative oxygenation event at ~1.4 Ga.

Scott et al. (2008) presented the first record of Mo concentrations from euxinic shales through time, demonstrating that the mid-Proterozoic is characterized by values that rarely exceed 50 ppm. An updated record is shown in Figure 3.2 (next page, updated from Reinhard et al., 2013), and while the earlier pattern of maximum Mo concentrations of ~50 ppm throughout the mid-Proterozoic remains, the Velkerri Formation uniquely exceeds this threshold (>100 ppm; 29,30). This observation suggests that euxinic conditions were less prevalent at ~1.4 Ga compared to other times in the mid-Proterozoic. Further, a recent compilation of rhenium (Re) concentration data from anoxic shales throughout Earth's history revealed that while the maximum Re enrichment in the upper Velkerri Formation is similar to those of other mid-Proterozoic shales, the average concentration is uniquely high for the time interval (Sheen et al., 2018). Oceanic Re and Mo exhibit similar redox sensitivities in that both accumulate very slowly in sediments underlying well-oxygenated waters; however, Re differs from Mo by not requiring the presence of $H_2S_{(aq)}$ to facilitate rapid uptake under reducing conditions (Crusius et al., 1996). In this way, the concentration of Re in anoxic shales is thought to reflect the pervasiveness of anoxia in the global oceans (not discriminating between anoxic waters rich in Fe(II) or H_2S^-). The uniform Re enrichments of the upper Velkerri Formation make the average Re concentration for the unit significantly higher than those observed in other mid-Proterozoic shales included in the study (apart from the ~1.1 Ga Tourist Formation discussed below). Based on an element mass-balance model using these formational averages, Sheen et al. (Sheen et al., 2018) concluded that while the average Re enrichment in the lower Velkerri Formation is consistent with a fully anoxic ocean, the heightened average Re concentration of the upper

Velkerri Formation can be explained by a mere 2-13% of the contemporaneous seafloor residing beneath anoxic waters.

Additional evidence for a decrease in the areal extent of euxinic conditions at ~1.4 Ga was recently presented in the form of Mo isotope data (reported as δ^{98}Mo, permil deviations in the ratio of ^{98}Mo /^{95}Mo) from the Xiamaling Formation (Diamond et al., 2018). In oxygenated waters, adsorption to the surface of Mn-oxides carries a strong preference for the lighter Mo isotope (^{95}Mo; Barling et al., 2011; Siebert et al., 2003; Barling and Anbar, 2004; Poulson Brucker et al., 2009). Adsorption to iron-oxides induces a smaller fractionation, though both processes leave the residual seawater molybdate pool enriched in the heavier isotope (^{98}Mo). In strongly euxinic waters, by contrast (i.e., those with high and persistent dissolved sulfide concentrations), relatively small fractionations are observed between the dissolved Mo reservoir and authigenic solid-phase Mo in sediments (Nägler et al., 2011). Additionally, due to the rapid sequestration of Mo in euxinic settings, uptake is often nearly quantitative, leading to little or no preservation of isotopic fractionations related to the multiple processes involved. For these reasons, it is often suggested that the δ^{98}Mo value of sediments deposited beneath euxinic waters should closely match that of the coeval oceans—and this value should increase proportionally when larger regions of the oceans are well oxygenated, favoring the accumulation of Mn-oxides.

In summary, because Mo deposition in oxic settings carries a strong fractionation toward lighter Mo, and euxinic deposition can be expected to carry relatively little to no isotopic fractionation, the isotopic ratio of oceanic Mo can be modulated by the prevalence

of oxic conditions globally (Arnold et al., 2004). While the Mo isotope system contains many nuances unaccounted for in this simplified view, it is generally thought that the lack of high δ^{98}Mo values in the Proterozoic (as shown in Figure 3.2) reflects the relative scarcity of significant Mn-oxide sinks during that time (e.g., Kendall et al., 2015; Chen et al., 2015). The maximum δ^{98}Mo value reported by Diamond et al. (2018) from the Xiamaling Formation, however, is +1.7‰—that is, a value significantly higher than other mid-Proterozoic data and, again, qualitatively indicative of less reducing oceans at ~1.4 Ga.

Uranium (U) isotope data (δ^{238}U) have also been cited as evidence for expanded oxic and suboxic conditions at ~1.4 Ga. Like other redox-sensitive metals, U is highly soluble in its oxidized form but sequestered rapidly into sediments under reducing conditions (Morford and Emerson, 1999; Dunk et al., 2002). Unlike the Mo isotope system, however, the reduced sink for U carries a significant fractionation, favoring the heavier U isotope (^{238}U) and rendering authigenic sedimentary U beneath anoxic waters ~0.6‰ heavier than coeval seawater (Weyer et al., 2008; Montoya-Pino et al., 2010; Andersen et al., 2014). Yang et al. (2017) reported δ^{238}U values in black shales of the upper Velkerri Formation that are too high to be consistent with a fully anoxic ocean. In other words, if a large fraction of the global seafloor rests beneath anoxic waters, rapid and widespread uptake of heavy U will cause the residual seawater reservoir to become enriched in the lighter U isotopes (decreasing the δ^{238}U value). Consequently, sediments deposited in any one anoxic setting will preserve lower δ238U values. Using an isotope mass-balance model, Yang et al. (2017) calculated that the δ^{238}U values from the upper Velkerri

Formation were consistent with no more than 25% of the seafloor lying beneath anoxic waters.

Heightened iodine concentrations in the Tieling Formation, a stromatolitic carbonate unit that directly underlies the Xiamaling Formation, also suggest expanded oxic conditions at ~1.4 Ga (Hardisty et al., 2017). Iodine concentrations in carbonate rocks have been shown to scale proportionally with the magnitude and stability of surface ocean oxygenation. This relationship arises from the fact that iodine will readily substitute into the carbonate lattice during precipitation if it is present as the oxidized species iodate (IO_3^-) but will be wholly excluded in its reduced form iodide (I^-; 68). Hardisty et al. (2017) presented a record of iodine concentrations in carbonates spanning a large portion of Earth history and demonstrated that the mid-Proterozoic was a unique time in that iodine was present in most samples—but at very low levels. The only exception to this pattern is the Tieling Formation, which stands out as having values comparable to the Lomagundi interval of the Paleoproterozoic, roughly 2.2 to 2.0 Ga, and the Neoproterozoic, roughly 0.8 Ga—two intervals linked with increasing confidence to relatively high environmental O_2 compared to the mid-Proterozoic (Hardisty et al., 2014; 2017; Lu et al., 2017; Blättler et al., 2018).

A second event at ~1.1 Ga?

After ~1.4 Ga, the geochemical indicators that point to heightened oceanic O_2 concentrations return to ranges characteristic of the earlier mid-Proterozoic. There are,

however, suggestions of a second rise in oceanic-atmospheric O_2 at ~1.1 Ga, expressed in the isotopic composition of Cr in carbonates and a pronounced spike in Re concentrations of organic-rich shales (Figure 3.3; Gilleaudeau et al., 2016; Sheen et al., 2018).

As outlined above, the Cr-isotope paleoredox proxy relies on the recognition of isotopically fractionated Cr in sedimentary rocks, reflecting redox transformations in the subaerial weathering environment and during subsequent transport (e.g., Frei et al., 2014). This tool has been most widely applied to iron-rich chemical precipitates, like iron formations, and organic-rich shales (e.g., Frei et al., 2104; Planavsky et al., 2014; Cole et

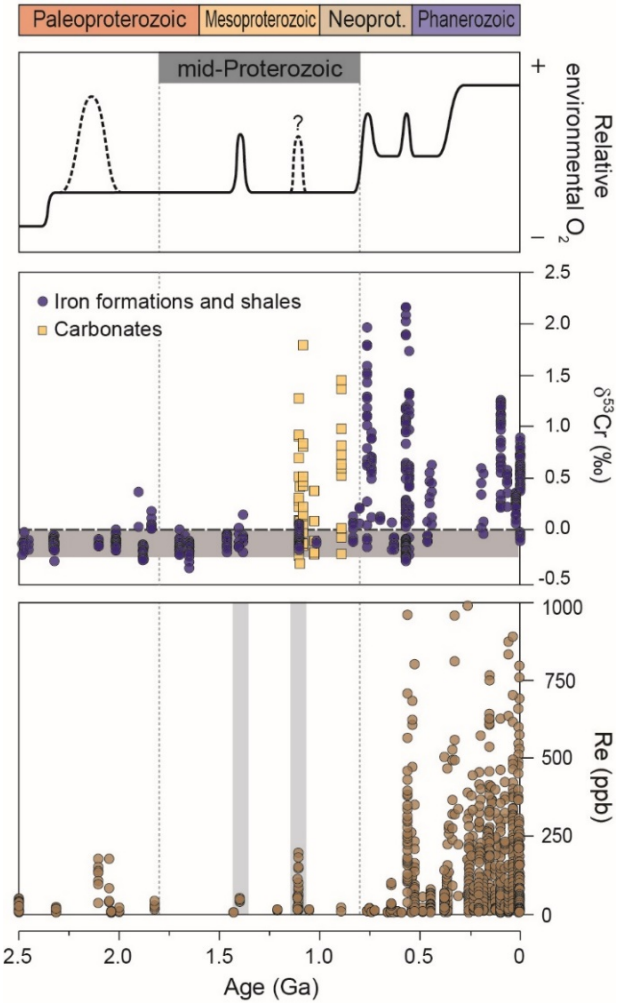

Figure 3. 3. Simplified history of environmental oxygenation through Proterozoic and Phanerozoic time with data supporting a possible second event at ~1.1 Ga. Top panel shows relative oceanic-atmospheric O_2 over the past 2.5 billion years (derived from many sources, see Sperling et al., 2015; Lyons et al., 2014; Canfield et al., 2008; Kump et al., 2008; Wallace et al., 2017 and refs. therein), dashed lines indicate less certain events (Lomagundi interval of the Paleoproterozoic and ~1.1 Ga event discussed here). Middle panel shows all available Proterozoic and Phanerozoic δ^{53}Cr data; blue circles show data from iron- and organic-rich marine sediments, orange squares show data from marine carbonates (compiled from data in Cole et al., 2016 and Gilleaudeau et al., 2016). Bottom panel shows rhenium concentration data from organic-rich marine shales (modified from Sheen et al., 2018).

al., 2016). The assumption that these marine sediments record the $\delta^{53}Cr$ value of overlying waters is grounded in the expectation that Cr reduction in such oxygen-lean systems should be rapid and complete, leading to no isotopic fractionation in the resultant reduced reservoir (Reinhard et al., 2014). Recent work has proposed that carbonate rocks may also serve as faithful recorders of oceanic $\delta^{53}Cr$ values (Gilleaudeau et al., 2106), although such applications of the proxy remain largely unexplored (e.g., with respect to the potential effects of post-depositional alteration). Oxidized Cr(VI) can substitute into the crystal lattice of carbonate minerals during precipitation. It has been shown, however, that Cr incorporated into both natural and experimentally grown carbonates can carry variable fractionations from surrounding waters, potentially resulting from partial Cr(VI) reduction through biological activity (Rodler et al., 2015; Pereira et al., 2016). Gilleaudeau et al. (2016) presented a record of $\delta^{53}Cr$ values from a suite of 1.1-0.9 Ga carbonates, identifying the presence of strongly fractionated values at ~1.1 and ~0.9 Ga (Figure 3.3). The presence of these two intervals of strong fractionation stand in contrast to the shale $\delta^{53}Cr$ record, which preserves significant fractionations only after ~0.8 Ga (Cole et al., 2016). At present, these are the only carbonate δ53Cr data available for the mid-Proterozoic. Given this, it is unclear whether the presence of fractionated Cr in carbonates is (1) a ubiquitous feature in the geological record, caused by factors intrinsic to the incorporation of Cr into the carbonate lattice or those contributing to the precipitation of the carbonate itself (i.e., biological interactions), or (2) if the data of Gilleaudeau et al. (2016) represent an event or transition in surface environmental redox conditions.

Few additional proxy data exist for the interval from ~1.4 to ~0.9 Ga, although the Re concentration dataset mentioned above does contain results that span this interval (Sheen et al., 2018). Interestingly, the most pronounced departure from the pattern of low mid-Proterozoic Re concentrations is in the ~1.1 Ga Tourist Formation of the El Mreiti Group, Mauritania (Sheen et al., 2018)—the same formation that was found to contain highly fractionated carbonate $\delta^{53}Cr$ values (Gilleaudeau et al., 2016). While these strong enrichments in Re have only been observed in one location at this time, the fact that $\delta^{53}Cr$ values and Re concentrations—two completely independent proxies—both point to heightened biospheric O_2 concentrations at this time is noteworthy. The Re data, however, return to near crustal values after ~1.1 Ga, and strong enrichments are not observed again until the late Ediacaran (Sheen et al., 2018). This relationship suggests that if a genuine oxygenation event did occur at ~1.1 Ga, it was likely transient.

While transient oxygenation at ~1.1 Ga is a tantalizing possibility, the available data are far less convincing than the collective evidence for the ~1.4 Ga event. Further, the strong Re enrichments at ~1.1 Ga, if taken at face value, would suggest a surprisingly high level of mid-Proterozoic oxygenation given the ease with which Re is depleted otherwise. We include 1.1 Ga in the discussion, however, because we lack an alternative explanation for the intriguing Re results. Further, our intent is to stimulate an ongoing conversation (e.g., Mukherjee and Large, 2016) about dynamic biospheric redox during the mid-Proterozoic and by summarizing the admittedly tenuous state of the art, catalyze additional research.

Implications for evolving eukaryotic life

The combined records of $\delta^{53}Cr$ values from marine shales (Cole et al., 2016) and mass-independent fractionation of sulfur isotopes (Reinhard et al., 2013) reveal a long mid-Proterozoic period of mostly intermediate but still low pO_2 values in the ocean-atmosphere system. Multiple lines of geochemical evidence suggesting higher oceanic O_2 at specific times within the mid-Proterozoic, however, point to the possibility of at least two instances during which environmental O_2 concentrations transiently rose beyond this range. Intriguingly, ~1.4 and ~1.1 Ga coincide roughly with important chapters in the histories of two pre-Pangea supercontinents—specifically the breakup of Nuna and the formation of Rodinia, respectively (Hanson et al., 2004; Ernst et al., 2008; Li et al., 2008; Zhang et al., 2009; Evans and Mitchell, 2011). During supercontinent breakup, related activity in large igneous province can supply voluminous basalt to Earth's surface, which can in turn weather rapidly to deliver abundant phosphorous to the oceans, stimulating productivity and subsequent organic carbon burial (e.g., Horton, 2015). At the same time, rift basins along the new continental margins become important loci for burial of sediment and associated organic matter. Similarly, uplift of large mountain ranges during continent-continent collisions and associated delivery of nutrients and sediment to shelf systems can stimulate organic carbon burial and net O_2 accumulation (Des Maris 1994; Campbell and Allen, 2008).

The recognition of dynamic fluctuations in mid-Proterozoic oceanic redox conditions raises critical questions about possible relationships to biotic evolution. Specifically, if long-term average mid-Proterozoic conditions, dominated by low O_2, acted

mostly to inhibit the ultimate emergence of Metazoa, what consequences might transient oxygenation have had? Despite indications for changing biospheric redox conditions throughout the Proterozoic, it is extremely challenging to extrapolate these data to quantitative estimates of surface-ocean O_2, although iodine data from the ~1.4 Ga Tieling Formation (Hardisty et al., 2017) point to at least locally oxygenated surface waters at that time. In addition to the proxy data discussed above, another recent study of the Xiamaling Formation used a carbon export and oxidation model to estimate atmospheric pO_2 based on the total organic carbon contents of the rocks, though several of the assumptions made in the model have been subsequently challenged in the literature (Zhang et al 2016; c.f., Planavsky et al., 2016 and Diamond et al., 2018)

It is clear from the geochemical records summarized here that the purported oxygenation events at ~1.4 and ~1.1 Ga were qualitatively different than changes observed later in the Neoproterozoic (e.g., Scott et al., 2008; Partin et al., 2013; Hardisty et al., 2017; Sheen et al., 2018; Kendall et al., 2015; Chen et al., 2015; Lu et al., 2010). Many of the same geochemical proxies have been used to propose redox fluctuations in the Neoproterozoic, and the magnitude of the chemical responses at that time were significantly larger, suggesting more intense expansions of oxygenated conditions. This contrast, however, does not necessarily mean that the transient oxygenation events in the mid-Proterozoic had a negligible effect on the evolutionary trajectory of eukaryotes—on the contrary. Perhaps it is not a coincidence that both size and diversity of eukaryotic microfossils in the Proterozoic succession of the North China craton reach a maximum in the Wumishan Formation, just below the Tieling Formation (Shi et al., 2014). Further,

many authors have attributed the first occurrence of crown group eukaryotes to the fossil Bangiomorpha pubescens found in the Hunting and Angmaat formations of Arctic Canada (Butterfield et al., 2000; Knoll et al., 2013), the age of which has recently been updated to ~1.05 Ga (Gibson et al., 2017).

As more geochemical data become available, the picture of system-scale redox fluctuations throughout Earth's history is emerging. All indications suggest a mid-Proterozoic world with low long-term average pO_2, though dynamic fluctuations may have been prominent feature. The proxy data indicate that these fluctuations became larger and more frequent during the Neoproterozoic, potentially accompanied by incremental increases in baseline pO_2, and eventually resulted in shelfal habitats that were stably oxygenated on longer timescales (Scott et al., 2008; Partin et al., 2013; Hardisty et al., 2017; Sheen et al., 2018). Nonetheless, specific questions about the relationship between these environmental changes and metazoan evolution remain open, and while the scope of the remaining challenges is great, the increasing resolution of geochemical and paleontological records coupled with the increasing sophistication of biogeochemical modeling is paving a path forward.

References:

Algeo, T. J., & Lyons, T. W. (2006). Mo–total organic carbon covariation in modern anoxic marine environments: Implications for analysis of paleoredox and paleohydrographic conditions. Paleoceanography, 21(1).

Andersen, M. B., Romaniello, S., Vance, D., Little, S. H., Herdman, R., & Lyons, T. W. (2014). A modern framework for the interpretation of 238U/235U in studies of ancient ocean redox. Earth and Planetary Science Letters, 400, 184-194.

Arnold, G. L., Anbar, A. D., Barling, J., & Lyons, T. W. (2004). Molybdenum isotope evidence for widespread anoxia in mid-Proterozoic oceans. Science, 304(5667), 87-90.

Barling, J., Arnold, G. L., & Anbar, A. D. (2001). Natural mass-dependent variations in the isotopic composition of molybdenum. Earth and Planetary Science Letters, 193(3-4), 447-457.

Barling, J., & Anbar, A. D. (2004). Molybdenum isotope fractionation during adsorption by manganese oxides. Earth and Planetary Science Letters, 217(3-4), 315-329.

Bertine, K. K., & Turekian, K. K. (1973). Molybdenum in marine deposits. Geochimica et Cosmochimica Acta, 37(6), 1415-1434.

Blättler, C. L., Claire, M. W., Prave, A. R., Kirsimäe, K., Higgins, J. A., Medvedev, P. V., et al. (2018). Two-billion-year-old evaporites capture Earth's great oxidation. Science, 360(6386), 320-323.

Brocks, J. J., Jarrett, A. J., Sirantoine, E., Hallmann, C., Hoshino, Y., & Liyanage, T. (2017). The rise of algae in Cryogenian oceans and the emergence of animals. Nature, 548(7669), 578.

Shi, M., Feng, Q., & Zhu, S. (2014). Biotic evolution and its relation with geological events in the Proterozoic Yanshan Basin, North China. Science China Earth Sciences, 57(5), 903-918.

Butterfield, N. J. (2000). Bangiomorpha pubescens n. gen., n. sp.: implications for the evolution of sex, multicellularity, and the Mesoproterozoic/Neoproterozoic radiation of eukaryotes. Paleobiology, 26(3), 386-404.

Butterfield, N. J. (2009). Oxygen, animals and oceanic ventilation: an alternative view. Geobiology, 7(1), 1-7.

Butterfield, N. J. (2018). Oxygen, animals and aquatic bioturbation: An updated account. Geobiology, 16(1), 3-16.

Campbell, I. H., & Allen, C. M. (2008). Formation of supercontinents linked to increases in atmospheric oxygen. Nature Geoscience, 1(8), 554.

Canfield, D. E., Poulton, S. W., Knoll, A. H., Narbonne, G. M., Ross, G., Goldberg, T., & Strauss, H. (2008). Ferruginous conditions dominated later Neoproterozoic deep-water chemistry. Science, 321(5891), 949-952.

Catling, D. C., Glein, C. R., Zahnle, K. J., & McKay, C. P. (2005). Why O_2 Is Required by Complex Life on Habitable Planets and the Concept of Planetary" Oxygenation Time". Astrobiology, 5(3), 415-438.

Chen, X., Ling, H. F., Vance, D., Shields-Zhou, G. A., Zhu, M., Poulton, S. W., et al. (2015). Rise to modern levels of ocean oxygenation coincided with the Cambrian radiation of animals. Nature Communications, 6, 7142.

Cole, D. B., Reinhard, C. T., Wang, X., Gueguen, B., Halverson, G. P., Gibson, T., et al. (2016). A shale-hosted Cr isotope record of low atmospheric oxygen during the Proterozoic. Geology, 44(7), 555-558.

Cox, G. M., Jarrett, A., Edwards, D., Crockford, P. W., Halverson, G. P., Collins, A. S., et al. (2016). Basin redox and primary productivity within the Mesoproterozoic Roper Seaway. Chemical Geology, 440, 101-114.

Crowe, S. A., Døssing, L. N., Beukes, N. J., Bau, M., Kruger, S. J., Frei, R., & Canfield, D. E. (2013). Atmospheric oxygenation three billion years ago. Nature, 501(7468), 535.

Crusius, J., Calvert, S., Pedersen, T., & Sage, D. (1996). Rhenium and molybdenum enrichments in sediments as indicators of oxic, suboxic and sulfidic conditions of deposition. Earth and Planetary Science Letters, 145(1-4), 65-78.

Diamond, C. W., Planavsky, N. J., Wang, C., & Lyons, T. W. (2018). What the~ 1.4 Ga Xiamaling Formation can and cannot tell us about the mid-Proterozoic ocean. Geobiology.

Des Marais, D. J. (1994). Tectonic control of the crustal organic carbon reservoir during the Precambrian. Chemical Geology, 114(3-4), 303-314.

Dunk, R. M., Mills, R. A., & Jenkins, W. J. (2002). A reevaluation of the oceanic uranium budget for the Holocene. Chemical Geology, 190(1-4), 45-67.

Eary, L. E., & Rai, D. (1987). Kinetics of chromium (III) oxidation to chromium (VI) by reaction with manganese dioxide. Environmental Science & Technology, 21(12), 1187-1193.

Erickson, B. E., & Helz, G. R. (2000). Molybdenum (VI) speciation in sulfidic waters:: stability and lability of thiomolybdates. Geochimica et Cosmochimica Acta, 64(7), 1149-1158.

Ernst, R. E., Wingate, M. T. D., Buchan, K. L., & Li, Z. X. (2008). Global record of 1600–700 Ma Large Igneous Provinces (LIPs): implications for the reconstruction of the proposed Nuna (Columbia) and Rodinia supercontinents. Precambrian Research, 160(1-2), 159-178.

Evans, D. A., & Mitchell, R. N. (2011). Assembly and breakup of the core of Paleoproterozoic–Mesoproterozoic supercontinent Nuna. Geology, 39(5), 443-446.

Farquhar, J., Bao, H., & Thiemens, M. (2000). Atmospheric influence of Earth's earliest sulfur cycle. Science, 289(5480), 756-758.

Frei, R., Gaucher, C., Poulton, S. W., & Canfield, D. E. (2009). Fluctuations in Precambrian atmospheric oxygenation recorded by chromium isotopes. Nature, 461(7261), 250.

Gibson, T. M., Shih, P. M., Cumming, V. M., Fischer, W. W., Crockford, P. W., Hodgskiss, M. S., et al. (2017). Precise age of Bangiomorpha pubescens dates the origin of eukaryotic photosynthesis. Geology.

Gilleaudeau, G. J., Frei, R., Kaufman, A. J., Kah, L. C., Azmy, K., Bartley, J. K., et al. (2016). Oxygenation of the mid-Proterozoic atmosphere: clues from chromium isotopes in carbonates.

Hanson, R. E., Crowley, J. L., Bowring, S. A., Ramezani, J., Gose, W. A., Dalziel, I. W., et al. (2004). Coeval large-scale magmatism in the Kalahari and Laurentian cratons during Rodinia assembly. Science, 304(5674), 1126-1129.

Hardisty, D. S., Lu, Z., Planavsky, N. J., Bekker, A., Philippot, P., Zhou, X., & Lyons, T. W. (2014). An iodine record of Paleoproterozoic surface ocean oxygenation. Geology, 42(7), 619-622.

Hardisty, D. S., Lu, Z., Bekker, A., Diamond, C. W., Gill, B. C., Jiang, G., et al. (2017). Perspectives on Proterozoic surface ocean redox from iodine contents in ancient and recent carbonate. Earth and Planetary Science Letters, 463, 159-170.

Helz, G. R., Miller, C. V., Charnock, J. M., Mosselmans, J. F. W., Pattrick, R. A. D., Garner, C. D., & Vaughan, D. J. (1996). Mechanism of molybdenum removal from the sea and its concentration in black shales: EXAFS evidence. Geochimica et Cosmochimica Acta, 60(19), 3631-3642.

Helz, G. R., Bura-Nakić, E., Mikac, N., & Ciglenečki, I. (2011). New model for molybdenum behavior in euxinic waters. Chemical Geology, 284(3-4), 323-332.

Horton, F. (2015). Did phosphorus derived from the weathering of large igneous provinces fertilize the Neoproterozoic ocean?. Geochemistry, Geophysics, Geosystems, 16(6), 1723-1738.

Kashiwabara, T., Takahashi, Y., & Tanimizu, M. (2009). A XAFS study on the mechanism of isotopic fractionation of molybdenum during its adsorption on ferromanganese oxides. Geochemical Journal, 43(6), e31-e36.

Kendall, B., Creaser, R. A., Gordon, G. W., & Anbar, A. D. (2009). Re–Os and Mo isotope systematics of black shales from the Middle Proterozoic Velkerri and Wollogorang formations, McArthur Basin, northern Australia. Geochimica et Cosmochimica Acta, 73(9), 2534-2558.

Kendall, B., Komiya, T., Lyons, T. W., Bates, S. M., Gordon, G. W., Romaniello, S. J., et al. (2015). Uranium and molybdenum isotope evidence for an episode of widespread ocean oxygenation during the late Ediacaran Period. Geochimica et Cosmochimica Acta, 156, 173-193.

Knoll, A. H., Wörndle, S., & Kah, L. C. (2013). Covariance of microfossil assemblages and microbialite textures across an upper Mesoproterozoic carbonate platform. Palaios, 28(7), 453-470.

Kotaś, J., & Stasicka, Z. (2000). Chromium occurrence in the environment and methods of its speciation. Environmental pollution, 107(3), 263-283.

Kump, L. R. (2008). The rise of atmospheric oxygen. Nature, 451(7176), 277.

Levin, L. A., & Gage, J. D. (1998). Relationships between oxygen, organic matter and the diversity of bathyal macrofauna. Deep Sea Research Part II: Topical Studies in Oceanography, 45(1-3), 129-163.

Levin, L. A. (2003). Oxygen minimum zone benthos: adaptation and community response to hypoxia. Oceanography and Marine Biology: An Annual Review.

Liu, X. M., Kah, L. C., Knoll, A. H., Cui, H., Kaufman, A. J., Shahar, A., & Hazen, R. M. (2015). Tracing Earth's O_2 evolution using Zn/Fe ratios in marine carbonates.

Love, G. D., Grosjean, E., Stalvies, C., Fike, D. A., Grotzinger, J. P., Bradley, A. S., et al. (2009). Fossil steroids record the appearance of Demospongiae during the Cryogenian period. Nature, 457(7230), 718.

Love, G. D., & Summons, R. E. (2015). The molecular record of Cryogenian sponges–a response to Antcliffe (2013). Palaeontology, 58(6), 1131-1136.

Li, Z. X., Bogdanova, S. V., Collins, A. S., Davidson, A., De Waele, B., Ernst, R. E., et al. (2008). Assembly, configuration, and break-up history of Rodinia: a synthesis. Precambrian research, 160(1-2), 179-210.

Lu, Z., Jenkyns, H. C., & Rickaby, R. E. (2010). Iodine to calcium ratios in marine carbonate as a paleo-redox proxy during oceanic anoxic events. Geology, 38(12), 1107-1110.

Lu, W., Wörndle, S., Halverson, G. P., Zhou, X., Bekker, A., Rainbird, R. H., et al. (2017). Iodine proxy evidence for increased ocean oxygenation during the Bitter Springs Anomaly.

Luo, G., Ono, S., Beukes, N. J., Wang, D. T., Xie, S., & Summons, R. E. (2016). Rapid oxygenation of Earth's atmosphere 2.33 billion years ago. Science advances, 2(5), e1600134.

Lyons, T. W., Reinhard, C. T., & Planavsky, N. J. (2014). The rise of oxygen in Earth's early ocean and atmosphere. Nature, 506(7488), 307.

Mills, D. B., & Canfield, D. E. (2014). Oxygen and animal evolution: Did a rise of atmospheric oxygen "trigger" the origin of animals?. BioEssays, 36(12), 1145-1155.

Montoya-Pino, C., Weyer, S., Anbar, A. D., Pross, J., Oschmann, W., van de Schootbrugge, B., & Arz, H. W. (2010). Global enhancement of ocean anoxia during Oceanic Anoxic Event 2: A quantitative approach using U isotopes. Geology, 38(4), 315-318.

Morford, J. L., & Emerson, S. (1999). The geochemistry of redox sensitive trace metals in sediments. Geochimica et Cosmochimica Acta, 63(11-12), 1735-1750.

Mukherjee, I., & Large, R. R. (2016). Pyrite trace element chemistry of the Velkerri Formation, Roper Group, McArthur Basin: Evidence for atmospheric oxygenation during the Boring Billion. Precambrian Research, 281, 13-26.

Nägler, T. F., Neubert, N., Böttcher, M. E., Dellwig, O., & Schnetger, B. (2011). Molybdenum isotope fractionation in pelagic euxinia: evidence from the modern Black and Baltic Seas. Chemical Geology, 289(1-2), 1-11.

Nursall, J. R. (1959). Oxygen as a prerequisite to the origin of the Metazoa. Nature, 183(4669), 1170.

Och, L. M., & Shields-Zhou, G. A. (2012). The Neoproterozoic oxygenation event: Environmental perturbations and biogeochemical cycling. Earth-Science Reviews, 110(1-4), 26-57.

Partin, C. A., Bekker, A., Planavsky, N. J., Scott, C. T., Gill, B. C., Li, C., et al. (2013). Large-scale fluctuations in Precambrian atmospheric and oceanic oxygen levels from the record of U in shales. Earth and Planetary Science Letters, 369, 284-293.

Pavlov, A. A., & Kasting, J. F. (2002). Mass-independent fractionation of sulfur isotopes in Archean sediments: strong evidence for an anoxic Archean atmosphere. Astrobiology, 2(1), 27-41.

Pereira, N. S., Vögelin, A. R., Paulukat, C., Sial, A. N., Ferreira, V. P., & Frei, R. (2016). Chromium-isotope signatures in scleractinian corals from the Rocas Atoll, Tropical South Atlantic. Geobiology, 14(1), 54-67.

Planavsky, N. J., Reinhard, C. T., Wang, X., Thomson, D., McGoldrick, P., Rainbird, R. H., et al. (2014). Low Mid-Proterozoic atmospheric oxygen levels and the delayed rise of animals. Science, 346(6209), 635-638.

Planavsky, N. J., Cole, D. B., Reinhard, C. T., Diamond, C., Love, G. D., Luo, G., et al. (2016). No evidence for high atmospheric oxygen levels 1,400 million years ago. Proceedings of the National Academy of Sciences, 113(19), E2550-E2551.

Poulson Brucker, R. L., McManus, J., Severmann, S., & Berelson, W. M. (2009). Molybdenum behavior during early diagenesis: Insights from Mo isotopes. Geochemistry, Geophysics, Geosystems, 10(6).

Reinhard, C. T., Planavsky, N. J., Robbins, L. J., Partin, C. A., Gill, B. C., Lalonde, S. V., et al. (2013a). Proterozoic ocean redox and biogeochemical stasis. Proceedings of the National Academy of Sciences, 110(14), 5357-5362.

Reinhard, C. T., Planavsky, N. J., & Lyons, T. W. (2013b). Long-term sedimentary recycling of rare sulphur isotope anomalies. Nature, 497(7447), 100.

Reinhard, C. T., Planavsky, N. J., Wang, X., Fischer, W. W., Johnson, T. M., & Lyons, T. W. (2014). The isotopic composition of authigenic chromium in anoxic marine sediments: A case study from the Cariaco Basin. Earth and Planetary Science Letters, 407, 9-18.

Reinhard, C. T., Planavsky, N. J., Olson, S. L., Lyons, T. W., & Erwin, D. H. (2016). Earth's oxygen cycle and the evolution of animal life. Proceedings of the National Academy of Sciences, 113(32), 8933-8938.

Reinhard, C. T., Planavsky, N. J., Gill, B. C., Ozaki, K., Robbins, L. J., Lyons, T. W., et al. (2017). Evolution of the global phosphorus cycle. Nature, 541(7637), 386.

Rodler, A., Sánchez-Pastor, N., Fernández-Díaz, L., & Frei, R. (2015). Fractionation behavior of chromium isotopes during coprecipitation with calcium carbonate: implications for their use as paleoclimatic proxy. Geochimica et Cosmochimica Acta, 164, 221-235.

Scott, C., Lyons, T. W., Bekker, A., Shen, Y. A., Poulton, S. W., Chu, X. L., & Anbar, A. D. (2008). Tracing the stepwise oxygenation of the Proterozoic ocean. Nature, 452(7186), 456.

Scott, C., & Lyons, T. W. (2012). Contrasting molybdenum cycling and isotopic properties in euxinic versus non-euxinic sediments and sedimentary rocks: Refining the paleoproxies. Chemical Geology, 324, 19-27.

Sheen, A. I., Kendall, B., Reinhard, C. T., Creaser, R. A., Lyons, T. W., Bekker, A., et al. (2018). A model for the oceanic mass balance of rhenium and implications for the extent of Proterozoic ocean anoxia. Geochimica et Cosmochimica Acta, 227, 75-95.

Shi, M., Feng, Q., & Zhu, S. (2014). Biotic evolution and its relation with geological events in the Proterozoic Yanshan Basin, North China. Science China Earth Sciences, 57(5), 903-918.

Siebert, C., Nägler, T. F., von Blanckenburg, F., & Kramers, J. D. (2003). Molybdenum isotope records as a potential new proxy for paleoceanography. Earth and Planetary Science Letters, 211(1-2), 159-171.

Sperling, E. A., Frieder, C. A., Raman, A. V., Girguis, P. R., Levin, L. A., & Knoll, A. H. (2013). Oxygen, ecology, and the Cambrian radiation of animals. Proceedings of the National Academy of Sciences, 110(33), 13446-13451.

Sperling, E. A., Wolock, C. J., Morgan, A. S., Gill, B. C., Kunzmann, M., Halverson, G. P., et al. (2015). Statistical analysis of iron geochemical data suggests limited late Proterozoic oxygenation. Nature, 523(7561), 451.

Summons, R. E., Bradley, A. S., Jahnke, L. L., & Waldbauer, J. R. (2006). Steroids, triterpenoids and molecular oxygen. Philosophical Transactions of the Royal Society B: Biological Sciences, 361(1470), 951-968.

Towe, K. M. (1970). Oxygen-collagen priority and the early metazoan fossil record. Proceedings of the National Academy of Sciences, 65(4), 781-788.

Tribovillard, N., Riboulleau, A., Lyons, T., & Baudin, F. (2004). Enhanced trapping of molybdenum by sulfurized marine organic matter of marine origin in Mesozoic limestones and shales. Chemical Geology, 213(4), 385-401.

Vorlicek, T. P., Kahn, M. D., Kasuya, Y., & Helz, G. R. (2004). Capture of molybdenum in pyrite-forming sediments: role of ligand-induced reduction by polysulfides 1. Geochimica et Cosmochimica Acta, 68(3), 547-556.

Waldbauer, J. R., Newman, D. K., & Summons, R. E. (2011). Microaerobic steroid biosynthesis and the molecular fossil record of Archean life. Proceedings of the National Academy of Sciences, 108(33), 13409-13414.

Wallace, M. W., Shuster, A., Greig, A., Planavsky, N. J., & Reed, C. P. (2017). Oxygenation history of the Neoproterozoic to early Phanerozoic and the rise of land plants. Earth and Planetary Science Letters, 466, 12-19.

Weyer, S., Anbar, A. D., Gerdes, A., Gordon, G. W., Algeo, T. J., & Boyle, E. A. (2008). Natural fractionation of 238U/235U. Geochimica et Cosmochimica Acta, 72(2), 345-359.

Yang, S., Kendall, B., Lu, X., Zhang, F., & Zheng, W. (2017). Uranium isotope compositions of mid-Proterozoic black shales: Evidence for an episode of increased ocean oxygenation at 1.36 Ga and evaluation of the effect of post-depositional hydrothermal fluid flow. Precambrian Research, 298, 187-201.

Zhang, S. H., Zhao, Y., Yang, Z. Y., He, Z. F., & Wu, H. (2009). The 1.35 Ga diabase sills from the northern North China Craton: implications for breakup of the Columbia (Nuna) supercontinent. Earth and Planetary Science Letters, 288(3-4), 588-600.

Zhang, S., Wang, X., Wang, H., Bjerrum, C. J., Hammarlund, E. U., Costa, M. M., et al. (2016). Sufficient oxygen for animal respiration 1,400 million years ago. Proceedings of the National Academy of Sciences, 113(7), 1731-1736.

Zink, S., Schoenberg, R., & Staubwasser, M. (2010). Isotopic fractionation and reaction kinetics between Cr (III) and Cr (VI) in aqueous media. Geochimica et Cosmochimica Acta, 74(20), 5729-5745.

Chapter 4

On the application of paleoredox proxies: a case study from the Xiamaling Formation

Preface:

No part of this chapter has been published in any form and solely reflects the views and opinions of myself, Charles Diamond.

Forward

As is briefly outlined in Chapter 1, the group of authors led by Don Canfield and Shuichang Zhang published a paper in direct response to the publication of Chapter 2 (Zhang et al., 2019, *Geobiology*). At the time Zhang et al., 2019 was published, it was the eighth paper on the Xiamaling Formation that these authors had published, five of them were related to atmospheric oxygen. Now, while I would rather not get too personal here, I feel like this bears exploring for a moment. As an early graduate student, just beginning to understand the depth of my task, I embarked on a project. By the time I published my first paper, a competing group had already published five papers on the same rocks, two of which were in *PNAS*, one in *AJS*, and all of which disagreed completely with what we were claiming. As if this were not dismal enough already, the group responded to our paper with one of their own, a point-by-point deconstruction of our argument as presented.

It is worth mentioning for anyone that is not aware, Don Canfield is not only a Fellow of the National Academy of Sciences, but he is also on the editorial board of *PNAS*.

To say he is an icon in our field would be putting it lightly—he literally wrote a pop-culture book about its history titled *Oxygen*. The lead author on much of this group's work is Shuichang Zhang, a senior professor of petroleum geochemistry at the Research Institute of Petroleum Exploration and Development, China National Petroleum Corporation. This is by no means a team of underachievers.

What follows in this chapter is a response to Zhang et al., 2019. It contains a deconstruction of all relevant arguments that had been made by Zhang and colleagues at the time that I wrote it. Since then, they have published multiple additional times on this and closely related subjects. While there have been others, their most recent contributions reported abundant biomarkers made by eukaryotic algae and purple sulfur bacteria in the Xiamaling Formation. These results are in direct conflict with both the work of Genming Luo and colleagues (2015) and with published and unpublished results from Gordon Love's lab group. Interestingly, significant debate surrounded much older rocks containing similar biomarkers. In that case, these molecules likely came from contamination by the drilling fluid used to extract the cores. It turns out these molecules are common in oils from much younger sources. Perhaps they should check for oleanane.

It has been stated above, but I will say it again here. This is my writing, and it reflects my thinking. This debate has been both a source of strife and motivation over the years. Had it not been there, I would not have thought as deeply about these things, and for that I am grateful. I will say, though, I am glad the graduate student involved in this saga was me. It was far from easy, intellectually or emotionally, but I've been through worse.

Introduction

Over the past several decades, an enormous body of geochemical proxy data has amassed that speaks to the changing landscape of oceanic and atmospheric redox conditions throughout Earth history (reviewed by Lyons et al., 2014, though significant work has continued since). These proxies vary widely in their applicability, but all are grounded in an understanding of modern biogeochemical cycling and sedimentary geochemistry. Some of these data are unambiguous and their interpretations are widely agreed upon—the record of mass-independent-fractionation of sulfur isotopes for example (reviewed by Johnston, 2011). Many other proxies, though, are less clear cut, and an unequivocal interpretation requires the constraint of multiple other local or global factors (the iron-speciation proxy for instance, reviewed recently by Raiswell et al., 2018). Nevertheless, most datasets support a timeline of progressive oxygenation of surface environments, beginning with a strongly reducing Archean ocean-atmosphere system and ending with O_2 levels that resemble the modern for at least the latter half of the Phanerozoic. The intervening Proterozoic and early Paleozoic likely harbored conditions that exist somewhere in between, which at times could have been quite dynamic.

This first order view is by no means new (e.g., Garrels et al., 1973) and seems to be shared by most workers in the field. Mapping out the nuances of Proterozoic redox change, however, has been a topic of considerable interest among geobiologists, and there has not always been a consensus view. This is not surprising as the implications of rising global O_2 are far-reaching and the Proterozoic rock record can be painfully sparse. There are vast stretches of time for which very few data exist, underscoring the importance of

each formation that has been preserved. The ~1.4 billion-year-old Xiamaling Formation of the North China Craton is one such formation that has received substantial recent attention (e.g., Luo et al., 2015; Zhang et al., 2016; Wang et al., 2017; Zhang et al., 2018; Wang et al., 2018; Diamond et al., 2018). Interestingly, while multiple research groups have been exploring the records preserved in the Xiamaling Formation and have produced suites of geochemical data that are very consistent with one another, they have arrived at different interpretations of these data (partially addressed in Zhang et al., 2019). It is my intention here to explore some of the arguments that underpin these interpretations and highlight forks in the road that have led these groups to different conclusions.

Background

The Xiamaling Formation was deposited unconformably on top of a multiple km thick sequence of Paleo- to Mesoproterozoic rocks (e.g., Qu et al., 2014). The underlying strata have been interpreted to record the rifting of the craton from the supercontinent Nuna and subsequent establishment of a long-lived passive margin (Meng et al., 2011). A stromatolitic shallow-water carbonate, the Tieling Formation, directly underlies the Xiamaling Formation. In many locations within the Xiamaling depositional basin, the upper contact of the Tieling is characterized by a thick weathering rind, evidence of an extended period of subaerial exposure before sediments of the Xiamaling began to accumulate (Qu et al., 2014).

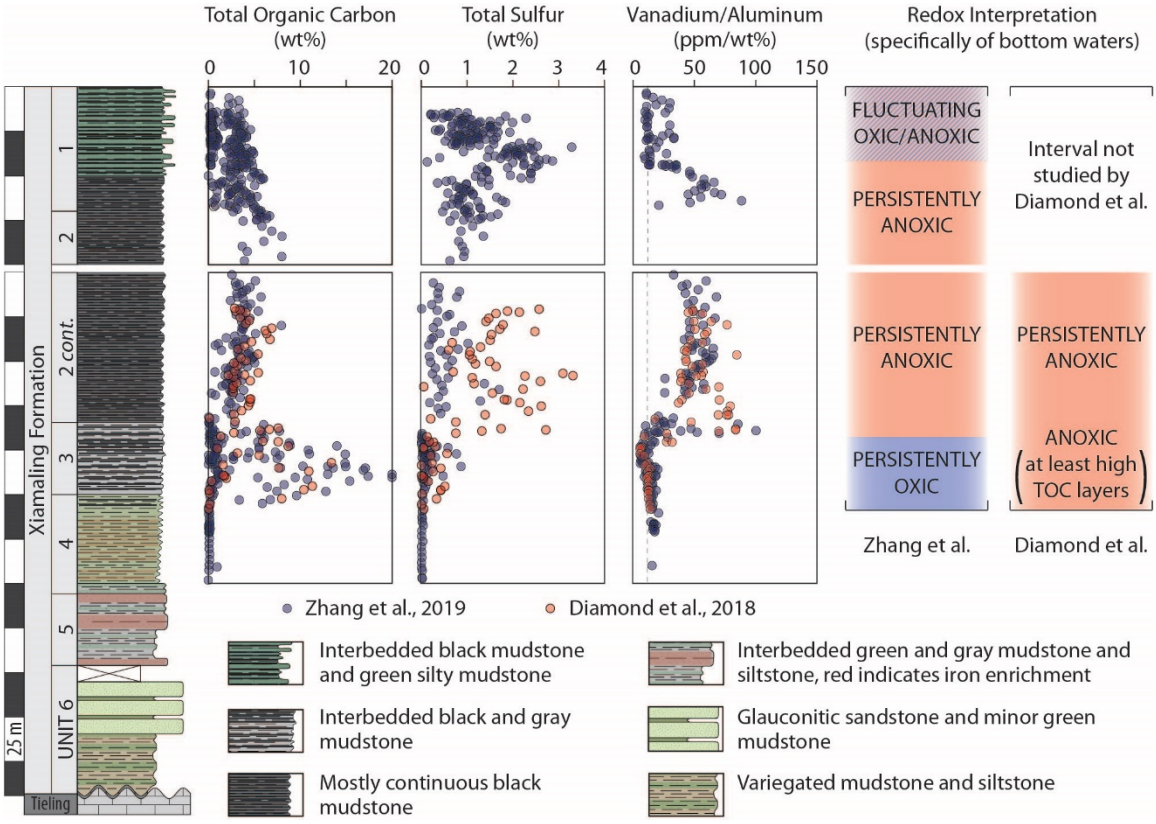

Figure 4.1. Comparison of data from Diamond et al., 2018 (orange circles) and Zhang et al., 2019 (blue circles). From left to right, these panels show weight percent total organic carbon (TOC), total sulfur, and the relative ratio of vanadium and aluminum concentrations The stratigraphy of the Xiamaling Formation is schematically represented to the left, to scale and as it correlates to the data as plotted (note scale break in unit 2). Redox interpretations from each author group are represented to the right as they appear stratigraphically.

The lower Xiamaling Fm. is characterized by coarse clastics that can be extremely enriched in iron and aluminum in places, which fine upward into interbedded green and red mudstones (Figure 4.1; Qu et al., 2014; Wang et al., 2017). Above this is a ~50 m interval of cm-scale interbedded black and gray shales, where black layers can have total organic carbon (TOC) contents as high as 20 wt% (Figure 4.1; Zhang et al., 2016; Diamond et al., 2018). Continuing upward, this interval grades into ~200 m of mostly continuous black shale with considerably lower TOC (~2-6 wt%; Wang et al., 2017; Diamond et al.,

2018). The uppermost ~50 m of the formation is characterized by a return to cm-scale interbedded black and gray shales, where dark layers continue to contain 2-6 wt% TOC and gray layers are TOC lean (<0.5 wt%; Wang et al., 2017; Zhang et al., 2017).

These three upper units have been informally divided based on this general pattern, and for consistency I will refer to them in the parlance of Zhang and colleagues, unit 1 being the uppermost, and units 2 and 3 underlying this in ascending order (Figure 4.1). Given that these three units contain significant organic-rich shale, they could be amenable to many traditionally used geochemical redox proxies (e.g., redox-sensitive trace metal concentrations and isotope systems).

Interpretations from Zhang and colleagues

Units 2 and 3

In 2016, Zhang et al. (*PNAS*) presented a combined inorganic and organic geochemical dataset from units 2 and 3 of the Xiamaling Formation. In this contribution, the authors argued that unit 3 was deposited in persistently oxic conditions that existed beneath an overlying oxygen-minimum-zone (OMZ), which was rich in hydrogen sulfide (H_2S^-). The interpretation that the sediments of unit 3 were deposited in persistently oxic conditions, despite containing up to 20 wt% TOC, was based on the distribution of redox-sensitive trace metals, specifically the concentrations of molybdenum, vanadium, and uranium (Mo, V, and U respectively; Zhang et al, 2016). In a first order sense, these metals are highly soluble in oxygenated waters but become insoluble or particle reactive under anoxic conditions (reviewed in Tribovillard et al., 2006; Mo requires the presence of H¬2S

to achieve strong particle reactivity). In typical marine waters, this redox sensitivity results in sedimentary enrichments when overlying waters are anoxic or sulfidic. Following from this, Zhang and colleagues interpreted small enrichments in Mo and U concentration coupled with a lack of V enrichment in unit 3 as reflecting deposition in oxic conditions (Figure 4.1). Unit 2, on the other hand, contains significant enrichments in all three metals, and while not explicitly addressed by Zhang et al. (2016), subsequent work from these authors interprets unit 2 to have been deposited in persistently anoxic conditions.

Interpretation that the oxic depositional environment of unit 3 existed beneath a sulfidic OMZ was based on the presence of 2,3,6-trimethyl aryl isoprenoid biomarkers (Zhang et al., 2016). These compounds are diagenetic breakdown products of carotenoid pigments associated with green sulfur bacteria, obligate anaerobic phototrophs that use sunlight to photo-oxidize H_2S^-. This observation requires that portions of the photic zone were anoxic during deposition. Thus, together with the observed Mo, U, and V concentrations, the authors posited that the water column contained a shallow OMZ with oxic waters beneath. The authors sought to bolster this interpretation through comparison to trace metal enrichment patterns within and beneath modern OMZs.

Zhang et al. (2016) went on to construct a carbon export and oxidation model that extrapolates atmospheric O_2 from a calculation of water column O_2 consumption during settling and deposition of organic matter. The model assumes that water at depth is sourced from the surface (where it is in equilibrium with the atmosphere) via transport along isopycnal surfaces, with a range of residence times calibrated by modern observations. Given these assumptions, the model calculates the duration over which the waters would

be exposed to settling organic matter, and with a prescribed remineralization rate, it then calculates the minimum surface water O_2 concentration required for the water to remain oxic despite O_2 consumption through respiration. Model outputs were calculated for particular sedimentary TOC concentrations (15 wt% in the main text), and independent variables only include new production and settling velocity. Using organic matter reactivity based on modern low latitude observations and the range of water residence times that the authors considered reasonable, they estimate a range of minimum atmospheric O_2 concentrations between 4% and greater than 100% of present levels (Zhang et al., 2016).

Somewhat counterintuitively, as new biological production increases in the model, the minimum atmospheric O_2 level required to keep bottom waters oxygenated actually decreases. This result means that the lowest modeled atmospheric O_2 occurs when new production and settling velocity are highest. This result runs counter to the general assumption that higher export production and settling velocity would place a higher respiratory demand on deep waters and therefore require higher O_2 to maintain oxic conditions. If I understand the model correctly, this result stems from the depositional water depth being calculated as a direct function of new production and settling velocity (rather than independently constrained or assumed) and the inclusion of a factor to compensate for decreasing organic matter reactivity during settling as more labile compounds are consumed first. In other words, because TOC is defined, the same amount of organic matter must reach the sediment water interface regardless of depth, but if export production is higher, the model assumes a deeper site and as a result, the organic matter is less reactive when it reaches these deeper waters, so it consumes less benthic O_2. Hence, this model

condition does not require the atmosphere to contain any O_2 at all to maintain weakly oxygenated conditions at the sediment-water interface. This model is interesting and certainly provides foundation for useful discourse, but aspects of it seem extremely sensitive to the calculated water depth which is very difficult to constrain independently. It is also important to note that the validity of the atmospheric O_2 estimates are wholly dependent on the interpretation that the high TOC shales of unit 3 (up to 20 wt%) were deposited beneath oxic bottom waters, an interpretation that has since been challenged in the literature.

The same group of authors offered an additional line of evidence for oxic depositional conditions for the high TOC shales of unit 3 in 2018 (Wang et al., 2018). This purely organic geochemical argument posits that the conversion of hopanes to a particular series of rearranged C_{30} hopanes (17α(H)-diahopanes or C_{30}* hopanes) requires the participation of molecular oxygen. Hopanes are the diagenetic product of hopanols, specialized membrane lipids produced in substantial quantity by bacteria. Analogous biomolecules known as sterols are produced ubiquitously by eukaryotes, which breakdown to steranes through diagenesis. Given this generality, the presence of hopanes and steranes in the rock record can provide information about the relative contributions of these clades to local primary production.

Wang et al. (2018) observed that unit 3 of the Xiamaling Formation contains abundant C30 hopanes and their rearranged counterparts, while unit 2 contains very little of either (Figure 4.2). The authors do not address the general lack of C_{30} hopanes in unit 2, instead focusing on the presence or absence of the rearranged forms. They suggest that

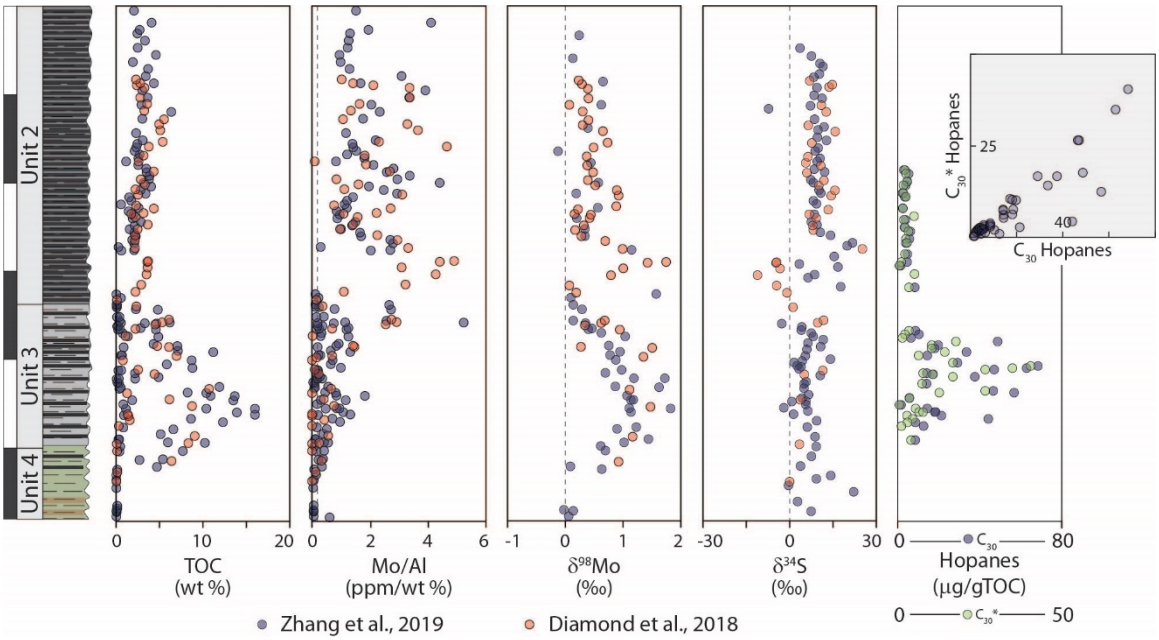

Figure 4.2. Stratigraphic plots of other relevant geochemical data. Total organic carbon is again plotted at the left. Moving to the right, panels show the relative ratio of molybdenum and aluminum concentrations, the isotopic composition of molybdenum (expressed as $\delta^{98}Mo$), the isotopic composition of sulfur in pyrite (expressed as $\delta^{34}S$), and the concentrations of both normal and rearranged C_{30} hopanes as reported by Wang et al., 2018.

their absence from unit 2 sediments reflects anoxic conditions, while their presence in unit 3 is an indication of the participation of O_2 (Wang et al., 2018). This interpretation is very novel, and the authors admit that the use of hopanes in such a way has rarely been proposed previously. Nonetheless, they support their interpretation by drawing analogy to several studies of more recent, mostly terrestrial and lacustrine environments.

The exact mechanism by which hopanes are converted to their rearranged forms, however, remains debated. A previous biomarker study of the Xiamaling Formation by an independent group (Luo et al., 2015) also reported (and commented on) high concentrations of rearranged hopanes. The authors of this study, however, concluded that the high abundance of rearranged hopanes likely reflected an acid-clay catalyzed

rearrangement that has been previously discussed in the literature (e.g., Moldowan et al., 1991). On a more fundamental level, what is clear about the formation of the rearranged series of hopanes is that it requires the hopane precursors. Unit 2 of the Xiamaling contains very low levels of C_{30} hopanes, so it should not be surprising that their rearranged counterparts are nearly absent as well (Figure 4.2). A cross-plot of total abundance of C_{30} and C_{30}* hopanes from units 2 and 3 makes this clear. For this reason, it seems entirely inappropriate to compare the absolute levels of rearranged hopanes in units 2 and 3.

Further, the authors claim that the samples used are free from contamination because the cores were drilled with freshwater as a lubricant (rather than petroleum-based products) and their biomarker profiles are markedly different from overlying Jurassic coal measures. This does not rule out the possibility of contamination by migrating subsurface fluids or through laboratory procedures, though, and there is cause for concern. The Supporting Information of Zhang et al. (2016) clearly shows the presence of steranes, indication of an appreciable eukaryotic contribution to sedimentary organic matter. Significant work in recent years has gone into attempting to recover Proterozoic steranes, and to date, the oldest confirmed detectable steranes come from the ~800 Ma Visingsö Group of Sweden (see discussions in Brocks et al., 2017 and Isson et al., 2018). Recovery of steranes from the Xiamaling Formation would push this date back by almost a factor of two. The study by Luo et al. (2015) mentioned above did not report detectable steranes.

Unit 1

Zhang and colleagues have also attempted to reconstruct atmospheric O_2 concentrations based on the uppermost unit 1 of the Xiamaling Formation (Zhang et al.,

2017). This unit is characterized by cm-scale interbedded black and cyan mudstones and siltstones, where black layers contain 2 to 4 wt% TOC and cyan layers contain less than 0.5 wt% TOC. Redox sensitive trace metals, iron-speciation, and hydrogen-index suggest that the organic rich layers were deposited in anoxic conditions, while the organic lean, cyan layers were deposited in oxic conditions. Rather than attributing this alternation to periodic changes in primary production, as would be the standard hypothesis for similar alternating sequences in younger time intervals, the authors speculate that these variations instead reflect a continuous rate of export production that was exposed to differing redox conditions during settling and deposition—leading to an order of magnitude (or more) difference in organic matter preservation. While I certainly acknowledge the dominating role that O_2 concentration plays on differing levels of organic matter preservation, it does beg the question of why the water column fluctuated periodically between oxic and anoxic, particularly if it was not changes in export production that drove it.

Zhang et al. (2017) goes on to construct a model that quantifies bottom water O_2 concentrations based on the O_2 exposure time required to produce order of magnitude differences in organic matter preservation. The model calculates this by first constraining the O_2 penetration depth into sediments required to achieve the necessary exposure time for a range of sedimentation rates and initial porosities, then calculates bottom water O_2 as a function of these parameters. The authors then suggest a minimum estimate of atmospheric O_2 by assuming that these bottom waters were in equilibrium with the atmosphere.

Indeed, this approach would provide a minimum estimate, as bottom water in such a scenario would be far removed from equilibrium with the atmosphere. In reality, waters at the surface would have had significantly more O_2, meaning that the model outputs actually imply much higher atmospheric O_2 (this very concept is the basis of the model used in the previously discussed Zhang et al., 2016). Furthermore, for the most logical sedimentation rate (one that was calculated based on a lower interval that contains multiple well dated volcanic layers) and an initial porosity of 0.9, the model suggests that O_2 needs to penetrate up to 34 cm into sediments to achieve the required range of exposure times (Zhang et al., 2017). This depth of O_2 penetration is rarely seen today, even with a well oxygenated environment and bioturbation. On a more fundamental level, it seems contradictory to the initial assumption that the cm-scale interbedded black and cyan shales experienced differing early diagenetic conditions. Nonetheless, after making several adjustments to the model, the authors arrive at a preferred bottom water O_2 concentration that, if in equilibrium with the atmosphere, would place atmospheric O_2 concentrations between 4 and 6% of present levels, consistent with their previous minimum estimate.

Interpretations from Diamond and colleagues

In 2018, Diamond et al. published an alternative interpretation of the depositional conditions of unit 2 and 3, suggesting that rather than having been deposited on the slope of a passive margin, they were deposited in a restricted marginal marine setting. Their interpretation was based on an inorganic geochemical dataset generated from a core taken not far from those studied by Zhang and colleagues. There has been some confusion about

the sampling locations of both Diamond et al. and Zhang et al., stemming from errors in geological maps published by both groups. The geologic map published in the Supporting Information of Zhang et al. (2016) places their study area in the Chicheng region, while subsequent publications by the same authors, presenting identical results, claim their work was carried out in the Xiahuayuan region (see Wang et al., 2017 for detailed description of coring and outcrop locations). While Diamond et al. (2018) state in the text that the samples used in the study were from the Xiahuayuan region, both Chicheng and Xiahuayuan are denoted by symbols on the geologic map shown in the original publication, and the figure caption erroneously states that the samples used in the study were from Chicheng. Importantly, this correction implies that the samples are from the same region, eliminating basinal heterogeneities as a basis for differing interpretations.

The location of Xiahuayuan is shown in Figure 4.3, on a paleogeographic reconstruction from Qiao et al. (2007a, 2007b, 2014). The findings of Qiao and coauthors' based on a wide range of field observations. They suggest that subduction initiated during

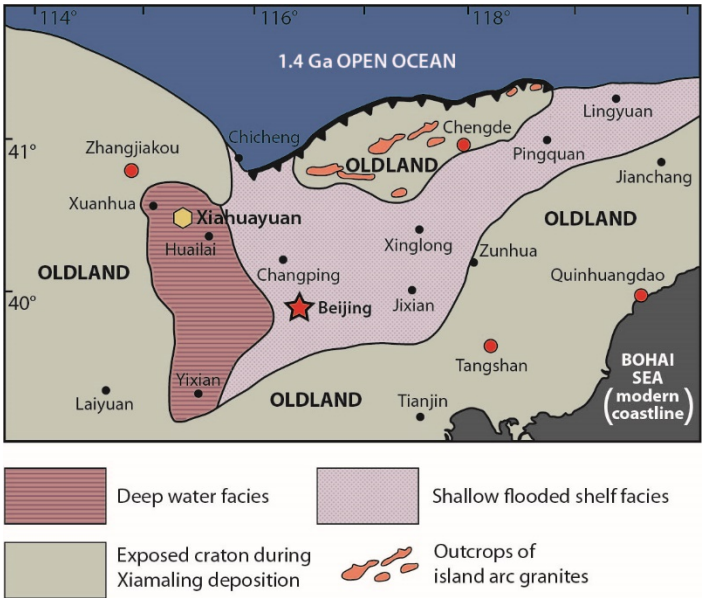

Figure 4.3. Distribution of Xiamaling Formation sediments with reconstructed paleo-coastline (modified from Qiao et al., 2007a). The location of the drill cores used by both groups of authors is shown by the yellow hexagon near Xiahuayuan. Note the deep, inland basin inferred to have existed in this area, separated from the open ocean by a shallower clastic shelf.

deposition of the Tieling Fm., leading to uplift (Qiao et al., 2014). The Xiamaling Fm. was interpreted as having been deposited in a back-arc extensional setting comprised mainly of a shallow clastic shelf facies with a deeper basin in the west, restricted from circulation with the open ocean by an active island arc (Qiao et al., 2007). Xiahuayuan is in this western, deep basinal facies.

Units 2 and 3

Diamond et al. presented many of the same inorganic geochemical measurements as the previous work of Zhang et al. (2016), identifying cm-scale oscillation between low and very high TOC in unit 3, followed by a consistent 2 to 6 wt% TOC in unit 2 (Figure 4.1). They also observed near crustal levels of Mo, V, and U in unit 3, with sharp increases in unit 2. Critical to their interpretation and in contrast to Zhang et al (2016), however, they presented total sulfur (S) concentration and sulfur isotope data (Figure 4.1) because of their proven value in paleoenvironmental interpretation (e.g., Canfield, 1989, 1998, 2001, 2005; Canfield and Teske,

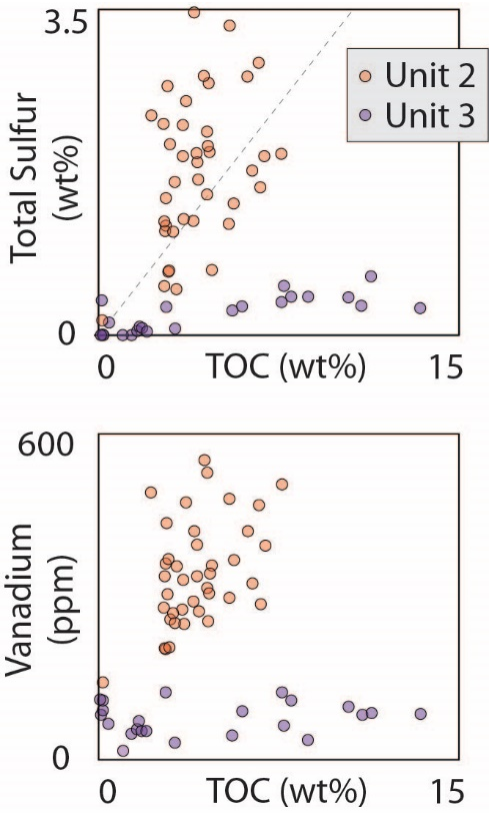

Figure 4.4. Cross-plots of total organic carbon and total sulfur (top) and vanadium (bottom). Samples from unit 2 and 3 are shown in orange and blue, respectively. Data from Zhang et al., 2019.

1996; Canfield et al., 2007, 2008) The S concentrations are surprisingly low in the high TOC layers of unit 3 (avg. 0.2 wt%) but increase by nearly an order of magnitude in unit 2 (avg. 1.7 wt%). This is an unusual result, as it produces two distinctly different carbon/sulfur ratios for the different units—the average C/S ratio in unit 2 is 2.7 while in unit 3 it is greater than 23 (cross-plots of wt% TOC and S are shown in Figure 4.4).

Pyrite (FeS_2) is a common constituent of marine sediments throughout geologic time and its abundance often covaries with TOC. This correlation arises because as sedimentary organic matter is respired and O_2 is depleted, organisms respire using alternative electron acceptors including sulfate (SO_4). The process of dissimilatory microbial sulfate reduction (MSR) generates H_2S^- that can react with iron in porewaters to form pyrite. It can also sulfurize organic matter or diffuse upward into the water column.

During MSR, an isotopic fractionation is imparted on the resulting H_2S^- pool, preferentially enriching it in the lighter S isotope. This fractionation can be large, although as the fraction of available SO_4^{2-} converted to H_2S^- increases, the S isotope ratio of the bulk H_2S^- pool (expressed as $\delta^{34}S_{pyr}$) will approach that of the original SO_4 reservoir. When all available SO_4^{2-} is converted to H_2S^-, the $\delta^{34}S$ value of the H_2S^- will be the same as the SO_4^{2-} from which it was generated (a thorough review of sulfur biogeochemistry and associated isotopic effects can be found in Canfield, 2001). In unit 3 of the Xiamaling Fm., the small amount of sulfur present has a δ value that is generally positive, most values falling between 0 and +15‰ (Figure 4.2). In the lower 20 m of unit 2, $\delta^{34}S$ decreases systematically to a minimum of -11‰ before rebounding to positive values upsection. The

decreasing limb of this negative trend begins at the same horizon where total S increases by nearly an order of magnitude.

Diamond et al. (2018) interpreted the low S concentration coupled with positive $\delta^{34}S$ values in unit 3 as reflecting a very small SO_4^{2-} reservoir in basinal waters during deposition, such that limited isotopic fractionations would be imparted on the small amount of H_2S^- generated. The simultaneous increase in S concentration and decrease in $\delta^{34}S$ at the unit 3/2 transition was interpreted to reflect a large increase in available SO_4^{2-}, allowing MSR to generate abundant H_2S^- while not exhausting available SO_4^{2-}. Rather than invoking a large increase in the SO_4^{2-} reservoir of the global oceans, Diamond et al. (2018) interpreted this increase to reflect a local, basin scale phenomenon—specifically, a large increase in the connectivity of the basin to the global ocean.

This idea is consistent with the observed patterns in redox sensitive trace metals as well. If the basin was largely restricted during deposition of the lower units of the Xiamaling Fm., basinal waters could have been brackish or even nearly fresh water, depending on local hydrographic and hydrological conditions. As a result, basinal SO_4^{2-} and trace metal inventories could have been drawn down to very low levels, limiting sedimentary enrichments regardless of the flux of organic carbon or redox conditions. An increase in the delivery of seawater into such a basin would have the effect of simultaneously increasing trace metal and SO_4^{2-} reservoirs, creating the sedimentary signals that are observed across the unit 3/2 transition. This scenario provides a parsimonious explanation for why redox sensitive trace metals are so low in the most TOC

enriched interval of the succession despite the likelihood that overlying waters were anoxic, and it is consistent with the paleogeography suggested by Qiao et al. (2007).

Molybdenum isotope data

The combined datasets presented by Zhang et al. and Diamond et al. are strikingly similar. This is encouraging as both sets of samples were obtained from nearby areas. A side-by-side comparison of the two datasets was recently published by Zhang et al. (2019) with the addition of a high-resolution Mo isotope dataset (δ^{98}Mo, Figure 4.2) that agrees very well with δ^{98}Mo data presented by Diamond et al. (2018). Interestingly, both δ^{98}Mo datasets capture values significantly higher than had been previously reported for the mid-Proterozoic. Diamond et al. (2018) interpreted this maximum value as a minimum estimate for coeval seawater δ^{98}Mo and argued that it indicated a more oxygenated global ocean than existed either before or after.

Molybdenum is a highly conservative element in oxygenated systems. It can adsorb to the surface of growing iron and manganese oxides, although this process is not a particularly efficient sink. When Mo is exposed to H_2S^-, however, it undergoes progressive sulfurization, converting the molybdate ion (MoO_4^{2-}) to tetrathiomolybdate (MoS_4^{2-}). Tetrathiomolybdate is considerably more particle reactive than its oxidized counterpart and will readily interact with sinking charged particles like organic matter. By this mechanism, sediments underlying sulfidic waters can become highly enriched in Mo. Critically, these different sinks for oceanic Mo have very different isotopic effects. The sorption of Mo to iron and manganese oxides carry strong fractionations, with the lighter isotopes of Mo preferentially enriched in the solid-phase oxides. The higher reactivity of

tetrathiomolybdate, on the other hand, allows for little or even no fractionation at all during sequestration in highly sulfidic systems. The modern ocean is well oxygenated and sulfidic conditions are relatively rare. As a result, Mo concentrations are considerably high and the δ^{98}Mo value is heavy (a recent review of Mo biogeochemistry and isotopic records was published by Kendall et al., 2017).

Both Diamond et al. (2018) and Zhang et al. (2019) reported high δ^{98}Mo in unit 3 sediments, which reach their heaviest values in the interval most enriched in organic carbon (Figure 4.2). This result is compatible with either uptake under highly sulfidic conditions or quantitative uptake of a very small Mo reservoir. The low sulfur contents and iron-speciation results demonstrate that conditions were not highly sulfidic at the time of deposition, and hence, Diamond et al. (2018) argued for quantitative uptake of a very limited reservoir, likely in weakly sulfidic porewaters. This process could have been achieved equivocally via quantitative uptake onto oxides in oxygenated conditions if the reservoir was very small, but in an open ocean sub-OMZ setting like Zhang and colleagues envisage, Mo would be strongly fractionated toward lighter δ^{98}Mo values. The δ^{98}Mo values in sub-OMZ sediments from the Peruvian margin that Zhang et al. (2019) draw comparison to, for example, are ~1‰ lighter than modern seawater. Recognizing this fact, Zhang et al. (2019) suggest that a yet unknown pathway for the capture of non-fractionated Mo was responsible for the high values found in unit 3.

Zhang et al. (2019) also argue that coeval seawater had a δ^{98}Mo value significantly lighter than the highest values reported by both studies. They suggest that heavier values are the result of post-depositional remobilization as they are only observed in low Mo

concentration samples. This is, to my knowledge, the first suggestion that sedimentary δ^{98}Mo values were driven heavier than coeval seawater in rocks of any age or by any known process. Regardless, a very similar maximum value was reported by Diamond et al. (2018) in unit 2, where the Mo concentrations are highest and all other geochemical indicators suggest sulfidic conditions.

Integrated views

Zhang and colleagues, now through nearly a dozen publications, have argued consistently that the entirety of unit 3 was deposited in oxic conditions. However, this interpretation seems to raise many questions. For example, we are left wondering how a final TOC of 20 wt% ended up in sediments deposited under oxic conditions beneath an OMZ, while at the same location a short time later, 3 to 6 wt% was sufficient to drive the system persistently and demonstrably euxinic. We also wonder why unit 1 would have been characterized by oscillation between oxic and anoxic water column conditions with sedimentary TOC contents fluctuating between <0.5 wt% and 2-5 wt%, respectively, yet unit 3, where TOC fluctuates between <0.5 wt% and up to 20 wt% over similar stratigraphic thicknesses, would reflect persistently oxic conditions. These and other, similarly blatant, inconsistencies are the backbone of the integrated argument presented by Zhang and colleagues. We are left instead explaining the unique geochemical patterns in unit 3 by limited connection to the open ocean, which muted trace metal enrichment despite at least intermittent anoxia—consistent with the previous work of Qiao et al. (2007a, 2007b, 2014; Figure 4.3), which envisions the depositional setting in a restricted back-arc basin.

Finally, the interpretation the unit 3 was deposited in oxygenated, sub-OMZ waters is inconsistent with the heavy δ^{98}Mo values reported by both groups, and it fails to explain the unusually low sulfur concentrations reported by Diamond et al. (2018). Zhang et al.

(2019) attributes this lack of sulfur to low iron availability limiting pyrite formation, yet Diamond et al. (2018) reported incomplete pyritization of the limited reactive iron pool that was present in unit 3. Given the abundance of organic matter, we are left with sulfate limitation to explain these findings. While sulfate may have been relatively low in the mid-Proterozoic open ocean (e.g., Kah et al., 2004), it was certainly adequate to drive abundant pyrite formation in most marine shales, such as those of units 1 and 2, suggesting local depletions during deposition of unit 3. Further, in the presence of abundant H_2S and the absence of reactive Fe, extensive sulfurization of organic matter would be expected, and with up to 20 wt% TOC, there would be ample opportunity for preserving excess sulfur. The difference between pyrite sulfur and total sulfur in unit 3 sediments is very small, though, indicating little to no organically bound sulfur (Diamond et al., 2018). Instead, these observations are all consistent with deposition in a highly restricted marginal marine setting.

Concluding remarks

It is more than a little ironic that the two groups have converged on the same conclusion; that the Xiamaling Formation contains evidence for relatively high oxygen during the mid-Proterozoic—despite extremely different approaches to interpreting essentially the same data. Each group might look at the other and conclude that they are generally right but for the wrong reasons. One might look at this particular debate and ask why these distinctions are relevant to anyone other than those listed on the author lines. Of course, the answer to this is obvious, and it is two-fold. It lies with both the importance of

this formation to the broader picture of the progression of environmental oxygenation through time and with a more existential question about the role of preconception and agenda in our (or any) field.

Some might take this combined body of work and surmise that the mid-Proterozoic witnessed a fairly stable 1-10% PAL atmospheric O_2. Others might interpret this formation as a suggestion of more dynamic conditions against a backdrop of lower atmospheric O_2. These distinctions are potentially critically important to understanding the role, if any, that environmental oxygenation played in pacing eukaryotic evolution. Advancing toward a resolution to that debate will only be possible with a significant improvement to our understanding of both environmental and biological evolution. Both groups discussed here have presented novel attempts at moving beyond previous standards for geochemical studies of individual formations, one through innovative modeling and the other through an integrated, high resolution, many multi-proxy investigation. Both seem to be saying the same thing about the forest at the time, but only one can be correct about the trees.

The other discussion point arising from this combined body of work is perhaps more important. The results that Diamond et al. (2018) presented were, in small part, at odds with previous interpretations about the mid-Proterozoic made by some of the authors. Despite this, the results and discussions were presented as dictated by logic. Further, these results have shaped the thinking of myself and Lyons, as made clear by the preceding and following chapters of this dissertation. The results presented by Zhang et al. (2016) support the notion that mid-Proterozoic atmospheric O_2 was 1-10% PAL, a conclusion of significant previous work by members of the authorship. The fact that the model of Zhang

et al. (2017) arrives at the same range, while I would argue that it has literally zero utility in estimating atmospheric O_2, is astounding. My perspective is obviously biased, but this seems remarkably convenient. In closing, I must say that I by no means intend to demonize the authorship for these contributions, there is an enormous amount of careful work and thoughtful insight presented within them. None of us are immune to the blinders that our working models and working groups create. This is just a dashboard light, reminding you to step out of the echo chambers once in a while and try to think objectively.

References

Brocks, J.J., Jarrett, A.J., Sirantoine, E., Hallmann, C., Hoshino, Y. and Liyanage, T., 2017. The rise of algae in Cryogenian oceans and the emergence of animals. Nature, 548(7669), p.578.

Canfield, D.E., 1989. Reactive iron in marine sediments. *Geochimica et Cosmochimica Acta*, *53*(3), pp.619-632.

Canfield, D.E., 1998. A new model for Proterozoic ocean chemistry. *Nature*, *396*(6710), pp.450-453.

Canfield, D.E., 2001. Biogeochemistry of sulfur isotopes. Reviews in mineralogy and geochemistry, 43(1), pp.607-636.

Canfield, D.E., Poulton, S.W., Knoll, A.H., Narbonne, G.M., Ross, G., Goldberg, T. and Strauss, H., 2008. Ferruginous conditions dominated later Neoproterozoic deep-water chemistry. *Science*, *321*(5891), pp.949-952.

Canfield, D.E., Poulton, S.W. and Narbonne, G.M., 2007. Late-Neoproterozoic deep-ocean oxygenation and the rise of animal life. *Science*, *315*(5808), pp.92-95.

Canfield, D.E., Raiswell, R. and Bottrell, S.H., 1992. The reactivity of sedimentary iron minerals toward sulfide. *American Journal of Science*, *292*(9), pp.659-683.

Diamond, C.W., Planavsky, N.J., Wang, C. and Lyons, T.W., 2018. What the~ 1.4 Ga Xiamaling Formation can and cannot tell us about the mid-Proterozoic ocean. Geobiology, 16(3), pp.219-236.

Garrels, R.M., Perry, E.A. and Mackenzie, F.T., 1973. Genesis of Precambrian iron-formations and the development of atmospheric oxygen. Economic Geology, 68(7), pp.1173-1179.

Isson, T.T., Love, G.D., Dupont, C.L., Reinhard, C.T., Zumberge, A.J., Asael, D., Gueguen, B., McCrow, J., Gill, B.C., Owens, J. and Rainbird, R.H., 2018. Tracking the rise of eukaryotes to ecological dominance with zinc isotopes. Geobiology, 16(4), pp.341-352.

Johnston, D.T., 2011. Multiple sulfur isotopes and the evolution of Earth's surface sulfur cycle. Earth-Science Reviews, 106(1-2), pp.161-183.

Kah, L.C., Lyons, T.W. and Frank, T.D., 2004. Low marine sulphate and protracted oxygenation of the Proterozoic biosphere. *Nature*, *431*(7010), pp.834-838.

Kendall, B., Dahl, T.W. and Anbar, A.D., 2017. The stable isotope geochemistry of molybdenum. Reviews in Mineralogy and Geochemistry, 82(1), pp.683-732.

Luo, G., Hallmann, C., Xie, S., Ruan, X., & Summons, R. E. (2015). Comparative microbial diversity and redox environments of black shale and stromatolite facies in the Mesoproterozoic Xiamaling Formation. Geochimica et Cosmochimica Acta, 151, 150-167.

Lyons, T.W., Reinhard, C.T. and Planavsky, N.J., 2014. The rise of oxygen in Earth's early ocean and atmosphere. Nature, 506(7488), p.307.

Meng, Q.R., Wei, H.H., Qu, Y.Q. and Ma, S.X., 2011. Stratigraphic and sedimentary records of the rift to drift evolution of the northern North China craton at the Paleo-to Mesoproterozoic transition. Gondwana Research, 20(1), pp.205-218.

Moldowan, J.M., Fago, F.J., Carlson, R.M., Young, D.C., an Duvne, G., Clardy, J., Schoell, M., Pillinger, C.T. and Watt, D.S., 1991. Rearranged hopanes in sediments and petroleum. Geochimica et Cosmochimica Acta, 55(11), pp.3333-3353.

Qiao, X.F., Gao, L.Z. and Zhang, C.H., 2007a. New idea of the Meso-and Neoproterozoic chronostratigraphic chart and tectonic environment in Sino-Korean Plate. Geological Bulletin of China, 26(5), pp.503-509.

Qiao, X.F., Gao, L.Z. and Peng, Y., 2007b. Mesoproterozoic earthquake events and breakup of the Sino-Korean Plate. Acta Geologica Sinica-English Edition, 81(3), pp.385-397.

Qiao, X.F. and Wang, Y.B., 2014. Discussions on the lower boundary age of the Mesoproterozoic and basin tectonic evolution of the Mesoproterozoic in North China Craton. Acta Geologica Sinica, 88(9), pp.1623-1637.

Qu, Y., Pan, J., Ma, S., Lei, Z., Li, L. and Wu, G., 2014. Geological characteristics and tectonic significance of unconformities in Mesoproterozoic successions in the northern margin of the North China Block. Geoscience Frontiers, 5(1), pp.127-138.

Raiswell, Rob, Dalton S. Hardisty, Timothy W. Lyons, Donald E. Canfield, Jeremy D. Owens, Noah J. Planavsky, Simon W. Poulton, and Christopher T. Reinhard. "The iron paleoredox proxies: A guide to the pitfalls, problems and proper practice." American Journal of Science 318, no. 5 (2018): 491-526.

Tribovillard, Nicolas, et al. "Trace metals as paleoredox and paleoproductivity proxies: an update." Chemical geology232.1-2 (2006): 12-32.

Wang, X., Zhang, S., Wang, H., Bjerrum, C.J., Hammarlund, E.U., Haxen, E.R., Su, J., Wang, Y. and Canfield, D.E., 2017. Oxygen, climate and the chemical evolution of a 1400 million year old tropical marine setting. American Journal of Science, 317(8), pp.861-900.

Wang, X., Zhao, W., Zhang, S., Wang, H., Su, J., Canfield, D.E. and Hammarlund, E.U., 2018. The aerobic diagenesis of Mesoproterozoic organic matter. Scientific reports, 8(1), p.13324.

Zhang, S., Wang, X., Wang, H., Bjerrum, C.J., Hammarlund, E.U., Costa, M.M., Connelly, J.N., Zhang, B., Su, J. and Canfield, D.E., 2016. Sufficient oxygen for animal respiration 1,400 million years ago. Proceedings of the National Academy of Sciences, 113(7), pp.1731-1736.

Zhang, S., Wang, X., Wang, H., Bjerrum, C.J., Hammarlund, E.U., Haxen, E.R., Wen, H., Ye, Y. and Canfield, D.E., 2019. Paleoenvironmental proxies and what the Xiamaling Formation tells us about the mid-Proterozoic ocean. Geobiology, 17(3), pp.225-246.

Chapter 5

Breaking the Boring Billion: A case for solid-Earth processes as drivers of system-scale environmental variability during the mid-Proterozoic

Preface:

The contents of this chapter, less the forward, have been published in a modified form as:

> Diamond, C.W., Ernst, R.E., Zhang, S.H. and Lyons, T.W., 2021. Breaking the Boring Billion: A Case for Solid-Earth Processes as Drivers of System-Scale Environmental Variability During the Mid-Proterozoic. Large Igneous Provinces: A Driver of Global Environmental and Biotic Changes, pp.487-501.

Forward

The manuscript presented in this chapter was the culmination of many discussions with Richard Ernst. Prior to initiating communication, Richard, Shuan-Hong Zhang, and colleagues published a paper linking black shale deposition around 1.4 billion years ago with large-scale volcanism and the breakup of the supercontinent Nuna. Given what modeling studies have shown with respect to widespread phosphorous limitation in the global oceans when atmospheric O_2 is low, coupled to the fact that mafic volcanic rocks, the kind that would be produced in abundance during the volcanism Richard and Shuan-Hong had written about, contain abundant phosphorous and weather easily. It seems like at least a useful discussion point that this could be related to the transiently heightened oceanic-atmospheric O_2 levels that were argued for in Chapter 3.

This was met with mixed reviews. Tim Lenton provided a particularly harsh critique, arguing that Large Igneous Province volcanism could never have provided enough phosphorous to affect any perturbation to the global carbon cycle. It is worth mentioning that he has published multiple times arguing against both the notion of low atmospheric O_2 and low phosphorous during the mid-Proterozoic. Additionally, he and colleagues pioneered the idea that the proliferation of non-vascular land plants, through the secretion of organic acids, enhanced the phosphorous weathering flux in the Middle Ordovician to the point that it disrupted the global carbon cycle and caused the rapid descent from strong greenhouse conditions into the Hirnantian Glaciation (a short lived but intense ice age at the end of the Ordovician). By no means am I saying that he and colleagues are necessarily incorrect about any of these things, rather just that these conversations seem to have merit. The manuscript that follows presents this argument, along with the supporting evidence.

Abstract

Emplacement and weathering of large igneous provinces (LIPs) can have dramatic effects on global climate and biogeochemical systems. In the Phanerozoic, these events are often linked to expanding oceanic anoxia, widespread deposition of organic-rich shales, and metazoan extinctions. In the Precambrian, LIP activity would have had similar potential to perturb global systems, though the outcome may have differed given different starting conditions. Specifically, against a backdrop of mostly low oxygen conditions, Precambrian LIP emplacement may have stimulated oxygenation of the atmosphere and shallow oceans, which could have favored innovations among eukaryotic life. Here, we

review the records of several oceanic-atmosphere redox proxies, summarize their utility, and compare them to the record of continental LIPs. While the mid-Proterozoic (1.8-0.8 Ga) is famous for long-term environmental stability, several independent proxies suggest the possibility that conditions were transiently more oxygenated at ~1.4 Ga. This time coincides roughly with a period of increased LIP activity that has been recently linked with widespread deposition of black shales. We explore the possibility that LIP-induced impacts on productivity might have favored organic matter burial, transient oxygenation, and potential advantages for aerobic life, focusing in particular on the feedbacks that maintained environmental balance for nearly a billion years. Our understanding of the evolution of Proterozoic environmental conditions is still nascent, but as records improve and we search for mechanisms that underpinned long-term stability or drove secular change, it is critical that the whole Earth system be considered.

Introduction

The environmental conditions of the surface of our planet have experienced dramatic change over the course of its ~4.54 billion-year history. These changes reflect a variety of influences, including long-term secular processes like planetary cooling, atmospheric H^2 escape, and increasing solar luminosity (e.g., Gough, 1981; Catling et al., 2001; Claire et al., 2006; Condie, 2013). The monotonic evolution of these processes, however, has been overprinted by a vast number of interconnected feedbacks and has been perturbed repeatedly by an array of stochastic planetary and solar system processes. System-scale climatic and environmental upheavals throughout Earth's history have been attributed to the amalgamation or breakup of supercontinents (e.g., Hoffman, 1998; Li et al., 2004; Campbell and Allen, 2008), emplacement of large igneous provinces (LIPs; e.g., Coffin and Eldholm, 1994; Zhang et al., 2018; Ernst, 2014; Cox et al., 2016; Ernst and Youbi 2017), and the impact of large extraterrestrial objects (e.g., Schulte et al., 2010). These processes have the potential to dramatically alter ocean-atmosphere chemistry, continental weathering rates, and the architecture of local or global ocean circulation. The combined effects of these phenomena can lead to many outcomes—warming or cooling, large changes in the rate and distribution of nutrient and sediment delivery to shelf systems, and oxygenation or deoxygenation of the oceans and atmosphere to name a few (Wingall, 2001; Goddéris et al., 2003; Campbell and Allen, 2008; Turgeon et al., 2008; Cox et al., 2016).

Throughout this history of inorganic processes, life has been evolving within and alongside these changing environments and, in turn, further modifying their chemical and

physical nature through metabolic and other activity. The combined effect of life's metabolic potential is nowhere more apparent than in the 21% of our present atmosphere comprised of oxygen (O_2). This O_2 is almost exclusively the product of oxygenic photosynthesis, which uses water as an electron donor to generate reduced organic carbon and O_2 as a byproduct. The story of the accumulation of this 21%, however, is far from simple and has continually played out as competing forces of photosynthetic O_2 production and O_2 consumption through aerobic respiration and oxidation of reduced compounds present at Earth's surface (reviewed in Lyons et al., 2014). These processes are in turn modulated by a host of both positive and negative feedbacks.

The accumulation of O_2 in the environment was not inconsequential for the life inhabiting it. At a fundamental level, O_2 is toxic to organisms that are comprised primarily of reduced carbon compounds. Once this impediment was overcome, however, aerobic metabolisms offer a significant increase in energy yield per unit of organic carbon remineralized over less efficient anaerobic metabolisms, and biology has evolved numerous ways to use reactive oxygen species in cellular regulatory process and growth (e.g., Hammarlund et al., 2018; Taverne et al., 2018). The high reactivity of O_2 also makes it a critical component of terrestrial weathering regimes and nearly every marine biogeochemical cycle. For these reasons, environmental O_2 has played a central role in the chemical evolution of the oceans.

The potential effects of oceanic oxygenation on the trajectory of biological evolution have received significant attention (e.g., Nursall, 1959; Anbar and Knoll, 2002; Payne et al., 2009, 2011; Johnston et al., 2012a; Sperling et al., 2013; Knoll, 2014;

Planavsky et al., 2014; Mills et al., 2014; Reinhard et al., 2016). This relationship is most clear when considering animal (Metazoan) evolution specifically. In modern ecosystems, animal diversity, abundance, and body size are all directly related to the redox state of the water column (e.g., Levin, 2003). Large animals with energetically demanding lifestyles are simply not able to meet their metabolic requirements in persistently low O_2 environments (Sperling et al., 2013). Additionally, such O_2-deprived ecosystems are typically characterized by low diversity and limited trophic tiering (Levin, 2003). This condition stands in stark contrast to the complex food webs generally assumed to support large predators under more oxygenated conditions. Further, widespread oceanic anoxia has been linked to many extinction events throughout the Phanerozoic (e.g., Erwin, 1994; Wignall and Twitchett, 1996; Caplan and Bustin, 1999).

However, these relationships become less straightforward when turning to the microbial world. While some processes that are nearly ubiquitous in the domain Eukarya require the presence of molecular O_2 (e.g., sterol biosynthesis; Summons et al., 2006), and the last common ancestor of all eukaryotes was capable of aerobic respiration (Müller et al., 2012), it is not clear how much oxygen early microbial eukaryotes would have needed or when these conditions would have been satisfied (Porter et al., 2018). Additionally, microbial eukaryotes are diverse and abundant in modern anoxic and sulfidic environments (e.g., Edgcomb et al., 2011; Orsi et al., 2012a), largely facilitated by partnerships with ecto- and endosymbionts (Orsi et al., 2012b). It is possible, therefore, that the availability of nutrients played a major, if not dominant, role in controlling the structure of ecosystems during the time when early eukaryotes were proliferating—specifically during the mid-

Proterozoic (1800-800 Ma; Reinhard et al., 2017). Further, nutrient availability and O_2 release to the oceans-atmosphere system are clearly coupled (Laakso and Schrag, 2014; Reinhard et al., 2016; Ozaki et al., 2018).

The mid-Proterozoic has been long recognized as a unique time in Earth history for the roughly billion-year lack of evidence for either continental glaciation or significant variation in the carbon isotope composition of marine carbonate ($\delta^{13}C$, Fig 5.1), earning it the name 'Boring Billion' (Buick et al., 1995; Brasier and Lindsay, 1998; Holland, 2006). This colloquialism has been further reinforced by an apparent stagnation of biological evolution during the time. While eukaryotes likely originated early in or just before the

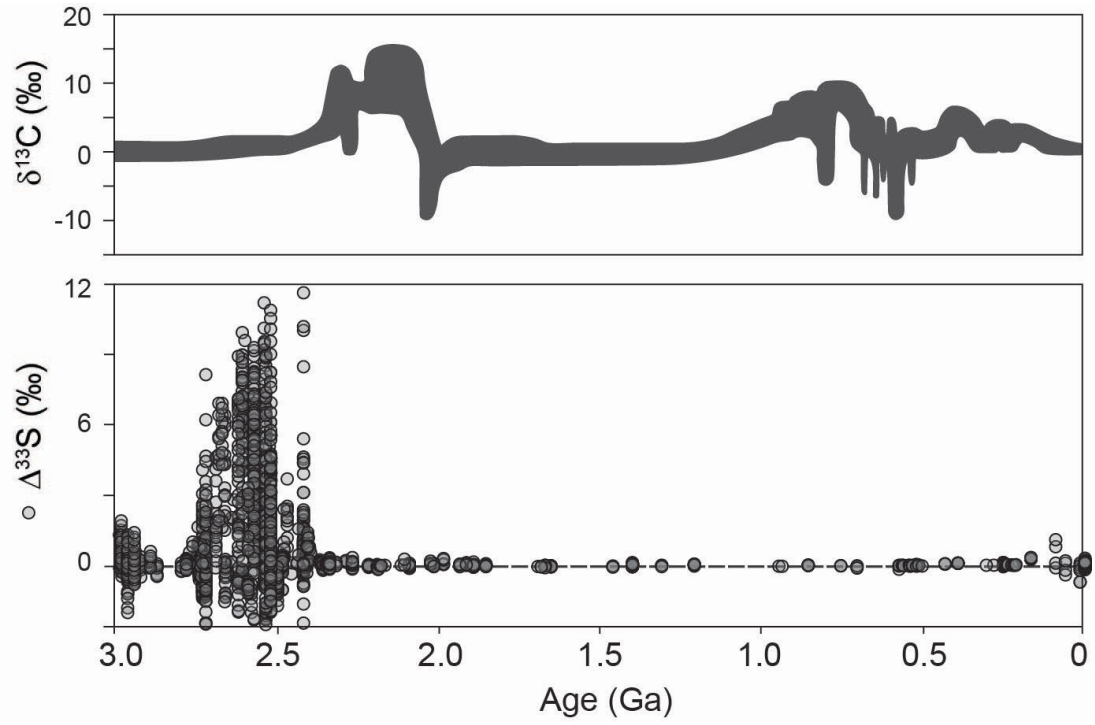

Figure 5.1. Record of carbon isotope values ($\delta^{13}C$) of marine carbonates (top) and mass-independent fractionation of sulfur isotopes ($\Delta^{33}S$, bottom). Note highly positive $\delta^{13}C$ values between ~2.2 and 2.0 Ga, followed by long interval of values ~0‰ and lack of fractionations in $\Delta^{33}S$ after ~2.4 Ga. Data in this figure are from many sources.

mid-Proterozoic, as a group they remained at low diversity and abundance until the early Neoproterozoic (Knoll et al., 2014; Cohen and Macdonald, 2015) It has also been suggested that the ocean-atmosphere system remained in a very low O_2 state throughout the mid-Proterozoic (e.g., Canfield, 2005; Planavsky et al., 2014). Attempts to link these observations have led multiple studies to suggest that this billion-year interval was characterized by a stable steady-state wherein iron-rich (ferruginous) conditions occupied much of the ocean, and primary production was stifled by low phosphorous (P) availability resulting from coprecipitation with iron minerals (Laakso and Schrag, 2014; Derry, 2015; Ozaki et al., 2018). The stability of such a scenario lies with the large amount of O_2 required to deplete the oceanic iron inventory and the difficulty in generating this O_2 when photosynthetic production is low (Ozaki et al., 2018). Importantly, this view of a nutrient starved mid-Proterozoic biosphere is not shared by all researchers (c.f. Daines et al., 2017; Lenton and Daines, 2017).

The mid-Proterozoic closed with major perturbations to climate and marine biogeochemical cycles, as well as escalating advances in eukaryotic complexity (Hoffman et al., 1998; Macdonald et al., 2010; Johnston et al., 2012b; Planavsky et al., 2014; Cohen and Macdonald, 2015). The 'snowball Earth' glaciations of the Cryogenian followed shortly after, beginning at ~717 Ma (Macdonald et al., 2010). Both before and after these glaciations, numerous transient oxygenation events are expressed in variety of independent redox proxies (e.g., Planavsky et al., 2014; Lu et al., 2017; Hardisty et al., 2017; Sahoo et al., 2016). However, the certainty of these events and their cause(s) remains to be resolved. Numerous theories have been proposed to explain the likely interrelated climatic, redox,

and evolutionary events in the Neoproterozoic, many of which point to the progressive breakup of the supercontinent Rodinia as a driving force behind environmental change (e.g., Goddéris et al., 2003; Horton, 2015; Cox et al., 2016). Supercontinent breakup can perturb global biogeochemical cycles through many factors, including the creation of rift basins as loci of organic carbon burial, the emplacement and subsequent weathering of LIPs, and through changes in global weathering patterns (Des Marais et al., 1992; Coffin et al., 1994; Donnadieu et al., 2004; Horton, 2015; Cox et al., 2016).

These processes, however, were by no means restricted to the Neoproterozoic. The supercontinent Nuna broke up in the mid-Proterozoic (Evans and Mitchell, 2011), and LIP volcanism has waxed and waned throughout Earth history (Ernst, 2014; Ernst and Youbi, 2017; Ernst et al., this volume). Recent work has also highlighted the possibility that environmental conditions in the mid-Proterozoic were not as stable as once thought (e.g., Canfield et al., 2018; Diamond et al., 2018a; Planavsky et al., 2018). It is our intent here to critically examine the records of environmental oxygenation and compare them to the record of continental LIP magmatism. Importantly, the history of environmental oxygenation tracks the balance of O_2 production and consumption, and LIP volcanism is one of many external factors that could force change on this balance.

The Precambrian record of environmental oxygenation

A first-order picture

An exploration of the mid-Proterozoic requires that we first consider the conditions in the preceding time intervals as context for assessing later environmental change. We

then focus on conditions during the mid-Proterozoic using diverse proxies that allow us to define and interpret the prevailing conditions and any significant offsets from the long-term trends. These 'events' can then be addressed within the framework of possible drivers, including LIP activity.

The Archean Earth was characterized by an anoxic ocean-atmosphere system. The transition out of this anoxic world took place between 2.4 and 2.3 Ga in an event known as the Great Oxidation Event (GOE; reviewed in Lyons et al., 2014). While this transition is evident in a variety of geological archives, the record of mass-independent fractionation (MIF) of sulfur isotopes delineates it most clearly (Fig 5.1; Farquhar et al., 2000; Farquhar and Wing, 2003; Luo et al., 2016; among others). Generation of this signal is attributed to photodissociation of SO_2 in the upper atmosphere, but its preservation in the geologic record requires low O_2 such that the reaction products can be transferred to sediments separately while avoiding oxidation (Pavlov and Kasting, 2002). It has been estimated that atmospheric partial pressure of O_2 (pO_2) on the order of 10-5 times present atmospheric levels (PAL) would be required to fully oxidize the products and result in isotopic homogenization, although modeling studies suggest pre-GOE atmospheric pO_2 may have been significantly lower (Pavlov and Kasting, 2002; Claire et al., 2006). The permanent disappearance of this signal from the record implies that atmospheric pO_2 has remained above 10^{-5} PAL since the GOE, placing a lower limit for the Proterozoic.

Shortly after the GOE, an anomalously large positive carbon isotope excursion known as the Lomagundi event is preserved in many carbonate successions around the world (e.g., Karhu and Holland, 1996; Martin et al., 2013). This event is characterized by

highly positive carbon isotope values ($\delta^{13}C$ >10‰) that appear consistently in approximately two hundred million years of carbonate stratigraphy (reviewed in Martin et al., 2013). The conventional interpretation of positive $\delta^{13}C$ values in carbonate rocks would argue for the sustained burial of enormous amounts of organic carbon (which is enriched in ^{12}C), leaving oceanic dissolved inorganic carbon (DIC) enriched in ^{13}C. This isotopically heavy DIC would then be preserved in coeval carbonate rocks that precipitate from it. Had this organic carbon originated from oxygenic photosynthesis, it would indicate the production of a large amount of O_2. Some evidence does suggest that surface oceans were more oxidizing during the Lomagundi interval compared to the remainder of the Paleo-Mesoproterozoic (e.g., Hardisty et al., 2014) and that substantial oxidizing power amassed in the form of oceanic sulfate (e.g., Planavsky et al., 2012; Blättler et al., 2018). This purported accumulation of oxidants is consistent with the notion of substantial organic carbon burial during the Lomagundi event, although its causes and consequences remain poorly understood.

By ~2.0 Ga, carbonate $\delta^{13}C$ values return to near 0‰ (Melezhik et al., 2007). Numerous lines of evidence have been used to argue that between 1.8-0.8 Ga the ocean-atmosphere system was in a perpetually low O_2 state (e.g., Canfield, 1998; Kah et al., 2004; Canfield, 2005; Scott et al., 2008; Reinhard et al., 2013; Partin et al., 2013; Planavsky et al., 2014; Lyons et al., 2014; Cole et al., 2016; Hardisty et al., 2017). Geochemical data consistent with widespread anoxia in the deep ocean and a weakly oxic surface ocean have been found in nearly every investigated formation from this time interval (Figure 5.2), but as we will discuss, there are exceptions.

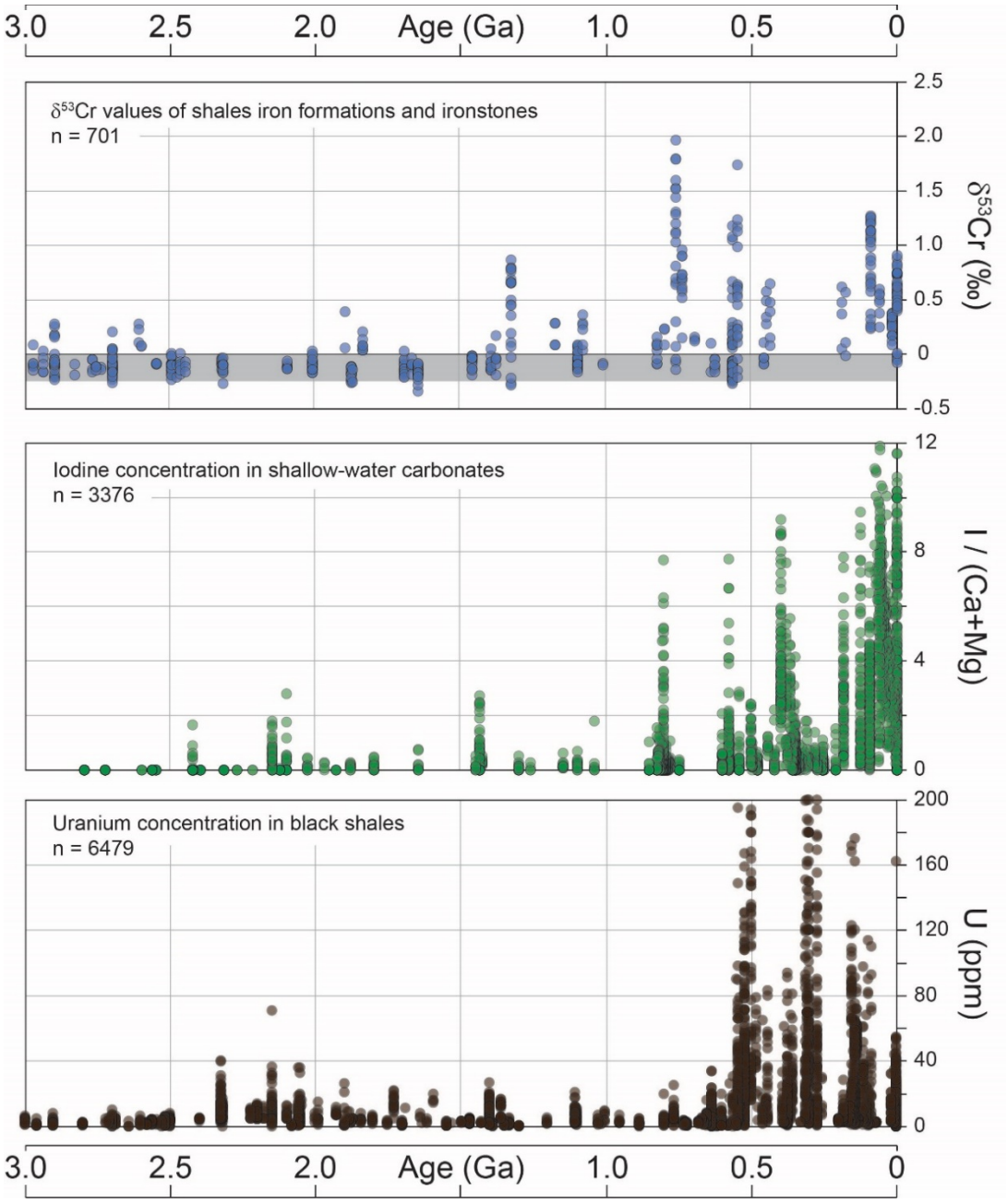

Figure 5.2. Records of select redox proxy data and continental LIPs. Top. Chromium isotopic composition of marine ironstones and shales. Middle. Iodine concentration of shallow water marine carbonates (normalized to sum of calcium and magnesium to correct for variable carbonate content). Bottom. Uranium concentration in organic rich marine shales. Data in figure are updated from Partin et al., 2013; Cole et al., 2016; Hardisty et al., 2017; and Lu et al., 2018.

In the following sections we review the records of three independent redox proxies and briefly outline their systematics. The isotopic composition of chromium ($\delta^{53}Cr$) preserved in sediments deposited under anoxic conditions is thought to reflect reactions in the terrestrial weathering environment and thus has the potential to record variations in atmospheric pO_2 (e.g., Frei et al., 2009). The concentration of iodine in shallow-water carbonate sediments reflects the presence of the oxidized iodate (IO_3^-) species in surface waters, which is highly sensitive to changes in the dissolved O_2 concentration of surface waters as well as frequent mixing with deeper, reducing water masses (e.g., Hardisty et al., 2017). The concentration of uranium (U) in organic-rich black shales can track the size of the oceanic U reservoir, which in turn can be modulated by the prevalence of anoxic bottom waters in the global oceans (e.g., Partin et al., 2013). In this way we will consider the signals in these datasets as a sort of globally integrated, one-dimensional depth profile of the ocean-atmosphere system, although local variation would obviously have been significant.

The chromium isotope composition of marine sediments

Chromium exists in the environment primarily in two valence states: Cr(III) and Cr(VI). The oxidation of Cr(III) to Cr(VI) requires a very high local redox potential and is almost exclusively facilitated in natural systems through interactions with solid phase manganese-oxides (Eary and Rai, 1987; Kotaś and Stasicka, 2000). While Cr(III) does attain some mobility in the environment through complexation with organic ligands (Puzon et al., 2008), Cr (VI) is highly soluble and hence highly mobile. A mobile Cr(VI) pool can

then be carried to the ocean via streams, where the possibility exists during transport for some Cr(VI) to be reduced back to Cr(III) through interactions with organic matter or other reductants (Banks et al., 2006). This partial reduction can leave an isotopic fingerprint on the mobile Cr (VI) pool, selectively reducing ^{52}Cr and leaving the residual Cr(VI) enriched in the heavier isotope (^{53}Cr; e.g., Zink et al., 2010). When this isotopically fractionated Cr(VI) encounters reducing conditions in the ocean it can be sequestered quantitatively into sediments, preserving traces of the redox cycling that occurred in the terrestrial environment (Frei et al., 2009; Planavsky et al., 2014). The crux of this system for the investigation of Precambrian redox is that without oxidative cycling of Cr, only small amounts of ligand bound Cr(III) will move through the system and remain for the most part isotopically unfractionated (Frei et al., 2009; Planavsky et al., 2014; Cole et al., 2016).

Two studies have attempted to place quantitative limits on the operation of the oxidative Cr cycle (Crowe et al., 2013; Planavsky et al., 2014). Taking slightly different approaches, both studies arrived at a very low atmospheric pO_2 level (<1% PAL) required to either induce the oxidation or to allow for survival of some Cr(VI) during transport (Crowe et al., 2013; Planavsky et al., 2014). Specific pO_2 estimates grounded in the Cr isotope system rely on soil weathering models, which are a crude approximation of the integrated operation of the global weathering process. For this reason, the constraints have significant error bars. Nevertheless, the lack of significant Cr fractionations throughout the majority of the Precambrian suggests that atmospheric pO_2 was low.

The $\delta^{53}Cr$ data shown in Figure 5.2 are updated from Cole et al. (2016), who examined the $\delta^{53}Cr$ compositions of a suite of black shales spanning almost three billion

years of Earth history. This work followed studies by Frei et al. (2009) and Planavsky et al. (2014), both of which primarily presented $\delta^{53}Cr$ values in iron formations and ironstones throughout Earth history. The data from these three publications show a lack of significantly fractionated $\delta^{53}Cr$ values in rocks older than the ~800 Ma shales from the Shaler Supergroup (Frei et al., 2009; Planavsky et al., 2014; Cole et al., 2016). Since Cole et al. (2016), one study identified fractionated $\delta^{53}Cr$ values in shales older than 800 Ma, the Taizi Formation of the Shennongjia Group, South China (Canfield et al., 2018). Shales in the upper Taizi Formation have been dated using whole rock U-Pb to 1332 ± 67 Ma (Li and Leng, 1991), and detrital zircons from the Dayanping Formation, lower in the Shennongjia Group, contain a minimum age of 1429 Ma (Li et al., 2013).

Another study has also presented $\delta^{53}Cr$ values from four carbonate successions spanning 1.1-0.9 Ga, identifying fractionated $\delta^{53}Cr$ values in all four (Gilleaudeau et al., 2016). The application of the Cr isotope proxy has not been fully evaluated in carbonate rocks, however, and multiple studies have shown the potential for fractionations associated with Cr incorporation into carbonates (Rodler et al., 2015; Pereira et al., 2016). One intriguing aspect of the shale and ironstone $\delta^{53}Cr$ record is that fractionated Cr is nearly absent from the record until roughly 800 Ma, begging questions about possible drivers and consequences of that shift.

Iodine concentrations in shallow water carbonates

Use of iodine (I) concentrations in carbonate rocks as a redox proxy is a fairly recent development. The proxy's utility stems from the fact that I exists in the environment

primarily as the reduced species iodide (I^-) or the oxidized iodate (IO_3^-), and laboratory studies have shown that while iodate will readily substitute into the carbonate lattice at a rate proportional to its concentration in solution, iodide will be wholly excluded from precipitating carbonate regardless of concentration (Lu et al., 2010). This observation suggests that the presence of I in carbonate rocks can be interpreted as reflecting the presence of iodate in local waters during precipitation (Lu et al., 2010). This utility is further strengthened by the fact that a relatively high redox potential is required to induce oxidation of iodide to iodate and this oxidation progresses slowly, even in well oxygenated waters. In contrast, iodate reduction occurs rapidly and completely as O_2 concentrations diminish (e.g., Rue et al., 1997). Were this not the case, we would expect to find iodine at high concentrations in most carbonates postdating the GOE, as surface waters have likely been weakly oxygenated continuously since that time based on the loss of the MIF sulfur signal. However, because the oxidation kinetics are slow, iodate concentrations in surface waters are likely highly sensitive to frequent upward mixing of anoxic waters or advection across a shallow redoxcline (Hardisty et al., 2017).

A combined record of all published I data is shown in Figure 5.2. The concentration of I is normalized to calcium (Ca) concentration to compensate for variable carbonate contents of rocks (or the sum of calcium and magnesium in dolomitic intervals; Lu et al., 2010; Hardisty et al., 2014). Prior to the GOE, I is absent in nearly every sample, as expected given the dominantly low O_2 conditions in the oceans. During the Lomagundi event, some I is present in many samples, suggesting that the surface ocean could have been fairly O_2 rich at that time (Hardisty et al. 2014). Throughout the mid-Proterozoic,

however, I/(Ca+Mg) values are consistently very low but non-zero (Hardisty et al., 2017). This observation suggests that either surface waters were persistently very low in O_2 or that frequent mixing with nearby reducing water masses outpaced iodide oxidation (Hardisty et al., 2017).

The only exception to the pattern of low but non-zero I/(Ca+Mg) in the mid-Proterozoic is found in the ~1.4 Ga Tieling Formation (Hardisty et al., 2017). The Tieling Formation is a shallow-water stromatolitic carbonate that underlies the ~1.385 Ga Xiamaling Formation (Zhang et al., 2015). Multiple arguments have been presented for heightened oceanic-atmospheric O_2 during deposition of the Xiamaling Formation (e.g., Zhang et al., 2016; Diamond et al., 2018b). In contrast, several formations in the 1.3-1.0 Ga range, after deposition of the Tieling Formation, were analyzed by Hardisty et al. (2017), and all contained low but non-zero I/(Ca+Mg) ratios, similar to those of the interval after the Lomagundi event but before the Tieling Formation.

This pattern of low iodine concentrations is broken again at ~810 Ma—specifically during the Bitter Springs carbon isotope anomaly (Lu et al., 2017) and again in the Ediacaran period during the Shuram carbon isotope excursion (Hardisty et al., 2017). These carbon isotope events are both recognized as departures from baseline $\delta^{13}C$ values of marine carbonates to substantially lower values. The concomitant I enrichments suggest that both events were associated with either large additions to the I budget of the oceans or a substantial expansion of oxygenated conditions manifested in a deepening of the redoxcline. The cause(s) of both isotopic excursions are still areas of very active research (e.g., Cui et al., 2017; Klaebe et al., 2017; Li et al., 2017; Shi et al., 2018), and there is far

from a consensus opinion. The connection of both events to heightened I/(Ca+Mg), though, and its relationship with local water-mass redox structure is consistent with the suggestion that these events could have been linked to the oxidation of large amounts of dissolved organic carbon, thus returning isotopically light carbon to the DIC pool (e.g., Fike et al., 2006). Iodine concentrations in carbonates are inherently influenced by local factors. Nevertheless, by examining a large dataset of globally distributed sections, a global trend emerges.

Uranium concentrations in marine black shales

Uranium (U), like many other transition metals, exhibits solubility behavior that is sensitive to redox. Uranium is highly soluble in well-oxygenated seawater generally present as the uranyl ion [$U(VI)O_2^{2+}$], which can form a suite of carbonate complexes (Maher et al., 2012). Under reducing conditions, U(VI) is reduced to U(IV), which is poorly soluble and readily precipitates as uraninite (UO_2; e.g., Morford and Emerson, 1999). While U sequestration into sediments underlying anoxic waters is rapid and efficient, in the modern U-cycle, uptake into sediments underlying suboxic waters represents a significant sink due to the prevalence of such settings and the importance of diagenetic U uptake in reducing porewaters (Dunk et al., 2002, Andersen et al., 2016). Additional sinks in the modern U cycle include adsorption onto Fe-Mn oxides, hydrothermal alteration of basaltic seafloor, and coprecipitation with biogenic carbonate and silica (Morford and Emersen 1999; Dunk et al., 2002).

Of all the sinks for U in the global oceans, sequestration under anoxic conditions is the most efficient. Because of this, the size of the oceanic U reservoir is highly sensitive to the prevalence of anoxia on a global scale (e.g., Partin et al., 2013). Importantly, when considering a single anoxic depositional setting, the maximum achievable enrichment in U will be proportional to the U concentration in overlying waters. This concept is true on a basinal scale and is necessary to satisfy mass-balance on a global scale. These combined attributes of the U-cycle make the record of enrichments in shales deposited under anoxic conditions through time capable of tracking the spatial extent of anoxia on a global scale (Partin et al., 2013).

The record initially published by Partin et al. (2013) has been updated with more recently published data and is shown in Figure 5.2. Like the pattern for I/(Ca+Mg), U concentrations are low in shales predating the GOE and rise in sediments immediately postdating it, most strongly between 2.2-2.0 Ga. Following this Lomagundi interval, the data return to a low range. There are some mid-Proterozoic values that reach the 20-30 ppm range, which is a significant increase over Archean sediments, although these still low maxima persist into the Cambrian. If the record is interpreted as tracking the expansion and contraction of anoxic conditions at a global scale, it suggests that much of the oceans remained in a very low O_2 state into the Phanerozoic. This interpretation is consistent with other independent redox proxies that indicate widespread anoxia well into the Paleozoic (e.g., Dhal et al., 2010; Sperling et al., 2015).

Stabilization of low mid-Proterozoic O_2

Like many aspects of the Precambrian world, stabilization of the Earth system at low atmospheric pO_2 presents somewhat of a conundrum (e.g., Laakso and Schrag, 2014; Derry, 2015). Why was the Earth seemingly locked into this state for such a long time? And how did it finally overcome the strong negative feedbacks that would have been required to keep it poorly oxygenated in the face of active tectonics and an evolving biosphere? Numerous modeling studies have been undertaken to address these questions, applying increasingly sophisticated numerical models to provide necessary constraints on the many interrelated processes simultaneously affecting the system (e.g., Laakso and Schrag, 2014; Reinhard et al., 2016; Daines et al., 2017; Laakso and Schrag, 2018; Ozaki et al., 2018).

A recent study by Ozaki et al. (2018) employed a novel C-N-P-O_2-S biogeochemical model to constrain the redox balance of the mid-Proterozoic ocean-atmosphere system. Simulations were run under both low (0.01-1% PAL) and relatively high (1-10%) pO_2 scenarios. In both cases, the ultimate condition that sustained low O_2 levels while also satisfying constraints on oceanic sulfate concentrations (derived from the geological record) was a dramatic reduction in organic carbon burial. This condition arose in their model from a nearly ten-fold reduction in the availability of P in the photic zone compared to modern levels, which limited primary production. This requirement for suppressed mid-Proterozoic productivity is consistent with other recent modeling efforts (Laakso and Schrag, 2014, 2018, 2019; Reinhard et al., 2017). The possibility of low marine P is also consistent with both a recent compilation of sedimentary P concentrations

through Earth history (Reinhard et al., 2017) and estimates of late Paleoproterozoic oceanic P concentrations from P/Fe ratios of iron formations (Jones et al., 2015). The scarcity of P in the ocean interior in these models is primarily the result of widespread iron-rich conditions in which iron-phosphate mineralization readily occurs (Derry, 2015) and suppressed biomass remineralization rates under low O_2 conditions (Kipp and Stüeken, 2017; Laakso and Schrag, 2018).

As alluded to above, this viewpoint is not universal. A study by Daines et al. (2017) argues instead for mid-Proterozoic oceanic productivity and nutrient levels between 50-100% of modern. In this model, low atmospheric O_2 levels are maintained by incomplete oxidative weathering of sedimentary organic matter exposed subaerially through uplift and erosion. The authors argue that this oxidation is highly sensitive to pO_2 levels in the ~10% PAL range and will produce a negative feedback that acts to stabilize O_2 at those intermediate levels (i.e., as more or less O_2 is produced, these changes are offset by an increase or decrease in the relative rate of oxidation of exposed sedimentary organic matter). This mechanism also produces an elegant explanation for the seemingly invariant $\delta^{13}C$ of carbonates throughout the mid-Proterozoic. When organic matter burial increases, removing isotopically light carbon from the system, pO_2 increases alongside it. This increase results in an increase in the fraction of organic carbon that undergoes oxidation rather than sedimentary recycling, thus consuming O_2 and ultimately returning isotopically light carbon to the oceanic DIC budget (Daines et al., 2017). In the model of Daines et al. (2017), widespread iron (II)-rich conditions have the potential to generate a positive feedback, stripping oceanic P inventories to a point that the GOE reverses and the Earth

returns to a wholly anoxic state. From the viewpoint of these authors, low Proterozoic O_2 is largely the result of the absence of land plants at the time, which contribute ~50% of the net O_2 production on the modern Earth (Daines et al., 2017).

Both models for the mid-Proterozoic environment provide intriguing insights into the factors that contributed to the observed trends in environmental proxies. Our understanding is still in a fairly nascent state, and aspects of each may be correct. Importantly for our purposes, both models argue for ocean-atmosphere O_2 levels, oceanic nutrient inventories, and global productivity that are all lower than the latter half of the Phanerozoic—how much lower is the point of contention. While these details are immensely important, the world inferred by either model would be strongly influenced by dramatic changes in productivity and organic matter burial that could be driven by strong environmental perturbation, such as might result from the breakup of a supercontinent.

The record of continental large igneous provinces

Large Igneous Provinces (LIPs) represent large volume (>0.1 Mkm3; frequently above 1 Mkm3), mainly mafic (-ultramafic) magmatic events of intraplate affinity (based on tectonic setting and/or geochemistry) that occur in both continental and oceanic settings and are typically either of short duration (<5 Ma) or consist of multiple short pulses over a maximum of a few 10s of Ma (Ernst, 2014; Ernst and Youbi 2017; Ernst et al., 2021). LIPs consist of volcanic packages (flood basalts) and a plumbing system of regional dyke swarms (linear, radiating, and circumferential), sill complexes, layered mafic-ultramafic (M-UM) intrusions, and crustal magmatic underplates. LIP events occur at variable rates

through time, although since 2500 Ma, there has been an average of one LIP event every 20–30 Ma (Figure 5.3; Ernst et al. this volume). Importantly to the discussion of environmental impacts in the mid-Proterozoic, associated flood basalts contain significant amounts of P and have the potential to weather rapidly given ample precipitation.

LIPs have been the focus of a significant amount of recent research, given their growing importance in constraining paleocontinental reconstructions (Ernst et al. 2013), as

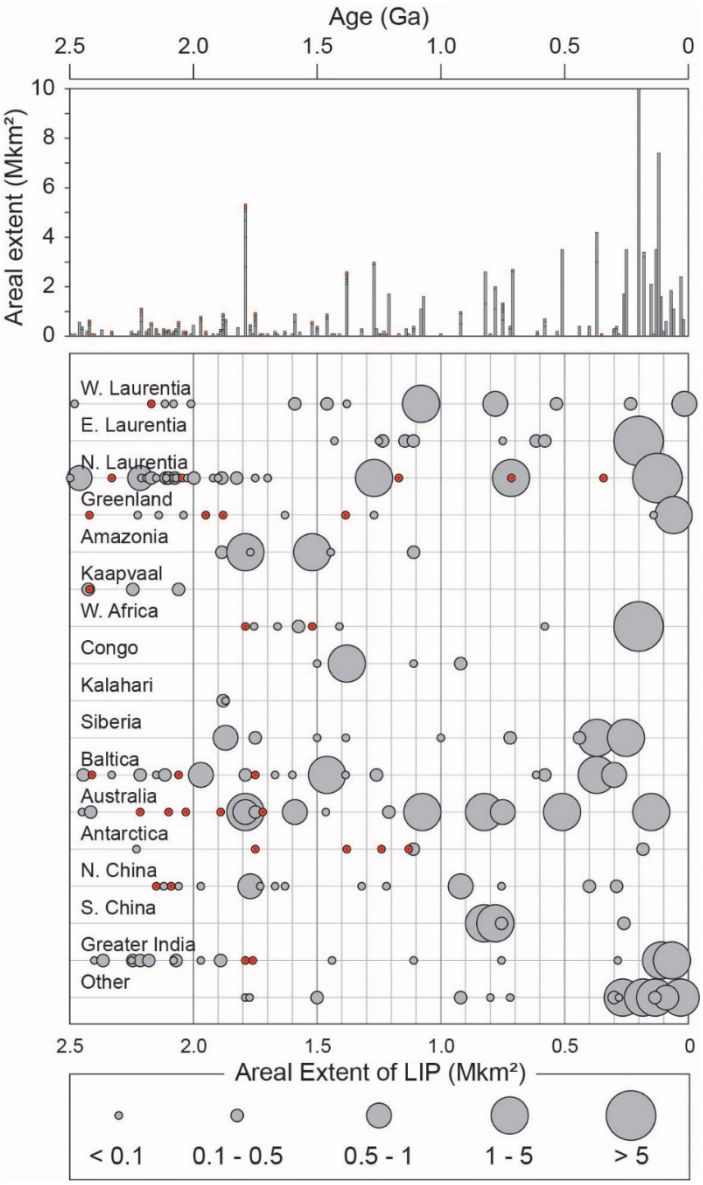

Figure 5.3. Top, Stacked bar chart of large igneous province activity for the past 2.5 billion-years using ten-million-year bins (events with unknown size represented as 0.1 Mkm2). Bottom, Large igneous province activity by craton over the same duration, events are represented with symbols proportional to size bins shown below. Data are from Ernst, 2014 and Zhang, et al., 2018.

a tool in exploration targeting (e.g., Ernst and Jowitt 2013), as analogs for voluminous planetary intraplate magmatism (e.g., Head and Coffin 1997; Ernst 2014), and for their causal role in dramatic climate change throughout Earth history (e.g., Ernst and Youbi 2017; Bond and Grasby 2017; Ernst et al., 2021). Here, we specifically consider their link with environmental change during the 'Boring Billion' (1.8-0.8 Ga) using the record of changing ocean-atmosphere redox conditions as an indicator.

As summarized in Zhang et al. (2018; this volume), there are temporal links between LIP magmatism and black shale deposition throughout Earth history. In the Phanerozoic, these events are often associated with metazoan mass extinctions due to habitat loss in the face of warming, ocean acidification, and/or anoxia (e.g., Wignall, 2001). Extensive LIP magmatism between ~1.39-1.36 Ga was documented by Zhang et al. (2018), and a causal link with the deposition of the similarly aged, organic-rich Xiamaling and Velkerri formations was suggested. While mid-Proterozoic environmental conditions differed fundamentally from those of the Phanerozoic, the effects of LIP activity would likely have been largely the same—that is, conditions that favored the development of anoxia through enhanced primary production and rising global temperatures, resulting in the widespread burial of organic-rich black shales. A critical consideration in this discussion, however, is that such conditions will also lead to the accumulation of O_2 in the surface ocean and atmosphere as photosynthetically derived organic matter is removed from the system. In other words, LIP activity in the Phanerozoic likely triggered extinction through expansion of anoxia in largely oxic oceans, while analogous activity in the

Proterozoic could have simulated organic matter production and burial, increasing surface water O_2 concentrations in oceans that were initially O_2-poor.

The main phase of LIP activity discussed by Zhang et al. (2018; 2021) is centered at ~1.38 Ga, with a smaller pulse of activity pre-dating this at ~1.42 Ga (Figure 5.2). This time slice correlates roughly with indications of heightened surface-ocean and atmospheric O_2 as recorded in the Tieling, Xiamaling, Velkerri, and Taizi formations (Zhang et al., 2016; Hardisty et al., 2017; Diamond et al., 2018b; Yang et al., 2018). It is possible that ongoing LIP activity throughout this time and its subsequent weathering provided a source of P to nearshore environments, leading to the deposition of large amounts of organic carbon and a significant gain in biospheric O_2. The exact timing, magnitude, and duration of oxygenation around 1.4 Ga is admittedly speculative, although as more data emerge, the case continues to grow stronger.

In addition to the mere presence of LIP volcanism, many other factors would have influenced their environmental impacts. These include the location of the LIP during eruption—that is, whether submarine or subaerial and the latitude-dependent climatic controls on weathering, among other factors. While the record of LIPs in the Proterozoic is obscured by poor preservation, appreciable activity at ca. 1.4 Ga appears to have been synchronous on numerous cratons (Fig 5.3; Zhang et al., 2018; 2021).

Potential effects of LIP volcanism in the mid-Proterozoic

The apparent long-term stability of the mid-Proterozoic implies a strong set of stabilizing feedbacks. The studies of Ozaki et al. (2018) and others suggest that diminished

marine P was central to maintaining this balance. Widespread iron-rich conditions in the ocean interior provide a critical link in the chain, maintaining low P through the continual precipitation of iron-phosphate minerals and via scavenging of P onto iron oxides (Derry 2015; Ozaki et al., 2018). The prospect of oxidizing a large reservoir of iron poses a further challenge, as formation of iron oxides would efficiently strip P from the water column. Upsetting this balance would seem to require either a large addition of P to the oceans or the arrival of a mechanism to export organic carbon more efficiently into sediments—though the latter may result in continued P scarcity as the vast majority of primary production today utilizes recycled P (Laakso and Schrag, 2018).

Global tectonics offer one possible solution. Widespread mafic volcanism, for example, could provide rapidly weathering P-rich material to stimulate production. This is not a new idea, and many authors have proposed tectonic controls for a variety of first-order observations throughout Earth history. Specifically, with respect to the oxygenation of Earth surface environments, Campbell and Allen (2008) first proposed that the step-wise oxygenation of our planet was paced by supercontinent cycles. They suggested that the uplift of large mountain belts during supercontinent assembly would lead to rapid and sustained weathering, delivering clastic sediment and nutrients to the oceans and, in turn, stimulate productivity and organic carbon burial. While our understanding of the evolution of ocean-atmosphere O_2 has improved significantly over the decade since Campbell and Allen's important paper, the suggestion that the formation and breakup of supercontinents could have profound impacts on organic carbon burial through large changes in weathering

patterns stands intact, and this cyclic activity surely played a role in shaping surficial systems throughout Earth history.

The suggestion that LIP derived P could upset the balance of feedbacks that maintained environmental stability in the mid-Proterozoic has also been made previously (e.g., Horton, 2015). The case presented by Horton (2015) argues that extensive LIP volcanism between 850-717 Ma, associated with the breakup of Rodinia, delivered abundant P to the ocean, stimulating productivity and organic carbon burial, ultimately resulting in a substantial drawdown of atmospheric CO_2 and the release of significant amounts O_2. This effect, Horton (2015) suggested, could have been responsible for oxygenation events reported in the Tonian period (e.g., Planavsky et al., 2014) and the onset of the Cryogenian glaciation.

Roberts (2013) also made a tectonic argument for control of mid-Proterozoic environmental conditions. Rather than focusing specifically on oxygenation, Roberts (2013) refers more generally to the stability of ocean-atmosphere chemistry during the 'Boring Billion' and the lack of variability in the $\delta^{13}C$ record. The author suggested that the supercontinent Nuna (Columbia) assembled between 2.0-1.8 Ga and remained nearly intact despite multiple breakup attempts—until being modified slightly to form Rodinia at ~1.1-0.9 Ga. While subduction and accretion would have continued around the edges of this single large landmass, the stable Nuna would have remained largely unmodified for these billion years, and Roberts (2013) suggested that this would have allowed for quiescence in global biogeochemical cycles.

It is now commonly asserted that the breakups of Nuna and Rodinia were very different, the former being much less complete. These differing behaviors may have had much to do with the apparently very different responses of the ocean-atmosphere system during the breakup of each. Some dispersion of Nuna's core did occur, however, between 1.45-1.35 Ga (Evans and Mitchell, 2011), and the conditions that would have been conducive to increased productivity and organic carbon burial during the more complete breakup of Rodinia would have been present at least to some extent. Namely, we can imagine the opening of rift basins, concomitant burial of organic matter, and large-scale mafic volcanism that could weather rapidly to deliver sediment and P into nearshore marine environments (e.g., Horton 2015; Cox et al., 2016). It is not immediately clear which of these factors would be most important for organic matter burial fluxes at the time, and the answer likely lies with many factors. The aforementioned modeling studies (Laakso and Schrag, 2014; 2018; Ozaki et al., 2108) suggest that a necessary component to stabilizing the mid-Proterozoic biosphere was lower marine productivity associated with P scarcity. If this was the case, rapid P delivery through the weathering of LIPs could have had a profound impact on the global carbon cycle.

Eruption of a LIP in the watershed of a coastal system could have resulted in a continuous source of nutrients directly into the nearshore surface environment via weathering, thereby sustaining elevated productivity for hundreds of thousands to millions of years, or more. Coastal systems are also inherently high sedimentation areas, further favoring the burial of this heightened organic matter export flux. Sustained high productivity along stretches of a coastal system could have provided an effective

mechanism for increasing ocean-atmosphere O_2 beyond the long-term, stable steady-state levels. Importantly, however, eruption and subsequent weathering of continental LIPs are events of finite duration, meaning that the weathering-driven nutrient flux and related productivity would have diminished as the LIP weathered and eroded.

This scenario provides a plausible mechanism for transient oxygenation events in the mid-Proterozoic world. In our review of published $\delta^{53}Cr$ values, I/(Ca+Mg) ratios, and U concentrations, there are clear suggestions of transient oxygenation in the atmosphere and surface ocean during the 1.4-1.35 Ga interval (Figure 5.2). Transient oxygenation in this interval has also been suggested on the basis of sedimentary molybdenum and uranium isotopic data and a novel carbon export and oxidation model (Yang et al., 2017; Diamond et al., 2018a; Zhang et al., 2016). This timing aligns well with the attempted breakup of Nuna and specifically with heightened activity in the continental LIP record (Figure 5.2; Zhang et al., 2018, 2021). Extensive LIP activity at that time has been documented on Baltica, Laurentia, Siberia, Amazonia, Kalahari, Congo, and East Antarctica (Figure 5.3; Ernst et al. 2008, 2021; Zhang et al., 2018, 2021).

Other transient oxygenation events have been proposed in the mid-Proterozoic (e.g., ~1.1 Ga; Diamond et al., 2018b), although limited data exist. Nevertheless, intriguing evidence suggests accelerated LIP activity at ~1.1 Ga as well (Ernst et al. 2013, de Kock et al., 2014). The Proterozoic rock record is sparse and significant gaps exist. Hence, it is possible that global redox conditions were more variable than the available records suggest, although the U record, for example, has high temporal resolution and attests to the persistence of anoxia in large portions of the deep ocean throughout the Proterozoic (Figure

5.2; Partin et al., 2013). Additionally, if significant events have gone undetected, the implicit, subsequent return to baseline conditions would seem to preclude any large unidirectional increase in biospheric O_2 prior to roughly 800 million years ago.

Conclusions

The long-held notion of environmental stasis during the so-called 'Boring Billion' has been questioned. Multiple independent proxies indicate that environmental O_2 concentrations could have transiently increased between 1.4-1.35 Ga (Figure 5.2; Zhang et al, 2016; Yang et al., 2017; Diamond et al., 2018b). This period coincides with a very large pulse of LIP volcanism related to the incomplete breakup of Nuna (Zhang et al., 2018; 2021). We briefly reviewed biogeochemical modeling studies that have attempted to constrain the many interrelated processes that ultimately controlled primary productivity and O_2 production during the mid-Proterozoic, and we went on to offer a possibility for how continental LIP volcanism would have affected such a system. The rapid weathering of extrusive volcanics and resultant delivery of P could sustain productivity in shallow shelf settings for an extended period—driving export production, organic matter burial, and the accumulation of O_2 in the surface ocean and atmosphere. Once the weathering flux diminished, conditions would presumably have relaxed back to the pre-perturbation steady state.

LIP emplacement and weathering offer one possible mechanism to force the surficial environment into a state that lies outside the bounds imposed by long-term stabilizing feedbacks. The temporal coincidence between enhanced LIP activity and environmental oxygenation at ~1.4 Ga suggests a possible connection. Significant LIP

activity (Franklin and Irkutsk LIPs events; Ernst et al. 2016) also accompanied the breakup of Rodinia beginning in the Early Neoproterozoic, much of it in close temporal proximity to the onset of the Sturtian glaciation (e.g., Macdonald et al., 2010; Horton, 2015; Cox et al., 2016).

If the breakup of Rodinia was solely responsible for the climatic upheavals of the Neoproterozoic, it begs the question of why the Earth-system responded so differently to the attempted breakup of Nuna. At least part of the answer lies with the likelihood that the breakups of these two supercontinents were qualitatively different (Roberts, 2014, Evans and Mitchell, 2011). The suggestion that the differing tectonic implications of each event acted in isolation, however, fails to consider the role that the evolving biosphere played in modulating Earth's biogeochemical response to each. Were the same supercontinental breakup to have occurred in both the mid- and Neoproterozoic, the climatic responses would not necessarily have been the same, given the significant biological evolution that took place in the interim. As more, diverse data are produced, our picture of the Proterozoic Earth continues to look, perhaps not surprisingly, more and more like a dynamic planet. As we search for an understanding of the cause-and-effect relationships that brought that world to be, it is critical that the roles and intersections of both geological and biological processes be considered.

References

Anbar, A. D., & Knoll, A. H. (2002). Proterozoic ocean chemistry and evolution: a bioinorganic bridge? Science, 297(5584), 1137-1142.

Andersen, M. B., Vance, D., Morford, J. L., Bura-Nakić, E., Breitenbach, S. F., & Och, L. (2016). Closing in on the marine 238U/235U budget. Chemical Geology, 420, 11-22.

Bachan, A., & Kump, L. R. (2015). The rise of oxygen and siderite oxidation during the Lomagundi Event. Proceedings of the National Academy of Sciences, 201422319.

Banks, M. K., Schwab, A. P., & Henderson, C. (2006). Leaching and reduction of chromium in soil as affected by soil organic content and plants. Chemosphere, 62(2), 255-264.

Blättler, C. L., Claire, M. W., Prave, A. R., Kirsimäe, K., Higgins, J. A., Medvedev, P. V., ... & Kreitsmann, T. (2018). Two-billion-year-old evaporites capture Earth's great oxidation. Science, 360(6386), 320-323.

Rodler, A., Sánchez-Pastor, N., Fernández-Díaz, L., & Frei, R. (2015). Fractionation behavior of chromium isotopes during coprecipitation with calcium carbonate: implications for their use as paleoclimatic proxy. Geochimica et Cosmochimica Acta, 164, 221-235.

Brasier, M. D., & Lindsay, J. F. (1998). A billion years of environmental stability and the emergence of eukaryotes: new data from northern Australia. Geology, 26(6), 555-558.

Buick, R., Des Marais, D. J., & Knoll, A. H. (1995). Stable isotopic compositions of carbonates from the Mesoproterozoic Bangemall Group, northwestern Australia. Chemical Geology, 123(1-4), 153-171.

Campbell, I. H., & Allen, C. M. (2008). Formation of supercontinents linked to increases in atmospheric oxygen. Nature Geoscience, 1(8), 554.

Canfield, D. E. (1998). A new model for Proterozoic ocean chemistry. Nature, 396(6710), 450.

Canfield, D. E. (2005). The early history of atmospheric oxygen: homage to Robert M. Garrels. Annu. Rev. Earth Planet. Sci., 33, 1-36.

Canfield, D. E., Zhang, S., Frank, A. B., Wang, X., Wang, H., Su, J., ... & Frei, R. (2018). Highly fractionated chromium isotopes in Mesoproterozoic-aged shales and atmospheric oxygen. Nature communications, 9(1), 2871.

Caplan, M. L., & Bustin, R. M. (1999). Devonian–Carboniferous Hangenberg mass extinction event, widespread organic-rich mudrock and anoxia: causes and consequences. Palaeogeography, Palaeoclimatology, Palaeoecology, 148(4), 187-207.

Catling, D. C., Zahnle, K. J., & McKay, C. P. (2001). Biogenic methane, hydrogen escape, and the irreversible oxidation of early Earth. Science, 293(5531), 839-843.

Claire, M. W., Catling, D. C., & Zahnle, K. J. (2006). Biogeochemical modelling of the rise in atmospheric oxygen. Geobiology, 4(4), 239-269.

Coffin, M. F., & Eldholm, O. (1994). Large igneous provinces: crustal structure, dimensions, and external consequences. Reviews of Geophysics, 32(1), 1-36.

Cohen, P. A., & Macdonald, F. A. (2015). The Proterozoic record of eukaryotes. Paleobiology, 41(4), 610-632.

Condie, K. C. (2013). Plate Tectonics & Crustal Evolution. Elsevier.

Cox, G. M., Halverson, G. P., Stevenson, R. K., Vokaty, M., Poirier, A., Kunzmann, M., ... & Macdonald, F. A. (2016). Continental flood basalt weathering as a trigger for Neoproterozoic Snowball Earth. Earth and Planetary Science Letters, 446, 89-99.

Cui, H., Kaufman, A. J., Xiao, S., Zhou, C., & Liu, X. M. (2017). Was the Ediacaran Shuram Excursion a globally synchronized early diagenetic event? Insights from methane-derived authigenic carbonates in the uppermost Doushantuo Formation, South China. Chemical Geology, 450, 59-80.

Daines, S. J., Mills, B. J., & Lenton, T. M. (2017). Atmospheric oxygen regulation at low Proterozoic levels by incomplete oxidative weathering of sedimentary organic carbon. Nature communications, 8, 14379.

Dahl, T. W., Hammarlund, E. U., Anbar, A. D., Bond, D. P., Gill, B. C., Gordon, G. W., ... & Canfield, D. E. (2010). Devonian rise in atmospheric oxygen correlated to the

radiations of terrestrial plants and large predatory fish. Proceedings of the National Academy of Sciences, 107(42), 17911-17915.

De Kock, M.O., Ernst, R., Söderlund, U., Jourdan, F., Hofmann, A., Le Gall, B., … & Fuchs, R. (2014). Dykes of the 1.11 Ga Umkondo LIP, Southern Africa: Clues to a complex plumbing system. Precambrian Research, 249, 129-143

Derry, L. A. (2015). Causes and consequences of mid-Proterozoic anoxia. Geophysical Research Letters, 42(20), 8538-8546.

Des Marais, D. J., Strauss, H., Summons, R. E., & Hayes, J. M. (1992). Carbon isotope evidence for the stepwise oxidation of the Proterozoic environment. Nature, 359(6396), 605.

Diamond, C. W., & Lyons, T. W. (2018a). Mid-Proterozoic redox evolution and the possibility of transient oxygenation events. Emerging Topics in Life Sciences, 2(2), 235-245.

Diamond, C. W., Planavsky, N. J., Wang, C., & Lyons, T. W. (2018b). What the~ 1.4 Ga Xiamaling Formation can and cannot tell us about the mid-Proterozoic ocean. Geobiology, 16(3), 219-236.

Donnadieu, Y., Goddéris, Y., Ramstein, G., Nédélec, A., & Meert, J. (2004). A 'snowball Earth'climate triggered by continental break-up through changes in runoff. Nature, 428(6980), 303.

Dunk, R., Mills, R., and Jenkins, W. (2002) A reevaluation of the oceanic uranium budget for the Holocene. Chemical Geology, 190(1-4):45–67.

Eary, L. E., & Rai, D. (1987). Kinetics of chromium (III) oxidation to chromium (VI) by reaction with manganese dioxide. Environmental Science & Technology, 21(12), 1187-1193.

Edgcomb, V., Orsi, W., Bunge, J., Jeon, S., Christen, R., Leslin, C., ... & Epstein, S. (2011). Protistan microbial observatory in the Cariaco Basin, Caribbean. I. Pyrosequencing vs Sanger insights into species richness. The ISME Journal, 5(8), 1344.

Ernst, R. E. (2014). Large igneous provinces. Cambridge University Press.

Ernst, R. E., & Youbi, N. (2017). How Large Igneous Provinces affect global climate, sometimes cause mass extinctions, and represent natural markers in the geological record. Palaeogeography, Palaeoclimatology, Palaeoecology, 478, 30-52.

Ernst, R. E., Wingate, M. T. D., Buchan, K. L., & Li, Z. X. (2008). Global record of 1600–700 Ma Large Igneous Provinces (LIPs): implications for the reconstruction of the proposed Nuna (Columbia) and Rodinia supercontinents. Precambrian Research, 160(1-2), 159-178.

Ernst, R. E., Hamilton, M. A., Söderlund, U., Hanes, J. A., Gladkochub, D. P., Okrugin, A. V., ... & Buchan, K. L. (2016). Long-lived connection between southern Siberia and northern Laurentia in the Proterozoic. Nature Geoscience, 9(6), 464.

Ernst, R. E., Bond, D. P. G., Zhang, S-H., Buchan, K. L., Grasby, S. E., Youbi, N., El Bilali, H., Bekker, A. (2020). LIP record through time and implications for secular environmental changes and GTS boundaries, In: Ernst, R.E., Dickson, A., Bekker, A. (ed.) Environmental Change and Large Igneous Provinces: The Deadly Kiss of LIPs,

Erwin, D. H. (1994). The Permo–Triassic extinction. Nature, 367(6460), 231.

Evans, D. A., & Mitchell, R. N. (2011). Assembly and breakup of the core of Paleoproterozoic–Mesoproterozoic supercontinent Nuna. Geology, 39(5), 443-446.

Farquhar, J., Bao, H., & Thiemens, M. (2000). Atmospheric influence of Earth's earliest sulfur cycle. Science, 289(5480), 756-758.

Farquhar, J., & Wing, B. A. (2003). Multiple sulfur isotopes and the evolution of the atmosphere. Earth and Planetary Science Letters, 213(1-2), 1-13.

Fike, D.A., Grotzinger, J.P., Pratt, L.M. and Summons, R.E. (2006). Oxidation of the Ediacaran ocean. Nature, 444(7120), 744.

Frei, R., Gaucher, C., Poulton, S. W., & Canfield, D. E. (2009). Fluctuations in Precambrian atmospheric oxygenation recorded by chromium isotopes. Nature, 461(7261), 250.

Galy, V., France-Lanord, C., Beyssac, O., Faure, P., Kudrass, H., & Palhol, F. (2007). Efficient organic carbon burial in the Bengal fan sustained by the Himalayan erosional system. Nature, 450(7168), 407.

Gilleaudeau, G. J., Frei, R., Kaufman, A. J., Kah, L. C., Azmy, K., Bartley, J. K., ... & Knoll, A. H. (2016). Oxygenation of the mid-Proterozoic atmosphere: clues from chromium isotopes in carbonates. Geochemical Perspectives Letters, 2, 178-187.

Goddéris, Y., Donnadieu, Y., Nédélec, A., Dupré, B., Dessert, C., Grard, A., ... & Francois, L. M. (2003). The Sturtian 'snowball'glaciation: fire and ice. Earth and Planetary Science Letters, 211(1-2), 1-12.

Gough, D. O. (1981). Solar interior structure and luminosity variations. In Physics of Solar Variations (pp. 21-34). Springer, Dordrecht.

Guilbaud, R., Poulton, S.W., Butterfield, N.J., Zhu, M. and Shields-Zhou, G.A. (2015). A global transition to ferruginous conditions in the early Neoproterozoic oceans. Nature Geoscience, 8(6), 4466.

Gumsley, A. P., Chamberlain, K. R., Bleeker, W., Söderlund, U., de Kock, M. O., Larsson, E. R., & Bekker, A. (2017). Timing and tempo of the Great Oxidation Event. Proceedings of the National Academy of Sciences, 114(8), 1811-1816.

Hardisty, D. S., Lu, Z., Planavsky, N. J., Bekker, A., Philippot, P., Zhou, X., & Lyons, T. W. (2014). An iodine record of Paleoproterozoic surface ocean oxygenation. Geology, 42(7), 619-622.

Hardisty, D. S., Lu, Z., Bekker, A., Diamond, C. W., Gill, B. C., Jiang, G., ... & Planavsky, N. J. (2017). Perspectives on Proterozoic surface ocean redox from iodine contents in ancient and recent carbonate. Earth and Planetary Science Letters, 463, 159-170.

Hoffman, P. F. (1999). The break-up of Rodinia, birth of Gondwana, true polar wander and the snowball Earth. Journal of African Earth Sciences, 28(1), 17-33.

Holland, H. D. (2006). The oxygenation of the atmosphere and oceans. Philosophical Transactions of the Royal Society of London B: Biological Sciences, 361(1470), 903-915.

Horton, F. (2015). Did phosphorus derived from the weathering of large igneous provinces fertilize the Neoproterozoic ocean? Geochemistry, Geophysics, Geosystems, 16(6), 1723-1738.

Huaikun, L., ChuanLin, Z., Zhenqun, X., Songnian, L., Jian, Z., Jianzhen, G., ... & Zhixian, W. (2013). Zircon and baddeleyite U-Pb geochronology of the Shennongjia Group in the Yangtze Craton and its tectonic significance. Acta Petrologica Sinica, 29(2), 673-697.

Johnston, D. T., Poulton, S. W., Goldberg, T., Sergeev, V. N., Podkovyrov, V., Vorob'Eva, N. G., ... & Knoll, A. H. (2012a). Late Ediacaran redox stability and metazoan evolution. Earth and Planetary Science Letters, 335, 25-35.

Johnston, D. T., Macdonald, F. A., Gill, B. C., Hoffman, P. F., & Schrag, D. P. (2012b). Uncovering the Neoproterozoic carbon cycle. Nature, 483(7389), 320.

Jones, C., Nomosatryo, S., Crowe, S. A., Bjerrum, C. J., & Canfield, D. E. (2015). Iron oxides, divalent cations, silica, and the early earth phosphorus crisis. Geology, 43(2), 135-138.

Kah, L. C., Lyons, T. W., & Frank, T. D. (2004). Low marine sulphate and protracted oxygenation of the Proterozoic biosphere. Nature, 431(7010), 834.

Karhu, J. A., & Holland, H. D. (1996). Carbon isotopes and the rise of atmospheric oxygen. Geology, 24(10), 867-870.

Kipp, M.A. and Stüeken, E.E. (2017). Biomass recycling and Earth's early phosphorus cycle. Science advances, 3(11), eaao4795.

Klaebe, R. M., Kennedy, M. J., Jarrett, A. J. M., & Brocks, J. J. (2017). Local paleoenvironmental controls on the carbon-isotope record defining the Bitter Springs Anomaly. Geobiology, 15(1), 65-80.

Knoll, A. H. (2014). Paleobiological perspectives on early eukaryotic evolution. Cold Spring Harbor Perspectives in Biology, 6(1), a016121.

Kotaś, J., & Stasicka, Z. (2000). Chromium occurrence in the environment and methods of its speciation. Environmental Pollution, 107(3), 263-283.

Laakso, T. A., & Schrag, D. P. (2014). Regulation of atmospheric oxygen during the Proterozoic. Earth and Planetary Science Letters, 388, 81-91.

Laakso, T. A., & Schrag, D. P. (2018). Limitations on limitation. Global Biogeochemical Cycles, 32(3), 486-496.

Laakso, T.A. and Schrag, D.P. (2019). A small marine biosphere in the Proterozoic. Geobiology, 17(2), 161-171.

Lenton TM & Daines SJ (2017). Biogeochemical Transformations in the History of the Ocean. Annual Review of Marine Science 9(1), 31-58.

Levin, L.A. (2003). Oxygen minimum zone benthos: adaptation and community response to hypoxia. Oceanogr. Mar. Biol. 41, 1–45

Li, C., Hardisty, D. S., Luo, G., Huang, J., Algeo, T. J., Cheng, M., ... & Jiao, N. (2017). Uncovering the spatial heterogeneity of Ediacaran carbon cycling. Geobiology, 15(2), 211-224.

Li, Q., & Leng, J. (1991). The Upper Precambrian in the Shennongjia Region. Science and Technology Publishing House, Tianjin.

Li, Z. X., Evans, D. A. D., & Zhang, S. (2004). A 90 spin on Rodinia: possible causal links between the Neoproterozoic supercontinent, superplume, true polar wander and low-latitude glaciation. Earth and Planetary Science Letters, 220(3-4), 409-421.

Lu, W., Wörndle, S., Halverson, G. P., Zhou, X., Bekker, A., Rainbird, R. H., ... & Lu, Z. (2017). Iodine proxy evidence for increased ocean oxygenation during the Bitter Springs Anomaly. Geochem. Perspect. Lett., 5, 53-57.

Lu, W., Ridgwell, A., Thomas, E., Hardisty, D. S., Luo, G., Algeo, T. J., ... & Edwards, C. T. (2018). Late inception of a resiliently oxygenated upper ocean. Science, eaar5372.

Lu, Z., Jenkyns, H. C., & Rickaby, R. E. (2010). Iodine to calcium ratios in marine carbonate as a paleo-redox proxy during oceanic anoxic events. Geology, 38(12), 1107-1110.

Luo, G., Ono, S., Beukes, N. J., Wang, D. T., Xie, S., & Summons, R. E. (2016). Rapid oxygenation of Earth's atmosphere 2.33 billion years ago. Science Advances, 2(5), e1600134.

Lyons, T. W., Reinhard, C. T., & Planavsky, N. J. (2014). The rise of oxygen in Earth's early ocean and atmosphere. Nature, 506(7488), 307.

Macdonald, F. A., Schmitz, M. D., Crowley, J. L., Roots, C. F., Jones, D. S., Maloof, A. C., ... & Schrag, D. P. (2010). Calibrating the cryogenian. Science, 327(5970), 1241-1243.
Maher, K., Bargar, J. R., & Brown Jr, G. E. (2012). Environmental speciation of actinides. Inorganic Chemistry, 52(7), 3510-3532.

Martin, A. P., Condon, D. J., Prave, A. R., & Lepland, A. (2013). A review of temporal constraints for the Palaeoproterozoic large, positive carbonate carbon isotope excursion (the Lomagundi–Jatuli Event). Earth-Science Reviews, 127, 242-261.

Melezhik, V. A., Huhma, H., Condon, D. J., Fallick, A. E., & Whitehouse, M. J. (2007). Temporal constraints on the Paleoproterozoic Lomagundi-Jatuli carbon isotopic event. Geology, 35(7), 655-658.

Mills, D. B., Ward, L. M., Jones, C., Sweeten, B., Forth, M., Treusch, A. H., & Canfield, D. E. (2014). Oxygen requirements of the earliest animals. Proceedings of the National Academy of Sciences, 111(11), 4168-4172.

Morford, J. L., and Emerson, S. (1999). The geochemistry of redox sensitive trace metals in sediments. Geochimica et Cosmochimica Acta, 63(11), 1735-1750.

Müller, M., Mentel, M., van Hellemond, J. J., Henze, K., Woehle, C., Gould, S. B., ... & Martin, W. F. (2012). Biochemistry and evolution of anaerobic energy metabolism in eukaryotes. Microbiology and Molecular Biology Reviews, 76(2), 444-495.

Nursall, J. R. (1959). Oxygen as a prerequisite to the origin of the Metazoa. Nature, 183(4669), 1170.

Orsi, W., Song, Y. C., Hallam, S., & Edgcomb, V. (2012a). Effect of oxygen minimum zone formation on communities of marine protists. The ISME journal, 6(8), 1586.

Orsi, W. D., Charvet, S., Vdacny, P., Bernhard, J. M., & Edgcomb, V. P. (2012b). Prevalence of partnerships between bacteria and ciliates in oxygen-depleted marine water columns. Frontiers in Microbiology, 3, 341.

Ozaki, K., Reinhard, C. T., & Tajika, E. (2018). A sluggish mid-Proterozoic biosphere and its effect on Earth's redox balance. Geobiology.

Partin, C. A., Bekker, A., Planavsky, N. J., Scott, C. T., Gill, B. C., Li, C., ... & Love, G. D. (2013). Large-scale fluctuations in Precambrian atmospheric and oceanic oxygen levels from the record of U in shales. Earth and Planetary Science Letters, 369, 284-293.

Pavlov, A. A., & Kasting, J. F. (2002). Mass-independent fractionation of sulfur isotopes in Archean sediments: strong evidence for an anoxic Archean atmosphere. Astrobiology, 2(1), 27-41.

Payne, J. L., Boyer, A. G., Brown, J. H., Finnegan, S., Kowalewski, M., Krause, R. A., ... & Smith, F. A. (2009). Two-phase increase in the maximum size of life over 3.5 billion years reflects biological innovation and environmental opportunity. Proceedings of the National Academy of Sciences, 106(1), 24-27.

Payne, J. L., McClain, C. R., Boyer, A. G., Brown, J. H., Finnegan, S., Kowalewski, M., ... & Smith, F. A. (2011). The evolutionary consequences of oxygenic photosynthesis: a body size perspective. Photosynthesis Research, 107(1), 37-57.

Pereira, N. S., Vögelin, A. R., Paulukat, C., Sial, A. N., Ferreira, V. P., & Frei, R. (2016). Chromium-isotope signatures in scleractinian corals from the Rocas Atoll, Tropical South Atlantic. Geobiology, 14(1), 54-67.

Planavsky, N. J., Bekker, A., Hofmann, A., Owens, J. D., & Lyons, T. W. (2012). Sulfur record of rising and falling marine oxygen and sulfate levels during the Lomagundi event. Proceedings of the National Academy of Sciences, 109(45), 18300-18305.

Planavsky, N. J., Reinhard, C. T., Wang, X., Thomson, D., McGoldrick, P., Rainbird, R. H., ... & Lyons, T. W. (2014). Low Mid-Proterozoic atmospheric oxygen levels and the delayed rise of animals. Science, 346(6209), 635-638.

Planavsky, N. J., Cole, D. B., Reinhard, C. T., Diamond, C., Love, G. D., Luo, G., ... & Lyons, T. W. (2016). No evidence for high atmospheric oxygen levels 1,400 million years ago. Proceedings of the National Academy of Sciences, 113(19), E2550-E2551.

Planavsky, N. J., Slack, J. F., Cannon, W. F., O'Connell, B., Isson, T. T., Asael, D., ... & Bekker, A. (2018). Evidence for episodic oxygenation in a weakly redox-buffered deep mid-Proterozoic ocean. Chemical Geology, 483, 581-594.

Puzon, G. J., Tokala, R. K., Zhang, H., Yonge, D., Peyton, B. M., & Xun, L. (2008). Mobility and recalcitrance of organo–chromium (III) complexes. Chemosphere, 70(11), 2054-2059.

Reinhard, C. T., Planavsky, N. J., Robbins, L. J., Partin, C. A., Gill, B. C., Lalonde, S. V., ... & Lyons, T. W. (2013). Proterozoic ocean redox and biogeochemical stasis. Proceedings of the National Academy of Sciences, 201208622.

Reinhard, C. T., Planavsky, N. J., Olson, S. L., Lyons, T. W., & Erwin, D. H. (2016). Earth's oxygen cycle and the evolution of animal life. Proceedings of the National Academy of Sciences, 113(32), 8933-8938.

Reinhard, C. T., Planavsky, N. J., Gill, B. C., Ozaki, K., Robbins, L. J., Lyons, T. W., ... & Konhauser, K. O. (2017). Evolution of the global phosphorus cycle. Nature, 541(7637), 386.

Roberts, N. M. (2013). The boring billion?–Lid tectonics, continental growth and environmental change associated with the Columbia supercontinent. Geoscience Frontiers, 4(6), 681-691.

Rue, E. L., Smith, G. J., Cutter, G. A., & Bruland, K. W. (1997). The response of trace element redox couples to suboxic conditions in the water column. Deep Sea Research Part I: Oceanographic Research Papers, 44(1), 113-134.

Sahoo, S. K., Planavsky, N. J., Jiang, G., Kendall, B., Owens, J. D., Wang, X., ... & Lyons, T. W. (2016). Oceanic oxygenation events in the anoxic Ediacaran ocean. Geobiology, 14(5), 457-468.

Schulte, P., Alegret, L., Arenillas, I., Arz, J. A., Barton, P. J., Bown, P. R., ... & Collins, G. S. (2010). The Chicxulub asteroid impact and mass extinction at the Cretaceous-Paleogene boundary. Science, 327(5970), 1214-1218.

Scott, C., Lyons, T. W., Bekker, A., Shen, Y. A., Poulton, S. W., Chu, X. L., & Anbar, A. D. (2008). Tracing the stepwise oxygenation of the Proterozoic ocean. Nature, 452(7186), 456.

Shi, W., Li, C., Luo, G., Huang, J., Algeo, T. J., Jin, C., ... & Cheng, M. (2018). Sulfur isotope evidence for transient marine-shelf oxidation during the Ediacaran Shuram Excursion. Geology, 46(3), 267-270.

Sperling, E. A., Frieder, C. A., Raman, A. V., Girguis, P. R., Levin, L. A., & Knoll, A. H. (2013). Oxygen, ecology, and the Cambrian radiation of animals. Proceedings of the National Academy of Sciences, 110(33), 13446-13451.

Sperling, E. A., Wolock, C. J., Morgan, A. S., Gill, B. C., Kunzmann, M., Halverson, G. P., ... & Johnston, D. T. (2015). Statistical analysis of iron geochemical data suggests limited late Proterozoic oxygenation. Nature, 523(7561), 451.

Summons, R. E., Bradley, A. S., Jahnke, L. L., & Waldbauer, J. R. (2006). Steroids, triterpenoids and molecular oxygen. Philosophical Transactions of the Royal Society of London B: Biological Sciences, 361(1470), 951-968.

Taverne, Y. J., Merkus, D., Bogers, A. J., Halliwell, B., Duncker, D. J., & Lyons, T. W. (2018). Reactive Oxygen Species: Radical Factors in the Evolution of Animal Life: A molecular timescale from Earth's earliest history to the rise of complex life. Bioessays, 40(3), 1700158.

Turgeon, S. C., & Creaser, R. A. (2008). Cretaceous oceanic anoxic event 2 triggered by a massive magmatic episode. Nature, 454(7202), 323.

Wallace, M. W., Shuster, A., Greig, A., Planavsky, N. J., & Reed, C. P. (2017). Oxygenation history of the Neoproterozoic to early Phanerozoic and the rise of land plants. Earth and Planetary Science Letters, 466, 12-19.

Wignall, P. B., & Twitchett, R. J. (1996). Oceanic anoxia and the end Permian mass extinction. Science, 272(5265), 1155-1158.

Wignall, P. B. (2001). Large igneous provinces and mass extinctions. Earth Science Reviews, 53(1), 1-33.

Yang, S., Kendall, B., Lu, X., Zhang, F., & Zheng, W. (2017). Uranium isotope compositions of mid-Proterozoic black shales: Evidence for an episode of increased ocean oxygenation at 1.36 Ga and evaluation of the effect of post-depositional hydrothermal fluid flow. Precambrian Research, 298, 187-201.

Zhang, S., Wang, X., Wang, H., Bjerrum, C. J., Hammarlund, E. U., Costa, M. M., ... & Canfield, D. E. (2016). Sufficient oxygen for animal respiration 1,400 million years ago. Proceedings of the National Academy of Sciences, 113(7), 1731-1736.

Zhang, S. H., Ernst, R. E., Pei, J. L., Zhao, Y., Zhou, M. F., & Hu, G. H. (2018). A temporal and causal link between ca. 1380 Ma large igneous provinces and black shales: Implications for the Mesoproterozoic time scale and paleoenvironment. Geology, 46(11), 963-966.

Zhang, S.H., Ernst, R.E., Pei, J. L., Zhao, Y., & Hu, G. H. (2020) LIPs (large igneous provinces) and anoxia events in 'the Boring Billion'. In: Ernst, R.E., Dickson, A., A., Bekker, A. (ed.) Environmental Change and Large Igneous Provinces: The Deadly Kiss of LIPs, accepted.

Zink, S., Schoenberg, R., & Staubwasser, M. (2010). Isotopic fractionation and reaction kinetics between Cr (III) and Cr (VI) in aqueous media. Geochimica et Cosmochimica Acta, 74(20), 5729-5745.

Chapter 6

Middle Ordovician paleoenvironmental evolution of the western Laurentian carbonate platform

Preface:

The contents of this chapter, less the forward, have been submitted for publication in a modified form, the anticipated reference for this publication is:

> Diamond, C.W., Edwards, C.T., Saltzman, M.R. and Lyons, T.W., 2021. Middle Ordovician paleoenvironmental evolution of the western Laurentian carbonate platform. Palaeogeography, Palaeoclimatology, Palaeoecology.

Forward

The final chapter presenting new data in this dissertation takes a large step forward in time to the Great Ordovician Biodiversification Event (GOBE). This 'event' was a protracted period spanning the Early and Middle Ordovician Period, during which animal evolution took unprecedented strides. My interest in this period began during my undergraduate work with Matt Saltzman at Ohio State, where I completed a thesis on carbon isotope data that we measured in samples from Meiklejohn Peak in western Nevada. It was a formative time for me as a scientifically minded individual, and I found the GOBE a fascinating topic. It was also an amazing opportunity that Matt made possible for me, and for that I am incredibly grateful.

The data that we produced at Ohio State appear in this Chapter with additional geochemical measurements that were made at UCR. These data, along with a detailed

sedimentological investigation, provide a detailed picture into about ten million years of the changing environmental conditions in a single location on the margin of modern North America. While there are not many groundbreaking conclusions to be drawn from this dataset, it does speak to the general conditions present in the shallow oceans at the time. It is also a nice demonstration of the methodology that I have adopted for the measurement of iodine in carbonate rocks.

Abstract

The Great Ordovician Biodiversification Event (GOBE) encompasses a series of rapid and sustained diversification pulses unparalleled in Earth history. Despite the uniqueness and magnitude of the GOBE, a singular driving force for this critical interval has not been identified. Multiple hypotheses have been presented, some pairing the GOBE as cause and effect with extrinsic factors such as changing global temperatures, ocean chemistry, or paleogeography, while others have pointed to factors intrinsic to biology itself, such as the proliferation of skeletonization, predator-prey escalation, or the development of complex tiered seafloor communities. Sufficient data are not available at present to ascertain what combination of these factors was the key to generating the GOBE.

Here, we present new paired carbon and sulfur isotope data ($\delta^{13}C_{carb}$, $\delta^{13}C_{org}$, and $\delta^{34}S_{CAS}$), along with iodine concentration data from a Darriwilian carbonate sequence exposed at Meiklejohn Peak in Nye county, Nevada. Within a detailed lithologic and biostratigraphic framework, these new data provide a robust correlation to chemostratigraphic zonation established in Baltica along with insights into the evolution

of Middle Ordovician biogeochemical cycling. The carbon isotope data demonstrate a significant increase in the fractionation between carbonate carbon and organic matter ($\Delta^{13}C$) during the onset of the middle Darriwilian carbon isotope excursion (MDICE), and new carbonate-associated sulfate (CAS) sulfur isotope data support a decrease in global pyrite burial during this time. Both of these observations support previous work arguing for an increase in the $[O_2]$ of the global oceans at this time. New iodine concentration data from Meiklejohn Peak also suggest a progressive and sustained increase in the $[O_2]$ of regional waters throughout the Darriwilian during a period of relative sea-level highstand. This expansion of stably well-oxygenated ecospace could have laid the foundation for rapid diversification during one of the largest pulses of the GOBE.

Introduction

The largest sustained biological diversification in animal history occurred during the Ordovician Period, the so-called Great Ordovician Biodiversification Event or GOBE (e.g. Sepkoski, 1981, 1995, 2002; Droser and Sheehan, 1997; Webby et al., 2004; Harper 2006; Harper et al., 2015). Despite the name, the GOBE is now understood to be not so much an event but rather a protracted period of enhanced origination, punctuated by several discrete pulses of rapid diversification (Webby et al., 2004; Zhan et al., 2005; Chen et al., 2006; Harper et al., 2006). The causal mechanisms for the GOBE have remained elusive and more than likely involve a complex interplay between both intrinsic and extrinsic factors (Harper et al., 2015). In order to further our understanding of various causal mechanisms, an improved understanding of the timing of events, both relative and absolute, is needed. Stable carbon isotope data from marine carbonates (δ^{13}Ccarb) along with biostratigraphy have been useful tools for global correlation, in particular the many positive δ^{13}Ccarb excursions present throughout the lower Paleozoic (e.g., Brenchly et al., 1994; Saltzman et al., 1998, 2000; Bergström et al., 2006; Kaljo et al., 2007; Ainsaar et al., 2010, Cramer et al., 2010; Munnecke et al., 2011; Calner et al., 2014).

These δ^{13}Ccarb excursions also serve as important markers of perturbations to the global carbon cycle, often related to episodes of enhanced organic carbon burial and dynamic changes in oceanic redox conditions (e.g., Kump and Arthur, 1999). One of the largest increases in global diversity of the GOBE (i.e., observed in multiple paleogeographic blocks) occurred in the Darriwilian stage of the Middle Ordovician (Rasmussen et al., 2007). At approximately this same time, the first major δ^{13}Ccarb

excursion of the Ordovician occurred, known as the Mid-Darriwilian Carbon Isotope Excursion (MDICE) (Ainsaar et al., 2004; Kaljo et al., 2007; Schmitz et al., 2010; Leslie et al., 2011; Calner et al., 2014; Edwards and Saltzman, 2016; Young et al., 2016), giving rise to the possibility that a causal link exists between the two (Edwards et al, 2017).

In addition to the potential for the $\delta^{13}C_{carb}$ record to elucidate perturbations to the global carbon cycle, further environmental information can often be gleaned from the record when coupled with other geochemical data (e.g., Gill et al., 2007, 2011; Hurtgen et al., 2009; Young et al., 2008, 2016; Saltzman et al., 2011; Pancost et al., 2013; Edwards and Saltzman, 2016). Many studies have examined paired analyses of carbon ($\delta^{13}C$) and sulfur isotopes ($\delta^{34}S$), as these two intimately linked biogeochemical cycles exert a first-order control on the oxidant budget of Earth's surface environments (e.g., Gill et al., 2007, 2011; Hurtgen et al., 2009; Jones and Fike, 2013; Young et al., 2016). Through the burial of reduced C and S species (i.e., organic carbon and iron sulfides), oxygen (O_2) is liberated to the ocean-atmosphere system, where it can then be consumed through the oxidation of reduced C and S in the ocean or exposed on land, completing the cycle (Holland, 1973; Kump and Garrels, 1986; Berner, 2006). The known isotopic fractionations associated with these processes have allowed mass-balance modeling approaches to estimate fluctuations in the O_2 budget of the ocean-atmosphere system through time (e.g., Kump and Garrels, 1986; Berner, 2006)

Other studies have used more direct approaches to estimate environmental O_2 levels, with examples that include the coupling of carbonate and organic carbon isotope data ($\delta^{13}C_{carb}$ and $\delta^{13}C_{org}$) and the iodine concentrations in shallow water carbonate rocks

typically presented as the ratio of iodine to the sum of calcium and magnesium (I/(Ca+Mg); e.g., Edwards et al., 2017; Lu et al., 2018). The magnitude of fractionation between photosynthetically derived organic matter and aqueous CO_2 has been shown to scale with both pCO_2 and pO_2, and hence, in the absence of changes in ambient pCO_2 or the community of primary producers, the magnitude of this fractionation ($\delta^{13}C_{carb}$ - $\delta^{13}C_{org}$, or $\Delta^{13}C$) can track local pO_2 (Berner et al., 2000). Iodine concentrations in carbonate rocks also have the potential to track local O_2 concentrations, as the oxidized iodate species (IO_3^-) will readily substitute into the lattice of precipitating carbonates at a rate proportional to its concentration in ambient waters, while the reduced iodide species (I^-) will be wholly excluded (Liu et al., 2010).

Here, we present paired $\delta^{13}C_{carb}$ and $\delta^{13}C_{org}$ data along with carbonate-associated sulfate (CAS) sulfur isotope data ($\delta^{34}S_{CAS}$) and I/(Ca+Mg) ratios from a thick and well-exposed Middle Ordovician carbonate succession at Meiklejohn Peak in western Nevada, USA (Figure 6.1). Multiple workers have previously studied the exposures at this location, and a detailed macro- and microfossil biostratigraphic framework has been established (Ross, 1972; Harris et al., 1979; Ross et al., 1991). Meiklejohn Peak is unique in western North America in that zonally diagnostic conodonts from both the North Atlantic province and the North American Midcontinent province have been identified in the sampled section, allowing for correlation to key stratigraphic sections worldwide (Harris et al., 1979).

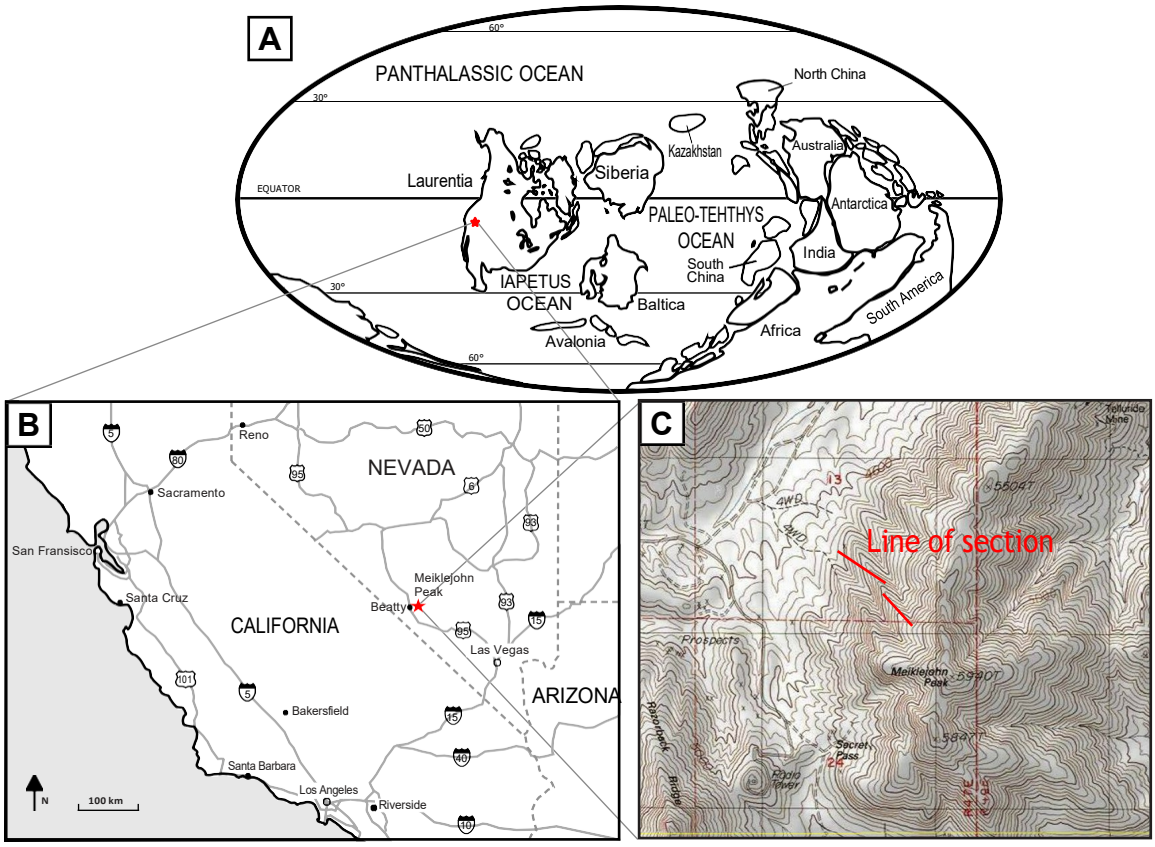

Figure 6.1. Location information for Meiklejohn Peak and the line of section. Panel A shows a paleogeographic reconstruction of the Middle Ordovician (after Cocks and Torsvik, 2002). Panel B and C show the modern location of Meiklejohn Peak (southwestern Nevada) and the line of section on a cropped USGS topographic map, respectively.

Background

Geologic setting

During the Middle Ordovician, Laurentia was roughly centered on the equator (Figure 6.1; Cocks and Torsvik, 2002). Passive margin deposition throughout this time resulted in a thick and mostly continuous carbonate succession before being interrupted, diachronously, by the deposition of the regionally extensive Eureka Quartzite (Poole et al., 1992). Meiklejohn Peak is situated in southwest Nevada, approximately 8 km southeast of

the town of Beatty and 4.5 km northeast of Bear Mountain (Figure 6.1). There are exposures of Ordovician limestone and calcareous shale along its western flank with a high angle fault dividing the northwest slope from the southwest, the south fault block having been uplifted relative to the north (Monsen et al., 1992). On both the northwest and southwest sides of Meiklejohn Peak, the top of the Goodwin Limestone, the Nine Mile Shale, and part of the Antelope Valley Limestone are exposed, though on the northwest side, the Goodwin Limestone and Nine Mile Shale dip below the surface rapidly, leaving only small exposures nearest to the fault (Ross et al., 1972, 1991; Monsen et al., 1992). Moving away from the fault to the north, the entire Antelope Valley Limestone is exposed along with the overlying Eureka Quartzite and Ely Springs Dolomite (Monsen et al., 1992).

The Antelope Valley Limestone is divided into three informal members (Ross et al., 1972). A section has been measured on the southwest side of Meiklejohn Peak containing a large biohermal mound within the lower member, which has been the focus of extensive study (e.g., Ross, 1961, 1972, 1975; Krause and Rowell, 1975; Krause, 2001). We instead followed the measured section of Harris et al. (1979), running along a nose on Meiklejohn's western flank (Figure 6.1). The entirety of the lower member is exposed in the measured section of Ross et al. (1969), however the middle and upper members have been truncated by erosion. While most of the lower member is below the surface in the line of section we followed, the middle and upper members are preserved and well exposed. Our measured section covers 270 m, beginning in the uppermost lower member and continuing to the base of the Eureka Quartzite. Samples were taken at 1.5 m intervals.

Biostratigraphy

A comprehensive biostratigraphic framework has been established for the Ordovician, primarily on the basis of graptolites and conodonts (Figure 6.2) (e.g. Bergström and Wang, 1995; Bergström et al., 2009; Cooper and Sadler, 2012). Meiklejohn Peak is unique in that it contains both North Atlantic and North American Midcontinent conodont species, many of which are useful for global correlation, namely Midcontinent species H. holodentata, P. polonicus, and C. sweeti and North Atlantic species E. suecicus and B. gerdae (Harris et al., 1979). H. holodentata is the oldest index fossil present and places the upper middle member in the H. holodentata zone, contemporaneous with the North Atlantic E. variabilis zone, which falls in the Darriwilian Dw2 Stage Slice of Bergström et al. (2009; Figure 6.2). The Midcontinent P. polonicus and N. Atlantic E. suecicus zones immediately follow the H. holodentata zone, with the P. polonicus zone extending slightly further. The majority of the upper member was deposited within this zone. Above the P. polonicus zone,

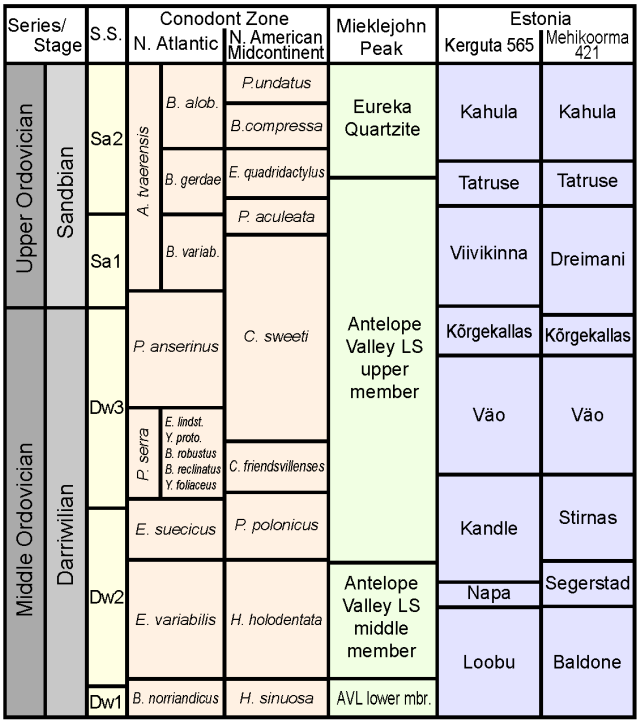

Figure 6.2. Biostratigraphic zonations for the Darriwilian and Sandbian. From left to right, columns show the geological time scale, Stage Slice breakdown, North Atlantic and North American midcontinent conodont zonations with representative index fossils, the formational stratigraphy of Meiklejohn Peak and two well studied cores form Baltica.

several zones known elsewhere are not represented by diagnostic fossils in this section, namely the Midcontinent C. friendsvillensis zone and the North Atlantic P. serra and P. anserinus zones (Figure 6.3, next page). This omission could indicate a highly condensed interval at the top of the section. Approximately 10 m above the last collection of P. polonicus, C. sweeti was collected, and B. gerdae (a member of the A. tvaerensis group) was collected 9 m above that (Harris et al., 1979). The space between the top of the P. polonicus zone and the bottom of the B. gerdae zone represents approximately 6 million years—the entirety of Darriwilian Dw3 and Sandbian Sa1 Stage Slices (Bergström et al., 2009; Cooper and Sadler, 2012).

Methods

Carbonate carbon and oxygen ($\delta^{13}C_{carb}$ & $\delta^{13}C_{org}$)

Carbonate samples were drilled, avoiding veins, spar, and obvious burrows, to obtain 1-2 g of powder for carbon isotope analysis. Carbonate carbon and oxygen isotope analyses were achieved using a Kiel Carbonate Device III coupled to a Finnigan Delta Plus VI gas source isotope ratio mass-spectrometer (IRMS) at Ohio State University and a Gas Bench II coupled to a Thermo-Finnigan Delta Plus XP gas source IRMS at Indiana University, both using standard methods. Sample powders were measured and placed in a vacuum oven at 100 °C for 8 hours to remove any volatile compounds and water, 100-500 µg were then acidified using H3PO4 at 72 °C for 4 minutes on the Kiel device or at least 8 hours using the Gas Bench. Precision was monitored by periodic measurement of NBS-18 and NBS-19 along with internal laboratory standards. Data were corrected, and results are

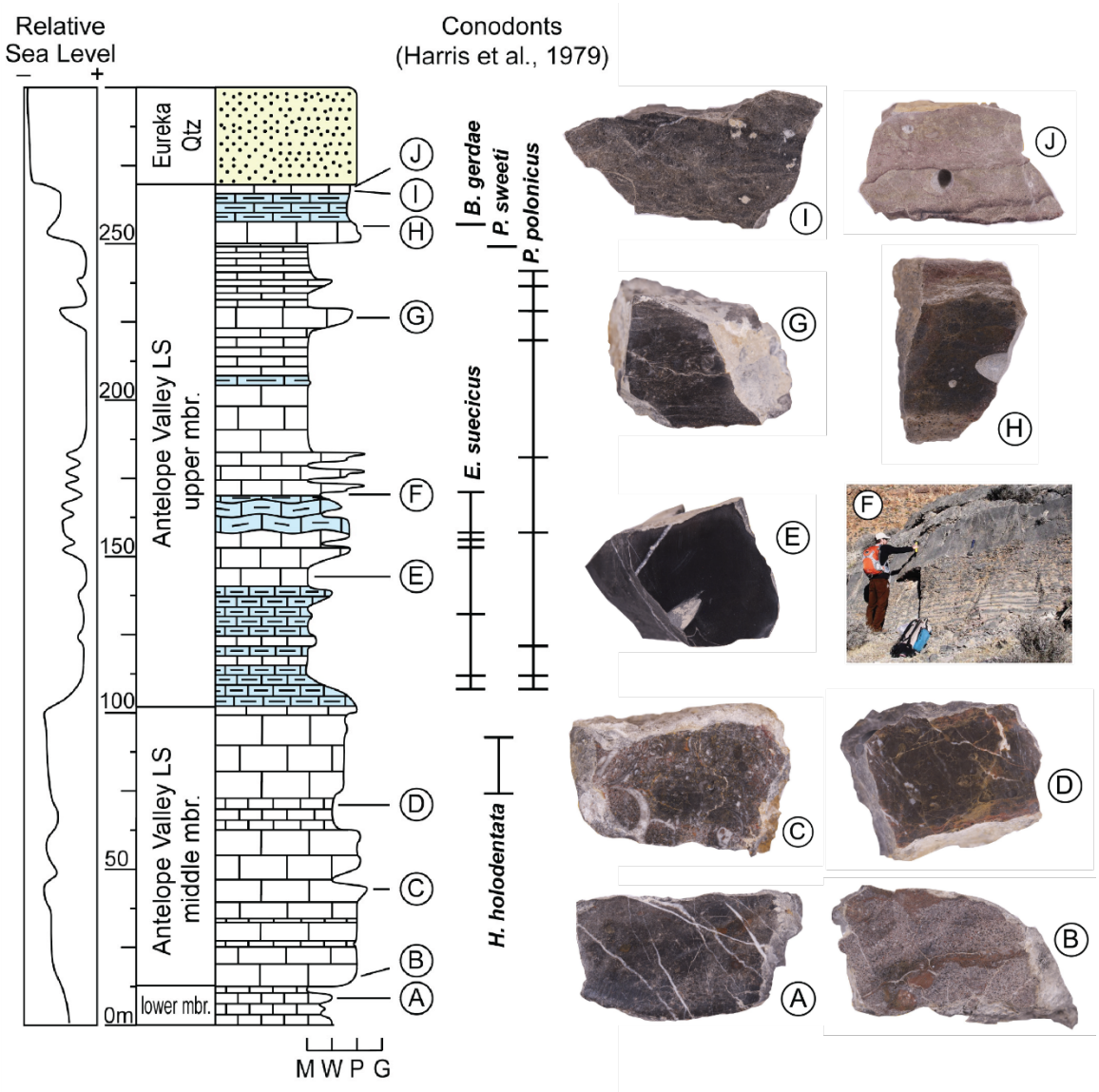

Figure 6.3. Stratigraphy of the Antelope Valley Limestone as exposed in the line of section. An inferred local sea level curve is shown to the left, followed by a generalized representation of the sedimentology. Significant conodont collections are shown in the center (Harris et al., 1979). To the right, photographs of polished surfaces on representative hand samples are shown, lettering corresponds to that in the stratigraphy to the left.

reported in standard delta notation as per mil (‰) deviations from the Vienna Pee Dee Belemnite (V-PDB) standard and standard mean ocean water (SMOW) for $\delta^{13}C_{carb}$ and $\delta^{18}O$, respectively. Repeat analyses of reference materials showed a standard deviation of 0.05‰ for $\delta^{13}C_{carb}$ and 0.10‰ for $\delta^{18}O$. The average reproducibility of repeated $\delta^{13}C_{carb}$ analyses was ± 0.08‰, and replicate analyses showed no laboratory bias.

Organic carbon ($\delta^{13}C_{org}$)

For analysis of organic carbon, 1-2 g of powder from each sample was acidified repeatedly using 6N HCl until no further reaction was observed. After each acidification, samples were centrifuged, and the supernatant was carefully decanted. Samples were then rinsed and decanted three times with ultrapure deionized water and dried for 48 hours at 75 °C. The residual insoluble material was homogenized, and a small fraction was measured for combustion using a Costech Elemental Analyzer. The $\Delta^{13}C$ of the resultant CO_2 gas was measured using a Finnigan Delta Plus IV via a CONFLO III open-split interface at The Ohio State University. The average reproducibility for repeated $\delta^{13}C_{org}$ analyses was ± 0.05‰. Results are reported in delta-notation as per mil deviations from V-PDB.

Carbonate-associated sulfate ($\delta^{34}S_{CAS}$)

Carbonate-associated sulfate sulfur isotope analyses were carried out at the University of California, Riverside. For these analyses, a 75-100 g hand sample was taken, and weathered surfaces along with any visible veins or sparry material were removed. The

samples were cleaned thoroughly with deionized water. Samples were then powdered using a clean steel ring mill. Extractions were carried out in a procedure similar to Gill et al. (2011).

Samples powders were first submerged in approximately 1 L of 10% NaCl solution and agitated periodically to remove any gypsum or anhydrite. After 24 hours, the solution was carefully decanted, and the samples were rinsed using DI water to ensure removal of any remnant NaCl solution that could contain sulfate. After the rinse water was carefully decanted and discarded, the samples were treated with a 4% NaOCl (hypochlorite) solution. Samples were agitated periodically and remained in the hypochlorite solution for 48 hours. The purpose of this treatment is to liberate any organically bound sulfur. After carefully decanting and discarding the hypochlorite solution, samples were rinsed repeatedly with deionized water until no detectable scent of the hypochlorite solution remained (a minimum of two rinses).

Samples were then dissolved completely using a 4N HCl solution and vacuum filtered (45 μm) to remove any insoluble fraction. The dissolution and filtering were carried out in small batches of three samples, and the HCl solution was added slowly and incrementally while monitoring reaction progression. Careful precaution was taken not to add excess HCl after all of the carbonate had reacted completely. Samples were then filtered immediately. These two steps were carried out quickly, typically in less an hour for each sample, to maintain the highest pH possible while still achieving 100% carbonate dissolution. The primary goal was to minimize exposure of any insoluble fraction of the

sample to an acidic solution, thus avoiding pyrite dissolution that could take place with prolonged exposure to low pH.

After filtration, a saturated BaCl2 solution (1.2N) was added to each solution to precipitate $BaSO_4$. Following addition of $BaCl_2$, samples were allowed to react at room temperature for a minimum of 48 hours to ensure full precipitation of SO_4^{2-} from solution. $BaSO_4$ was collected by vacuum filtration (45 μm) and dried at 50 °C. Each precipitate was then homogenized before being weighed into tin capsules loaded with excess V2O5 for isotope ratio analysis using a Thermo Delta V gas-source isotope ratio mass-spectrometer fitted with an elemental analyzer via a Conflo III interface. Sulfur isotope ratios are reported in standard delta-notation as per mil (‰) deviations from Vienna Canyon Diablo Troilite (V-CDT). Precision of analyses was monitored through routine analyses of NBS 127, IAEA SO-5, IAEA SO-6, and IAPSO SW. Standard deviations of replicate standard analyses were better than 0.3‰.

Iodine, calcium, and magnesium

Iodine measurements, normalized to the sum of major carbonate cations calcium and magnesium (I/(Ca+Mg)), were carried out at the University of California Riverside. The procedure followed was modified slightly from Lu et al. (2010). In this modified procedure, ~100 mg of sample powder was weighed and rinsed with 18 MΩ water to remove any surface-bound iodine or iodine salts. The sample was then digested in a volume of 3% HNO_3 sufficient to achieve quantitative dissolution assuming the sample powder was pure carbonate. Both the rinse and dissolution steps were carried out in 15 mL

centrifuge tubes and allowed to react in an ultrasonic bath for 15 minutes after agitation. After centrifugation, the digest supernatant was diluted in a matrix solution of 0.5% TMAH and ~0.375% HNO_3 for analysis via quadrupole inductively coupled plasma mass spectrometry (ICP-MS). The concentration of HNO_3 in the 0.5% TMAH matrix was such that the solution pH was 3.0, which is critical to prevent back precipitation of calcium salts when the sample digest is added. The sample dilution level used was such that the final measurement solutions would contain 50 ppm Ca assuming that the initial powders were pure calcite. In practice, [Ca] was lower than 50 ppm and variable, as samples generally contained some Mg and insoluble clastic material.

The sample solutions were then analyzed for the concentrations of major carbonate cations and iodine using an Agilent 7900 ICP-MS. Calibration standards were made from a single stock solution created using liquid single-element stock solutions in a ratio of concentrations similar to that expected from samples. A linear suite of eight standards was made using this stock solution, with [Ca] ranging from 0-50 ppm. Multiple reference materials were measured repeatedly throughout the run, including JCP-1 and two additional in-house carbonate reference materials. The average reproducibility of I/(Ca+Mg) for 45 analyses of these reference materials over three days was ~8.0%.

Results

Lithology

The lower member of the Antelope Valley Limestone is generally characterized by micrites to wackestones with some coarse packstone beds throughout (Figure 6.3A). Approximately 13 m of the uppermost lower member was sampled in our section on the northwest slope of Meiklejohn Peak. The lower-middle member contact was defined by medium gray, oscillating wackestones and micrites of the lower member below and the first occurrence of massively bedded, light gray, nodular packstone of the middle member above (Figure 6.3B).

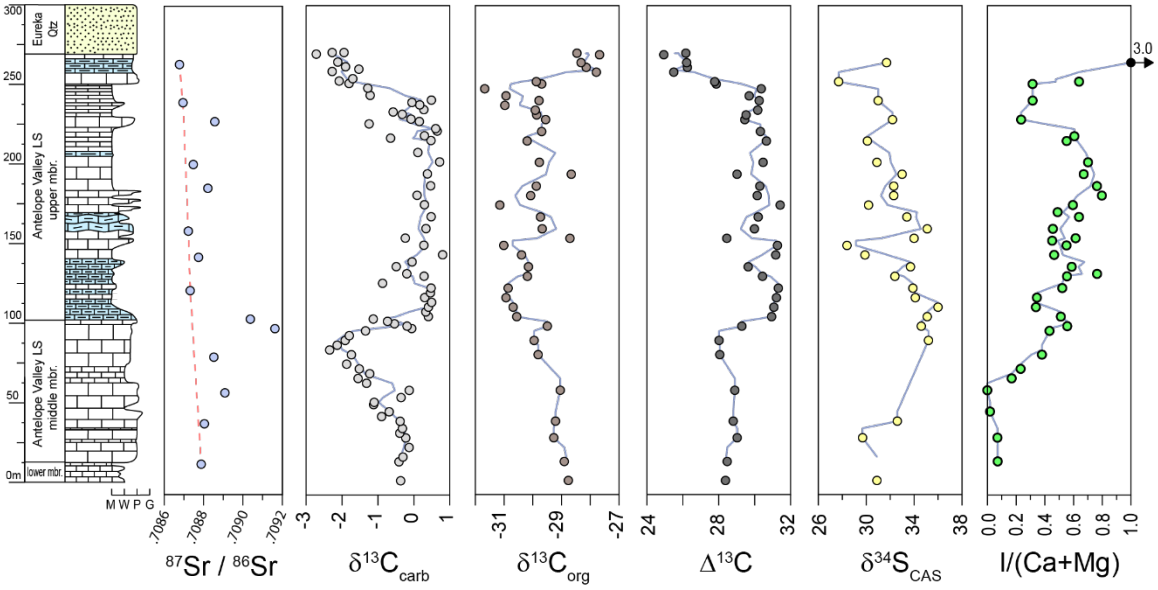

Figure 6.4. Geochemical data for samples from the middle and upper members of the Antelope Valley Limestone at Meiklejohn Peak. Panels, from left to right, show strontium isotope data ($^{87}Sr/^{86}Sr$), carbonate and organic carbon isotope data ($\delta^{13}C_{carb}$ and $\delta^{13}C_{org}$), the difference between $\delta^{13}C_{carb}$ and $\delta^{13}C_{org}$ ($\Delta_{13}C$), carbonate-associated-sulfate sulfur isotope data ($\delta^{34}S_{CAS}$), and iodine concentration data (expressed a normalized ratio to the sum of calcium and magnesium concentrations as ppm/wt%). All data are plotted stratigraphically as referenced to the stratigraphy shown at left.

The middle member is approximately 90 m thick and is almost entirely composed of massive, frequently oncolitic packstones. The middle 50 m is at times heavily burrowed, with silty burrows weathering to an orange brown. Resistant, ~1-m-thick, oncolitic beds are present at 51 m and 57 m in our measured section and thicker, 2-3 m, oncolitic beds occur at 75 m and 98 m. We placed the middle-upper member contact at 102 m in our section as defined by the last occurrence of a massive, light gray packstone of the middle member below and a transition into silty, thinner bedded, darker gray lime mudstone of the upper member above.

The upper member of the Antelope Valley Limestone at Meiklejohn Peak is approximately 170 m thick and is composed mainly of thinner bedded, homogeneous, dark gray micrite (Fig 6.3E). Several intervals contain thin silty micrite beds cyclically interbedded with cleaner micrites forming "ribbon" limestone. Beginning at 150 m in our section there is a ~35 m interval of more resistant packstone beds, toward the top of which there is a succession of repeated, ~2 m cycles of unbioturbated ribbon limestone, heavily bioturbated wackestones, and then massive packstone (Fig 6.3F). This sequence is followed by homogenous, dark gray micrite up section until approximately 20 m below the base of the overlying Eureka Quartzite where the rocks become coarser with interbedded clastic horizons. Nearing the Eureka, the fossiliferous packstones become increasingly sandier (Figure 6.3I and J). The Eureka-Antelope Valley Limestone contact was defined by the last occurrence of medium to dark gray packstone of the Antelope Valley Limestone below the contact, and above it a thick, massive, cliff-forming, buff orange quartzite.

$\delta^{13}C_{carb}$

Of the samples collected, 79 were analyzed for the isotopic composition of carbonate carbon. The $\delta^{13}C_{carb}$ results range from -2.7‰ to 0.8‰, and there are several discernable trends in the data (Figure 6.4). The lowest 85 m of our section show a steady negative trend beginning at values just below 0‰ and reaching -2.36‰ at 82.5 m. This trend is followed by rapid increase, which exceeds the heaviest values observed at the bottom of the section, plateauing at maximum values around 0.4‰. Both the negative trend and the subsequent rise to positive values are contained within the Antelope Valley middle member. The positive trend peaks very near to the middle-upper member contact. Positive values are then sustained through the next 135 m of the upper member before declining sharply in the uppermost 40 m of the section. The lightest values observed in the section occur in the uppermost samples, just below the Eureka Quartzite, measured at -2.7‰.

$\delta^{13}C_{org}$

Of the 79 samples that were analyzed for $\delta^{13}C_{carb}$, 40 were also analyzed for the isotopic composition of bulk organic carbon (Figure 6.4). These $\delta^{13}C_{org}$ data range from -31.7‰ to -27.7‰. The data show a negative trend through the Antelope Valley middle member, starting near -29‰ at the base of the section and decreasing to approximately -31‰ at the base of the upper member. This negative $\delta^{13}C_{org}$ trend of the middle member begins by roughly tracking $\delta^{13}C_{carb}$; however, the data continue to decrease as the $\delta^{13}C_{carb}$ data increase rapidly in the uppermost portion of the middle member. During the sustained positive $\delta^{13}C_{carb}$ interval of the upper member, $\delta^{13}C_{org}$ remains low, though there is some

variability in the data and a slight increasing trend exists moving up section. In the upper 25 m of the section, $\delta^{13}C_{org}$ rises abruptly from approximately -30‰ to -28‰.

$\Delta^{13}C$

The difference between the carbon isotope compositions of contemporaneously deposited carbonate and organic matter ($\delta^{13}C_{carb}$ - $\delta^{13}C_{org}$) is represented as $\Delta^{13}C$. In our section, $\Delta^{13}C$ values remain relatively constant in the middle member as $\delta^{13}C_{org}$ values track the negative trend in $\delta^{13}C_{carb}$ data (Figure 6.4). As $\delta^{13}C_{carb}$ values increase rapidly at the top of the middle member, however, the covariation with paired $\delta^{13}C_{org}$ data does not continue. Instead, the $\delta^{13}C_{org}$ data continue to trend toward lighter values, producing a steep increase in $\Delta^{13}C$ values from ~28‰ to ~31‰ coincident with the rapid increase in $\delta^{13}C_{carb}$. Throughout the broad interval of sustained positive $\delta^{13}C_{carb}$ values in the upper member, $\Delta^{13}C$ values remain relatively stable at ~30‰, though some variability on the order of 1‰ exists. In the uppermost portion of the section, $\Delta^{13}C$ values decrease abruptly. This shift from ~30‰ to ~26‰ occurs as $\delta^{13}C_{carb}$ data decrease by more than 2‰ and the paired $\delta^{13}C_{org}$ data increase by a similar amount.

$\delta^{34}S_{CAS}$

A subset (26) of the samples analyzed for both $\delta^{13}C_{carb}$ and $\delta^{13}C_{org}$ were also analyzed for $\delta^{34}S_{CAS}$ (Figure 6.4). The $\delta^{34}S_{CAS}$ data range from 27.7‰ to 36.0‰ (V-CDT). Only three samples were analyzed from the lower portion of our section, clustering around 31‰. An additional two samples were measured from the uppermost middle member and

show distinctly higher values, ~35‰, compared to those from the bottom of the section. Over the lower ~45 m of the upper member, $\delta^{34}S_{CAS}$ values trend negatively to a minimum of 28.4‰ before rebounding abruptly to greater than 34‰. The data from the remaining ~150 m of the upper member trend negatively up section, though some variability exists.

I/(Ca+Mg)

A subset (35) of the samples analyzed for δ^{13}Ccarb were also analyzed for iodine concentration (Figure 6.4). Carbonate-associated iodine data are typically normalized to the concentration of major carbonate cations, calcium and magnesium, to correct for the presence of detrital clastic material (e.g., Hardisty et al., 2014). The I/(Ca+Mg) data from out section range from below the detection limit to 0.80, though one outlier was measured just below the base of the Eureka Quartzite with a value of 3.03. In the lowermost 60 m of the section, I/(Ca+Mg) values are consistently low, below 0.10. In the upper 40 m of the middle member, there is an increasing trend moving up section, reaching I/(Ca+Mg) values in excess of 0.5 at the base of the upper member (102 m). The majority of the upper member is characterized by a slightly positive trend in I/(Ca+Mg) moving up section. This trend is interrupted in the upper 60 m of the section, where I/(Ca+Mg) values decrease to ~0.3, coincident with a change in lithology from packstone to micrite, and then increase abruptly approaching the gradational contact with the overlying Eureka Quartzite.

Discussion

Potential impacts of diagenesis

The MDICE has previously been reported on multiple paleocontinents, including South China, Baltica, the Argentinian Precordillera, Tarim, eastern Laurentia, and now from the Great Basin region of western Laurentia as well (Ainsaar et al., 2004; Kaljo et al., 2007; Schmitz et al., 2010; Leslie et al., 2011; Calner et al., 2014; Edwards and Saltzman, 2016; Young et al., 2016; Zhang and Munnecke, 2016). The global distribution of the event suggests that it was the product of a change in the $\Delta^{13}C$ composition of the global oceans, rather than a local or regional effect or the product of post depositional alteration. Still, the effects of diagenesis must be considered before any interpretation of past oceanographic conditions can be made.

Despite the fact that there is some isotopic exchange during stabilization of carbonate minerals, fine-grained carbonates should have a high potential for preserving seawater signals due to the rock-buffered nature of $\delta^{13}C_{carb}$ during early diagenesis (e.g., Banner and Hanson, 1990). This possibility is particularly likely in undisturbed sediments with a low porewater/rock ratio. However, some processes could enhance the degree to which this is not the case. Recrystallization and stabilization of carbonate minerals in the presence of migrating fluids, for example, could alter the primary $\delta^{13}C_{carb}$ signature, and extensive burrowing could enhance this process (Metzger and Fike, 2013).

One commonly used indicator of diagenetic alteration is covariation between $\delta^{13}C_{carb}$ and $\delta^{18}O_{carb}$ values. Due to the large difference in the concentrations of oxygen versus carbon in diagenetic fluids, $\delta^{18}O_{carb}$ values are, in general, much more easily altered

during recrystallization (Banner and Hanson, 1990). Although there are instances where $\delta^{13}C_{carb}$ and $\delta^{18}O_{carb}$ values can covary without requiring a diagenetic explanation, it is frequently assumed that if a diagenetic overprint is imparted upon the $\delta^{13}C_{carb}$ of a carbonate, the $\delta^{18}O_{carb}$ should be altered as well, leaving some pattern of covariation.

A cross-plot of all the $\delta^{13}C_{carb}$ and $\delta^{18}O_{carb}$ data from this study reveals no systematic covariation (Fig 6.5A); a linear best fit yields a slope of 0.25 with an R^2 value of 0.04. Interestingly, however, in the uppermost 20 m of our section, we do see a fairly strong covariation in $\delta^{13}C_{carb}$ and $\delta^{18}O_{carb}$. For these upper 10 measurements, a best-fit line has a slope of 3.29 and an R^2 value of 0.65. This observation suggests that the uppermost

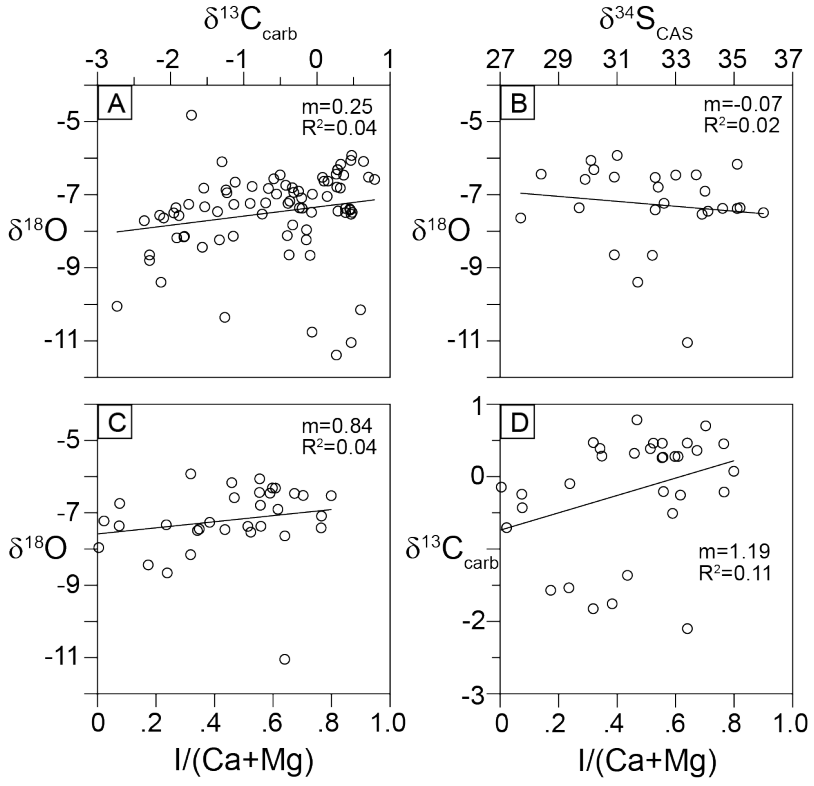

Figure 6.5. Cross-plots of $\delta^{13}C_{carb}$, $\delta^{18}O$, and I/(Ca+Mg). Note the lack of significant correlation between any of the data.

Antelope Valley Limestone experienced some alteration, and the observed covariation with a strong positive slope is consistent with recrystallization in the presence of meteoric fluids. This observation is further supported by the presence of the immediately overlying Eureka Quartzite, a time-transgressive unit that likely reflects the migration of beachfront facies during a large regression (McBride, 2012).

Below the uppermost 20 m of our section, $\delta^{18}O$ remains very stable, following a slight increasing trend from around -8‰ to -6‰. These values are similar to those previously reported for this time interval (e.g., Edwards and Saltzman, 2016) and follow the generally increasing long-term trend observed for the Early and Middle Ordovician (e.g., Trotter et al., 2008). These relationships suggest that $\delta^{13}C_{carb}$ values in the majority of our section have not been altered and are likely to preserve a primary seawater trend. Under these diagenetic conditions, $\delta^{34}S_{CAS}$ would also be expected to preserve primary trends. Even in the uppermost reaches of our section that likely experienced some meteoric alteration, carbonate-associated sulfate has the potential to preserve the primary $\delta^{34}S_{CAS}$ signal due to the rock-buffered nature of sulfur (Gill et al., 2008).

Iodine in marine carbonates is inherently susceptible to digenetic loss under reducing conditions. This likelihood arises from the redox-sensitive nature of iodine and related controls on incorporation into precipitating carbonate minerals. The oxidized iodate (IO_3^-) species will readily substitute into carbonate minerals during precipitation at a rate that is proportional to its concentration in the ambient solution; however, the reduced iodide (I^-) species will be wholly excluded, regardless of its concentration (Lu et al., 2010). This relationship implies that dissolution and reprecipitation of carbonate minerals under

reducing conditions will result in the release of iodine from the original carbonate into the diagenetic fluid, where it will remain even as new carbonate precipitates. This process, if the released iodine is reduced in solution, will tend to lower its concentration in the secondary carbonate. In contrast, few, if any, diagenetic scenarios would increase iodine concentration (Hardisty et al., 2017). Interestingly, the uppermost sample in our section, just below the gradation into coarse sands of the Eureka Quartzite, has a significantly higher I/(Ca+Mg) value compared to all other samples in this study. While these uppermost samples likely experienced some interaction with meteoric waters, it is likely that this high I/(Ca+Mg) value is a primary signature, reflecting precipitation in very shallow and well oxygenated waters.

Correlation of the MDICE to Baltoscandia

A thick and relatively continuous Ordovician carbonate platform/ramp succession can also be found in the subsurface of Estonia (e.g., Dronov and Rozhnov, 2007). During Ordovician time, the subcontinent of Baltica was situated on the eastern side of the Iapetus Ocean, north of 30°S (Figure 6.1A; Cocks and Torsvik, 2002). Several Estonian drill cores have been analyzed for $\delta^{13}C_{carb}$, and a robust chemostratigraphic framework has been established (Ainsaar et al., 2004; Kaljo et al., 2007; Ainsaar et al., 2010). Among the best-studied cores are Kerguta 565 and Mehikoorma 421, both of which have been examined paleontologically, and age diagnostic index fossils have been identified (Männik and Viira, 2005; Viira et al., 2006).

The MDICE has been identified in the Darriwilian interval of both of these cores, as well as having been observed in other contemporaneous Baltoscandian sections and on multiple other cratons (Ainsaar et al., 2007; Schmitz et al., 2010; Leslie et al., 2011; Albanesi et al., 2013; Bauert et al., 2014; Calner et al., 2014; Edwards and Saltzman, 2016). Age diagnostic conodont fossils in the Antelope Valley Limestone of Meiklejohn Peak suggest that the MDICE should be present (Harris et al., 1979), which is supported

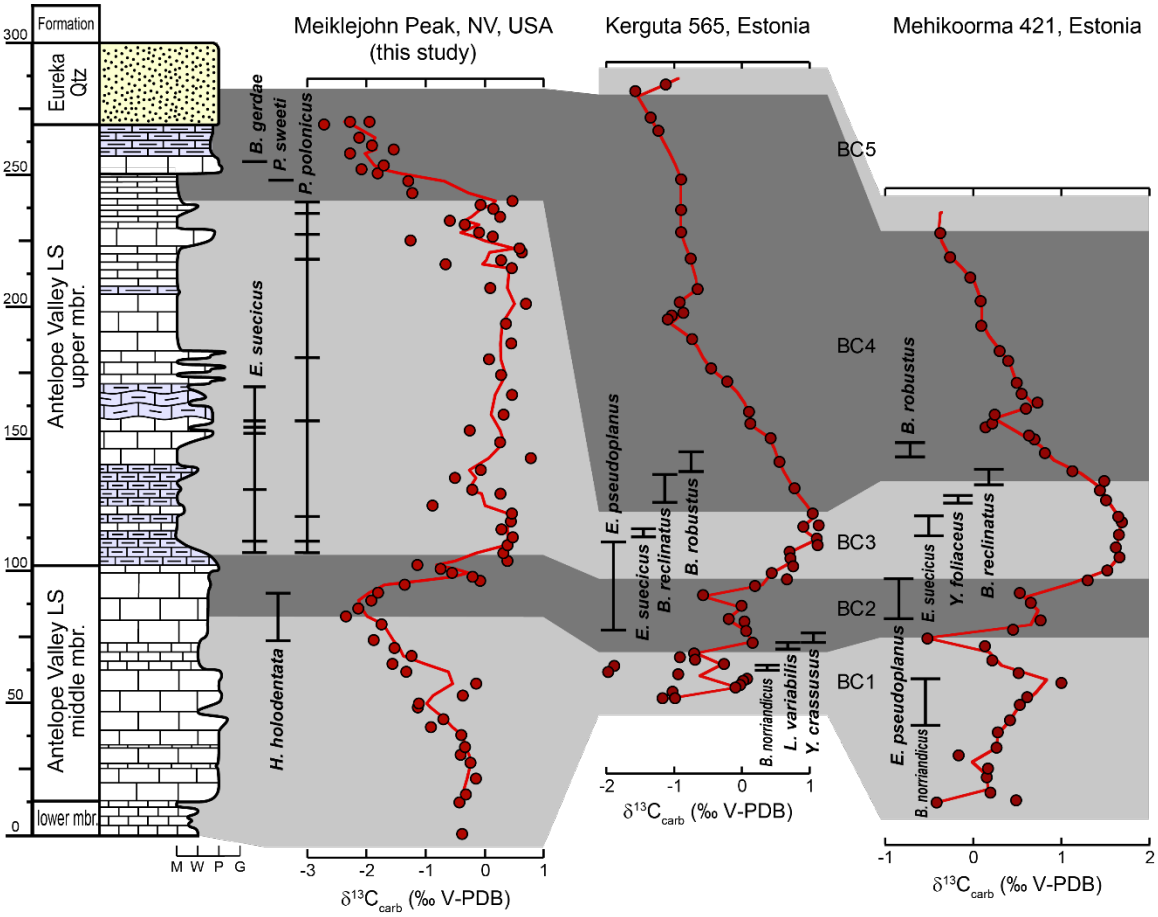

Figure 6.6. Correlation of the middle and upper members of the Antelope Valley Limestone to the chemostratigraphic zonation scheme of Ainsaar et al., 2010. Relevant conodont collections from each location are shown alongside with $\delta^{13}C$ data, the stratigraphy of Meiklejohn Peak is also shown at left.

independently by previously published Sr^{87}/Sr^{86} data from this section (Edwards et al., 2015; Fig 6.4). The trends in $\delta^{13}C_{carb}$ values from the northwest slope of Meiklejohn Peak presented here are consistent overall with observations of the MDICE elsewhere (Figure 6.6, previous page).

Ainsaar et al. (2010) proposed an Ordovician chemostratigraphic framework, dividing the MDICE into five intervals (i.e. BC1-5). Zone BC1 corresponds to the pre-excursion interval. We have correlated the lower 90 m of our section to this zone (Figure 6.6). The top of BC1 is defined by the isotopically lightest value in the pre-MDICE negative shift observed in most locations. Zone BC2 is defined by the increase during the onset of the MDICE. The correlation of this interval on the basis of $\delta^{13}C$ stratigraphy is strengthened by the presence of H. holodentata at Meiklejohn Peak and L. variabilis in the Kerguta 565 core, which are contemporaneous index species (Harris et al., 1979; Viira et al., 2006). In multiple Estonian sections, a very short-lived negative step is present in the increasing $\delta^{13}C$ trend of BC2. We observe a similar pattern in the BC2 zone of our dataset.

Zone BC3 is defined as the MDICE peak. In most sections where the MDICE has been documented, the peak is broad, and ^{13}C enriched values are maintained for several million years. The data presented here also show a period of sustained positive values, maintained through the majority of the upper member. The correlation of this interval to BC3 is supported by the presence of both E. suecicus and the contemporaneous Midcontinent species P. polonicus throughout the upper member of the Antelope Valley Limestone at Meiklejohn Peak (Figure 6.6) (Harris et al., 1979). The observed range of E. suecicus is restricted to the BC3 zone in Estonian sections where the MDICE has been

documented, coincident with the highest $\delta^{13}C_{carb}$ values. The uppermost collection of P. polonicus at Meiklejohn Peak (Harris et al., 1979) immediately precedes the drop in $\delta^{13}C_{carb}$ that we correlate with the BC4 zone of Ainsaar et al. (2010). As mentioned above, the horizons above this last observation of P. polonicus are very condensed. However, there is no apparent return toward less negative values, and for this reason, we have placed the remainder of the section in the BC4 zone (Figure 6.6).

More recent work from Bergström et al. (2015) has demonstrated the usefulness of the chemostratigraphic zones proposed by Ainsaar et al. (2010) in trans-Atlantic correlation. Significantly, the correlation presented herein goes one step beyond this, demonstrating that the $\delta^{13}C_{carb}$ trends that define this zonation system are present on the Panthalassic side of Laurentia as well, supporting its use in refinement of correlations outside the Iapetus region.

Interpretation of $\delta^{13}C_{carb}$

The rising limb of the MDICE occurs in close proximity to the middle-upper member boundary of the Antelope Valley Limestone at Meiklejohn Peak, which represents a transition from coarse wackestone/packstone to fine-grained, homogeneous lime muds. A decrease in grain size is also evident near the onset of the MDICE in eastern North America (Leslie et al., 2011), supporting the idea that this apparent deepening signifies a global eustatic event. The Ordovician sea-level curve of Nielsen (2004) also shows a transgression near the base of the E. suecicus and P. polonicus zones, further supporting this notion.

Although this shift in $\delta^{13}C_{carb}$ values occurs near a lithological boundary, its presence is consistent with a shift in the $\delta^{13}C_{carb}$ value of the global DIC reservoir, rather than a local effect due to a change in water depth. Specifically, the $\delta^{13}C_{carb}$ gradient in open seawater is generally such that deeper waters have a lighter $\delta^{13}C_{carb}$ value compared to shallower waters due to the export of ^{13}C depleted organic matter from the surface and its remineralization at depth. This is the opposite of the trend toward heavier $\delta^{13}C_{carb}$ values with deepening that is observed here. Additionally, the excursion has been observed in multiple localities at differing paleo-water depths. Globally distributed excursions throughout the Cambrian and Ordovician have previously been shown to track the oceanic DIC pool rather than a local $\delta^{13}C$ depth gradient, and the MDICE appears to be consistent with this (Ainsaar et al., 2004; Kaljo et al., 2007; Schmitz et al., 2010; Gill et al., 2011; Leslie et al., 2011; Edwards et al., 2015).

The transgression that is recorded in multiple sections at the onset of the MDICE could have significantly increased the organic carbon burial flux. Continental shelves and slopes represent the loci of the majority of organic carbon burial in the modern ocean. This is true because productivity is stimulated by coastal upwelling and continental runoff, and there is sufficient clastic and carbonate accumulation in these systems to achieve burial. During a transgression, the areal extent of shelf space increases, as does accommodation space in low-angle platform settings where sediment bypass could have limited accumulation and burial of organics under lowstand conditions. Transgression could, in turn, have led to vertical aggradation and sequestration of significant amounts of ^{13}C depleted organic matter.

In addition to changing the isotopic balance of the global carbon cycle, increasing organic matter burial also changes the balance of Earth's surface oxidant budget. Nearly all of the O_2 contained in Earth's ocean-atmosphere system is the product of oxygenic photosynthesis, and by increasing the burial of photosynthetically derived organic matter without correspondingly increasing sinks for the O_2 generated during production, a net increase in O_2 is achieved. During the MDICE, higher than background $\delta^{13}C$ values are maintained for several million years, suggesting several million years of elevated O_2 accumulation in surface environments. A change of this scale could have altered the redox landscape in the global oceans—deepening the chemocline in productive costal settings and stabilizing environmental conditions in areas that were prone to frequent incursions of anoxic or sulfidic waters from the cores of nearby oxygen minimum zones in earlier times. Modern benthic communities have been shown to exhibit threshold responses to low O_2 conditions in and around oxygen minimum zones (e.g., Levin, 2003; Woulds et al., 2007; Sperling et al., 2013). Hence, a small increase in surface ocean [O_2] could have made the difference between frequently inhospitable conditions in many locations and those in which a relatively rich community could have thrived.

Interpretation of $\delta^{34}S_{CAS}$

Along with the burial of organic carbon, the burial of reduced sulfur species represents a first-order driver of changes in the oxidant budget of the oceans (Berner, 1987). These two cycles are intimately linked through a variety of biotic interactions taking place both in the water column and within sediments. Given excess sulfate, enhanced

delivery of organic matter to sediments will increase net microbial sulfate reduction (MSR), which reduces sulfate (SO_4^{2-}) to hydrogen sulfide (H_2S^-). If H_2S^- produced through MSR is able to react with Fe2+, iron-sulfide minerals, principally pyrite, are formed and can be buried along with sediments, yielding a net addition of O_2 to the system (Berner, 1987).

Importantly, MSR has the potential to significantly fractionate sulfur isotopes (e.g., Habicht and Canfield, 1997). The H_2S^- produced through MSR can have a $\delta^{34}S$ value as much as 70‰ lighter than that of the sulfate pool from which it was generated, though fractionations this large are rarely observed in the rock record (e.g., Sim, Bosak, & Ono, 2011; Wing & Halevy, 2014). Many factors can influence the magnitude of the fractionation, including the size of the available sulfate reservoir, the fraction of that reservoir converted to H_2S^-, the degree of open versus closed system behavior, and the rate at which MSR progresses (e.g., Crowe et al., 2014; Gomes and Hurtgen, 2015). Nevertheless, an increase or decrease in MSR and resultant pyrite burial will generally leave the residual SO_4^{2-} reservoir heavier or lighter, respectively. Evaporite minerals like gypsum and anhydrite have the potential to record the $\delta^{34}S$ value of oceanic SO_4^{2-}. In the absence of evaporites, CAS has been shown to be a robust archive, as SO_4^{2-} is generally incorporated into precipitating carbonates without significant fractionation (e.g., Gill et al., 2007).

The $\delta^{34}S_{CAS}$ data presented here, while limited in resolution at the base of the section, begin at ~30‰, which is roughly consistent with other published $\delta^{34}S_{CAS}$ data from contemporaneous sections in eastern Laurentia (Thompson and Kah, 2012; Young et al.,

2016, Kozik et al., 2019). During the increasing limb of the MDICE, $\delta^{34}S_{CAS}$ values at Meiklejohn Peak are higher and stable at ~35‰, though moving up section, $\delta^{34}S_{CAS}$ values trend slowly and relatively continuously toward lighter values. A decrease in $\delta^{34}S_{CAS}$ values throughout the MDICE has been reported previously from multiple sections in eastern Laurentia, though the magnitude of the drop is greater than in our data (Thompson and Kah, 2012; Young et al., 2016). The large decrease reported from eastern Laurentia is also very rapid, inconsistent with the new data reported here (c.f., Thompson and Kah, 2012; Young et al., 2016). While general agreement among baseline values for these different sections appears to reflect a relatively homogeneous global sulfate reservoir, the spatial differences in the magnitude and rate of change during the MDICE highlights the importance of local controls and corresponding basin-to-basin heterogeneities. In other words, these signals are likely attributable to a combination of varying local factors superimposed on first-order global trends and related controls.

Young et al. (2016) interpret the overall negative shift to reflect a decrease in the burial flux of pyrite, suggesting that this could have resulted from an increase in oceanic [O_2] during the MDICE and a shift of the location of MSR to deeper within sediments, resulting in less overall MSR and more closed-system-type behavior. Though a decrease in the global pyrite burial flux is not generally what one would expect during a time of enhanced organic matter burial, it may not be inconsistent if the MDICE is viewed in the context of the related transgression. If we consider that the increase in organic carbon burial could have resulted from an increase in accommodation space in high sedimentation areas rather than from shifts toward anoxia in more restricted marine settings and/or oxygen

minimum zones, the possibility for inverse relationships in C and S becomes plausible. Specifically, this mechanism and the associated accumulation of O_2 from increased organic matter burial, along with cooling temperatures throughout this interval enhancing O_2 solubility (e.g., Trotter et al., 2008), could have created more stably oxic conditions in deep basinal waters, forcing the zone of MSR deeper into sediments and disfavoring the burial of light sulfur in pyrite.

Interpretation of $\Delta^{13}C$

Several factors contribute to the size of $\Delta^{13}C$, which again is the difference between co-occurring $\delta^{13}C_{carb}$ and $\delta^{13}C_{org}$ values. The largest contribution is from the fractionation imparted by photosynthesis (ε_p). In addition to ε_p, however, there are temperature-dependent fractionations within the dissolved inorganic carbon (DIC) pool (between $CO_2(aq)$, HCO_3^-, and CO_3^{2-}) and a fractionation during carbonate mineral precipitation between DIC and the resulting carbonate mineral, differing with primary carbonate mineralization (i.e., calcite vs. aragonite; Hayes et al., 1999).

Even narrowing down the cause of a change in $\Delta^{13}C$ to a change in ε_p, interpretation of this result is still not simple, as there is more than one way to generate an apparent change in ε_p. The ribulose 1,5-bisphosphate carboxylase/oxygenase enzyme (RuBisCO) catalyzes carbon fixation during photosynthesis. It does so using CO_2 as a substrate for the carboxylation of ribulose 1,5-bisphosphate (RuBP) and, in the process, imparts a fractionation on the isotopic composition of the carbon that is inevitably incorporated into the organism's biomass. The size of this fractionation can scale with the concentration of

CO_2(aq) in the water where the organism is growing (e.g., Rau et al., 1997). However, it can also scale with [PO_4^{3-}] and the growth rate of the organism (Bidigare et al., 1997, Joachimski et al., 2002). However, even ignoring these growth-rate effects, pCO_2 is still not the only factor controlling ε_p.

The RuBisCO enzyme serves both a carboxylase and oxygenase function and can operate using the same RuBP substrate along with O_2. When this reaction takes place, the products are used in photorespiration rather than photosynthesis, and carbon that was previously fixed by the organism is reoxidized into CO_2 in exchange for energy. This process takes place continuously in the presence of O_2 and today results in the reoxidation of approximately 25% of the carbon fixed by the carboxylation reaction (Andrews and Lorimer, 1987). The reoxidized carbon is then available within the cell to be used again in the Calvin cycle. Due to the competitive nature of RuBisCO, as intracellular [O_2] increases, the frequency of the photorespiration pathway increases. This recycling of CO_2 within the cell increases the net fractionation in the carbon isotope composition of the resultant organic matter.

Multiple laboratory studies have documented this relationship, showing that in both algae and vascular plants, as atmospheric pCO_2 is kept constant and pO_2 increases, the $\delta^{13}C_{org}$ value of biomass decreases and thus Δ increases (Berner et al., 2000; Beerling et al., 2002). Edwards et al. (2017) used high-resolution paired carbon isotope records throughout the Ordovician to show that a long-term increase in $\Delta^{13}C$ values exists in globally distributed sections, which they attributed to increasing O_2. The authors went on to argue that inferred increases oxygenation of the oceans played a significant role in pacing

early Paleozoic animal evolution—in particular during the GOBE. The model presented by Edwards et al. (2017) calculated a rapid rise in atmospheric pO_2 beginning in the Darriwilian. Consistent with the global data, there is an increase in $\Delta^{13}C$ values of ~3‰ coincident with the onset of the MDICE at Meiklejohn Peak.

However, as mentioned above, any interpretation of a shift in $\Delta^{13}C$ values must consider multiple possible forcing mechanisms. There is no evidence of a change in primary carbonate mineralization. Previous work points to low-Mg calcite as the primary carbonate mineral deposited throughout this time (Stanley and Hardie, 1998). The temperature-dependent fractionation between $CO_2(aq)$ and HCO_3^- should also not have changed significantly at this time. Global temperature declined persistently throughout the Early and Middle Ordovician but reached relative stability during the Darriwilian (Trotter et al., 2008). This combination leaves a change in ε_p as the likely cause of the observed change in $\Delta^{13}C$ values.

The most frequently invoked mechanism for increasing ε_p involves increasing $[CO_2(aq)]$. This explanation does not fit with the MDICE, however, because atmospheric pCO_2 was on a decreasing trajectory throughout the Middle and Upper Ordovician, as evidenced in the paleotemperature record of Trotter et al. (2008). It is also inconsistent with the interpretation of the MDICE as reflecting increased organic matter burial. In addition to these lines of reasoning, there is a threshold for $[CO_2(aq)]$ above which the relationship between $[CO_2(aq)]$ and $\Delta^{13}C$ becomes asymptotic. Given that atmospheric pCO_2 was much higher during the Ordovician compared to today, additional increases may not have had a large effect on isotope fractionation.

A change in the average growth rate of local primary producers or a change in the local phosphate inventory could have also influenced ε_p. This possibility cannot be ruled out give the available data, and further work should focus on community structure and nutrient availability during this critical time in evolutionary history. However, the suggestion that the observed changes in ε_p resulted from an increase in pO_2 are consistent with the interpretation of the MDICE as an organic carbon burial event.

Interpretation of I/(Ca+Mg)

As mentioned above, the incorporation of iodine into precipitating carbonate minerals is dependent on the redox state of iodine in solution. In this way, the concentration of iodine in shallow water carbonates can serve as an indirect measure of the redox state of those waters (e.g., Hardisty et al., 2017; Lu et al., 2018). This first order observation is confounded slightly by the oxidation-reduction kinetics of iodine. In waters with low $[O_2]$, IO_3^- will be reduced rapidly and quantitatively; however, I^- is somewhat slow to oxidize even in waters with high $[O_2]$ (Chance et al., 2014). These slow reaction kinetics, coupled with relatively shallow chemoclines and oxygen minimum zones along most productive basins/margins, offer a parsimonious explanation for the dominantly low I/(Ca+Mg) values of shallow water carbonates throughout the Paleozoic, despite the fact that surface waters were likely stably well oxygenated throughout this time (Lu et al., 2018).

At Meiklejohn peak, there is a clear trend of increasing I/(Ca+Mg) values in the middle and upper members (Fig 6.4). This trend plateaus in the middle member at modest but consistently elevated concentrations. The relative consistency of values, along with a

lack of obvious diagenetic indicators, suggests that these values are primary and reflect the relative concentration of IO_3^- in local waters during deposition. There is a large increase in the uppermost portions of the section to a maximum I/(Ca+Mg) value of greater than 3.0. This sharp increase is likely related to dramatic shallowing as evidenced by migration of the Eureka Quartzite sands into the depositional area.

In the middle member of the Antelope Valley Limestone, the observed increase in I/(Ca+Mg) values takes place through an interval of mostly continuous, massive packstones. The subsequent plateau in I/(Ca+Mg) values occurs in a dominantly micritic facies of the upper member. All else remaining equal, the transgression that is reflected in the middle-upper member transition and associated shoaling of the chemocline would bring deeper, oxygen-depleted waters closer to the site of deposition, and more frequent upward mixing of those waters would be expected, leading to a decrease in local $[IO_3^-]$ (Lu et al., 2018). However, the impact of this possibility seems to have been minimal in this case. Instead, throughout this interval of deeper water deposition, I/(Ca+Mg) values remain relatively high—consistent with dominantly more oxic conditions.

These high values throughout the upper member suggest a stably oxygenated platform and a decrease in the size and/or intensity of the OMZ on the western Laurentian margin. Importantly, this period of high I/(Ca+Mg) values corresponds to the positive plateau of $\delta^{13}C_{carb}$ values during the MDICE. A decrease in OMZ size or deepening of their position is not generally consistent with a carbon isotope excursion caused by an increase in organic carbon burial in the traditional sense. As discussed above, however, if this excursion was caused by an increase in accommodation space on shelves worldwide, rather

than a large increase in productivity, the organic matter burial necessary to generate the MDICE could have been achieved without invoking an increase in the size or strength of OMZs, consistent with the $\delta^{34}S_{CAS}$ records from this time.

While I/(Ca+Mg) data are inherently representative of local conditions, they do relate to variations in regional controls that may tie strongly to global-scale change. The data from Meiklejohn Peak suggest an overall increase in the $[O_2]$ of local waters and/or a reduction in the size of the OMZ located on the nearby slope. These possibilities could reflect an increase in ocean-atmosphere $[O_2]$ stemming from increased organic matter burial. More I/(Ca+Mg) data from this and other continental margins during the Middle Ordovician will be helpful in disentangling the possible mechanisms contributing to the trends in the data presented here. Importantly, though, this novel application of the iodine method provides a promising glimpse at the potential power of the proxy.

Conclusions

The MDICE stands out in the Middle Ordovician as the first indication of shifts in the global carbon cycle after a prolonged period of apparent stability. New $\delta^{13}C$ data presented here, coupled with detailed biostratigraphic work carried out previously, bolster the global chemostratigraphic correlations that have been laid out by Ainsaar et al. (2010) and others. In addition to its utility in chemostratigraphy and correlation, the MDICE takes place synchronously with one of the largest pulses of diversification associated with the GOBE. While correlation does not necessarily imply causation, published data have been used to argue for shifts in global biogeochemical cycles that could have impacted marine

animal communities (e.g., Young et al., 2016, Edwards et al., 2017)—these conclusions are not inconsistent with our results.

The MDICE has been linked with both enhanced organic carbon burial and oxygen accumulation (e.g., Edwards et al., 2017). The paired $\delta^{13}C$ data presented here are consistent with global data compiled by Edwards et al. (2017), also showing a step increase in $\Delta^{13}C$ coincident with the onset of the MDICE. New $\delta^{34}S_{CAS}$ data presented here are consistent with published data that have been used to suggest an increase in marine [O_2], resulting in a decrease in pyrite burial, during the MDICE (Young et al., 2016). New I/(Ca+Mg) data presented here are also consistent with this notion, suggesting an expansion of stably oxygenated conditions on the western Laurentian margin throughout the mid-Darriwilian.

In concert, the new data presented here speak to a mid-Darriwilian ocean where sea level was rising, and at the same time the chemocline was deepening. This combination could have created an enormous amount of shelf space that was continuously hospitable to animal communities for millions of years. Although this link is speculative, and previous experimental studies have shown the capacity for animals to live under very low oxygen levels, other work on modern oxygen minimum zones has demonstrated that there are threshold changes in ecological structure between 2-7% of modern surface ocean oxygen concentrations. These changes associated with higher oxygen contents are especially prominent in species-level diversity and carnivore size and abundance (Levin, 2003; Woulds et al., 2007; Sperling et al., 2013). Establishing a direct connection between the changing physical and chemical oceanographic state and coincident diversification in the

Middle Ordovician will require significant additional work. However, as evidence for increasing [O_2] in shallow marine settings during the GOBE continues to accumulate, detailed investigations of the geographic distributions of particular communities as they relate directly to local redox indicators in the same rocks provide a path forward.

References

Ainsaar, L., Meidla, T. and Tinn, O., 2004, May. Middle and Upper Ordovician stable isotope stratigraphy across the facies belts in the East Baltic. In WOGOGOB-2004 Conference Materials. Tartu University Press, Tartu (pp. 11-12).

Ainsaar, L., Kaljo, D., Martma, T., Meidla, T., Männik, P., Nõlvak, J., and Tinn, O., 2010, Middle and Upper Ordovician carbon isotope chemostratigraphy in Baltoscandia: A correlation standard and clues to environmental history: Palaeogeography, Palaeoclimatology, Palaeoecology, v. 294, no. 3–4, p. 189-201.

Albanesi, G.L., Bergström, S.M., Schmitz, B., Serra, F., Feltes, N.A., Voldman, G.G. and Ortega, G., 2013. Darriwilian (Middle Ordovician) δ^{13}Ccarb chemostratigraphy in the Precordillera of Argentina: Documentation of the middle Darriwilian Isotope Carbon Excursion (MDICE) and its use for intercontinental correlation. Palaeogeography, Palaeoclimatology, Palaeoecology, 389, pp.48-63.

Andrews, T.J. and Lorimer, G.H., 1987. Rubisco: structure, mechanisms, and prospects for improvement. In: Photosynthesis (pp. 131-218). Academic Press.

Banner, J.L. and Hanson, G.N., 1990. Calculation of simultaneous isotopic and trace element variations during water-rock interaction with applications to carbonate diagenesis. Geochimica et Cosmochimica Acta, 54(11), pp.3123-3137.

Bauert, H., Ainsaar, L., Poldsaar, K. and Sepp, S., 2014. δ^{13} C chemostratigraphy of the Middle and Upper Ordovician succession in the Tartu-453 drillcore, southern Estonia, and the significance of the HICE. Estonian Journal of Earth Sciences, 63(4).

Beerling, D.J., Lake, J.A., Berner, R.A., Hickey, L.J., Taylor, D.W. and Royer, D.L., 2002. Carbon isotope evidence implying high O_2/CO_2 ratios in the Permo-Carboniferous atmosphere. Geochimica et Cosmochimica Acta, 66(21), pp.3757-3767.

Bergstöm, S.M., Chen, X., Gutiérrez-Marco, J.C. and Dronov, A., 2009. The new chronostratigraphic classification of the Ordovician System and its relations to major regional series and stages and to δ^{13}C chemostratigraphy. Lethaia, 42(1), pp.97-107.

Bergstöm, S.M. and Wang, Z., 1995. Global correlation of Castlemainian to Darriwilian conodont faunas and their relations to the graptolite zone succession. In; Chen, X.,

Bergström, S.M. (Eds.), The Base of the Austrodentatus Zone as a Level for Global Subdivision of the Ordovician System. Nanjing University Press, Nanjing. pp. 92-98.

Bergström, S. M., Saltzman, M. M., and Schmitz, B., 2006, First record of the Hirnantian (Upper Ordovician) $\delta^{13}C$ excursion in the North American Midcontinent and its regional implications: Geological Magazine, v. 143, no. 05, p. 657-678.

Bergström, S.M., Saltzman, M.R., Leslie, S.A., Ferretti, A. and Young, S.A., 2015. Trans-Atlantic application of the Baltic Middle and Upper Ordovician carbon isotope zonation.

Berner, R.A., 1987. Models for carbon and sulfur cycles and atmospheric oxygen; application to Paleozoic geologic history. American Journal of Science, 287(3), pp.177-196.

Berner, R.A., 2006. GEOCARBSULF: a combined model for Phanerozoic atmospheric O_2 and CO_2. Geochimica et Cosmochimica Acta, 70(23), pp.5653-5664.

Berner, R.A., Petsch, S.T., Lake, J.A., Beerling, D.J., Popp, B.N., Lane, R.S., Laws, E.A., Westley, M.B., Cassar, N., Woodward, F.I. and Quick, W.P., 2000. Isotope fractionation and atmospheric oxygen: implications for Phanerozoic O_2 evolution. Science, 287(5458), pp.1630-1633.

Brenchley, P. J., Marshall, J. D., Carden, G. A. F., Robertson, D. B. R., Long, D. G., Meidla, T., Hints, L., and Anderson, T. F., 1994, Bathymetric and isotopic evidence for a short-lived Late Ordovician glaciation in a greenhouse period: Geology, v. 22, no. 4, p. 295-298.

Bidigare, R.R., Fluegge, A., Freeman, K.H., Hanson, K.L., Hayes, J.M., Hollander, D., Jasper, J.P., King, L.L., Laws, E.A., Milder, J. and Millero, F.J., 1997. Consistent fractionation of ^{13}C in nature and in the laboratory: Growth-rate effects in some haptophyte algae. Global Biogeochemical Cycles, 11(2), pp.279-292.

Calner, M., Lehnert, O., Wu, R., Dahlqvist, P., and Joachimski, M. M., 2014, $\delta^{13}C$ chemostratigraphy in the Lower–Middle Ordovician succession of Öland (Sweden) and the global significance of the MDICE: GFF, v. 136, no. 1, p. 48-54.

Chance, R., Baker, A.R., Carpenter, L. and Jickells, T.D., 2014. The distribution of iodide at the sea surface. Environmental Science: Processes & Impacts, 16(8), pp.1841-1859.

Chen, X., Zhang, Y.D., and Fan, J.X., 2006, A brief introduction to the evolutionary radiation of Ordovician graptolites: Biotic origination and radiation. Edited by J.-y. Rong, Z.-j. Fang, Z.-h. Zhou, X.-d. Wang, R.-b. Zhan, and X.-l. Yuan. Science Press, Beijing, China, p. 181-196.

Cocks, L.R.M. and Torsvik, T.H., 2002. Earth geography from 500 to 400 million years ago: a faunal and palaeomagnetic review. Journal of the Geological Society, 159(6), pp.631-644.

Cooper, R.A., Sadler, P.M., 2012. The Ordovician Period. In: Gradstein, F.M., Ogg, J.G., Schimtz, M.D., Ogg, G.M. (Eds.), The Geologic Time Scale 2012. Elsevier, Amsterdam, pp. 489–523.

Cramer, B. D., Loydell, D. K., Samtleben, C., Munnecke, A., Kaljo, D., Männik, P., Martma, T., Jeppsson, L., Kleffner, M. A., and Barrick, J. E., 2010, Testing the limits of Paleozoic chronostratigraphic correlation via high-resolution (< 500 ky) integrated conodont, graptolite, and carbon isotope (δ^{13}Ccarb) biochemostratigraphy across the Llandovery–Wenlock (Silurian) boundary: Is a unified Phanerozoic time scale achievable? Geological Society of America Bulletin, v. 122, no. 9-10, p. 1700-1716.

Crowe, S.A., Paris, G., Katsev, S., Jones, C., Kim, S.T., Zerkle, A.L., Nomosatryo, S., Fowle, D.A., Adkins, J.F., Sessions, A.L. and Farquhar, J., 2014. Sulfate was a trace constituent of Archean seawater. Science, 346(6210), pp.735-739.

Dronov, A., & Rozhnov, S. (2007). Climatic changes in the Baltoscandian basin during the Ordovician: sedimentological and palaeontological aspects. Acta Palaeontologica Sinica, 46, 108.

Droser, M. L., and Sheehan, P. M., 1997, Palaeoecology of the Ordovicianradiation; Resolution of Large-Scale Patterns with Individual Clade Histories, Palaeogeography and Environments: Geobios, v. 30, p. 221-229.

Edwards, C.T., Saltzman, M.R., Leslie, S.A., Bergström, S.M., Sedlacek, A.R., Howard, A., Bauer, J.A., Sweet, W.C. and Young, S.A., 2015. Strontium isotope (^{87}Sr/^{86}Sr) stratigraphy of Ordovician bulk carbonate: Implications for preservation of primary seawater values. Bulletin, 127(9-10), pp.1275-1289.

Edwards, C.T. and Saltzman, M.R., 2016. Paired carbon isotopic analysis of Ordovician bulk carbonate ($\delta^{13}C_{carb}$) and organic matter ($\delta^{13}C_{org}$) spanning the Great Ordovician Biodiversification Event. Palaeogeography, Palaeoclimatology, Palaeoecology, 458, pp.102-117.

Edwards, C.T., Saltzman, M.R., Royer, D.L. and Fike, D.A., 2017. Oxygenation as a driver of the Great Ordovician Biodiversification Event. Nature Geoscience, 10(12), pp.925-929.
Harper, D. A., 2006, The Ordovician biodiversification: setting an agenda for marine life: Palaeogeography, Palaeoclimatology, Palaeoecology, v. 232, no. 2, p. 148-166.

Gill, B.C., Lyons, T.W. and Saltzman, M.R., 2007. Parallel, high-resolution carbon and sulfur isotope records of the evolving Paleozoic marine sulfur reservoir. Palaeogeography, Palaeoclimatology, Palaeoecology, 256(3-4), pp.156-173.

Gill, B.C., Lyons, T.W. and Frank, T.D., 2008. Behavior of carbonate-associated sulfate during meteoric diagenesis and implications for the sulfur isotope paleoproxy. Geochimica et Cosmochimica Acta, 72(19), pp.4699-4711.

Gill, B.C., Lyons, T.W., Young, S.A., Kump, L.R., Knoll, A.H. and Saltzman, M.R., 2011. Geochemical evidence for widespread euxinia in the Later Cambrian ocean. Nature, 469(7328), pp.80-83.

Gomes, M.L. and Hurtgen, M.T., 2015. Sulfur isotope fractionation in modern euxinic systems: Implications for paleoenvironmental reconstructions of paired sulfate–sulfide isotope records. Geochimica et Cosmochimica Acta, 157, pp.39-55.

Habicht, K.S. and Canfield, D.E., 1997. Sulfur isotope fractionation during bacterial sulfate reduction in organic-rich sediments. Geochimica et Cosmochimica Acta, 61(24), pp.5351-5361.

Hardisty, D.S., Lu, Z., Planavsky, N.J., Bekker, A., Philippot, P., Zhou, X. and Lyons, T.W., 2014. An iodine record of Paleoproterozoic surface ocean oxygenation. Geology, 42(7), pp.619-622.

Hardisty, D.S., Lu, Z., Bekker, A., Diamond, C.W., Gill, B.C., Jiang, G., Kah, L.C., Knoll, A.H., Loyd, S.J., Osburn, M.R. and Planavsky, N.J., 2017. Perspectives on Proterozoic surface ocean redox from iodine contents in ancient and recent carbonate. Earth and Planetary Science Letters, 463, pp.159-170.

Harper, D. A. T., Zhan, R.-B., and Jin, J., 2015, The Great Ordovician Biodiversification Event: Reviewing two decades of research on diversity's big bang illustrated by mainly brachiopod data: Palaeoworld, v. 24, no. 1–2, p. 75-85.

Harris, A.G., Bergström, S.M., Ethington, R.L., and Ross, R.J., Jr., 1979. Aspects of Middle and Upper Ordovician conodont biostratigraphy of carbonate facies in Nevada and southeast California and comparison with some Appalachian successions. Brigham Young University Geological Studies, v. 26, pt. 3, p. 7-33.

Hayes, J.M., Strauss, H. and Kaufman, A.J., 1999. The abundance of ^{13}C in marine organic matter and isotopic fractionation in the global biogeochemical cycle of carbon during the past 800 Ma. Chemical Geology, 161(1-3), pp.103-125.

Holland, H.D., 1973. Systematics of the isotopic composition of sulfur in the oceans during the Phanerozoic and its implications for atmospheric oxygen. Geochimica et Cosmochimica Acta, 37(12), pp.2605-2616.

Hurtgen, M.T., Pruss, S.B. and Knoll, A.H., 2009. Evaluating the relationship between the carbon and sulfur cycles in the later Cambrian ocean: an example from the Port au Port Group, western Newfoundland, Canada. Earth and Planetary Science Letters, 281(3-4), pp.288-297.

Kaljo, D., Martma, T., and Saadre, T., 2007, Post-Hunnebergian Ordovician carbon isotope trend in Baltoscandia, its environmental implications and some similarities with that of Nevada: Palaeogeography, Palaeoclimatology, Palaeoecology, v. 245, no. 1, p. 138-155.
Joachimski, M.M., Pancost, R.D., Freeman, K.H., Ostertag-Henning, C. and Buggisch, W., 2002. Carbon isotope geochemistry of the Frasnian–Famennian transition. Palaeogeography, Palaeoclimatology, Palaeoecology, 181(1-3), pp.91-109.

Jones, D.S. and Fike, D.A., 2013. Dynamic sulfur and carbon cycling through the end-Ordovician extinction revealed by paired sulfate–pyrite $\delta^{34}S$. Earth and Planetary Science Letters, 363, pp.144-155.

Kozik, N.P., Young, S.A., Bowman, C.N., Saltzman, M.R. and Them II, T.R., 2019. Middle–Upper Ordovician (Darriwilian–Sandbian) paired carbon and sulfur isotope stratigraphy from the Appalachian Basin, USA: Implications for dynamic redox conditions

spanning the peak of the Great Ordovician Biodiversification Event. Palaeogeography, Palaeoclimatology, Palaeoecology, 520, pp.188-202.

Krause, F.F., 2001. Genesis and geometry of the Meiklejohn Peak lime mud-mound, Bare Mountain Quadrangle, Nevada, USA: Ordovician limestone with submarine frost heave structures—a possible response to gas clathrate hydrate evolution. Sedimentary Geology, 145(3-4), pp.189-213.

Krause, F.F. and Rowell, A.J., 1975. Distribution and systematics of the inarticulate brachiopods of the Ordovician carbonate mud mound, Meiklejohn Peak, Nevada. The University of Kansas Paleontological Contributions, 61, 74.

Kump, L.R. and Arthur, M.A., 1999. Interpreting carbon-isotope excursions: carbonates and organic matter. Chemical Geology, 161(1-3), pp.181-198.

Kump, L. and Garrels, R.M., 1986. Modeling atmospheric O_2 in the global sedimentary redox cycle. American Journal of Science, 286(5), pp.337-360.

Leslie, S.A., Saltzman, M.R., Bergström, S.M., Repetski, J.E., Howard, A. and Seward, A.M., 2011. Conodont biostratigraphy and stable isotope stratigraphy across the Ordovician Knox/Beekmantown unconformity in the central Appalachians. Ordovician of the World, 14, pp.301-308.

Levin, L.A., 2003. Oxygen minimum zone benthos: adaptation and community response to hypoxia. In; Gibson, R.N. and Atkinson, R.J.A. (Eds), Oceanogr. Marine Biol. Annu. Rev, 41, pp.1-45.

Lu, W., Ridgwell, A., Thomas, E., Hardisty, D.S., Luo, G., Algeo, T.J., Saltzman, M.R., Gill, B.C., Shen, Y., Ling, H.F. and Edwards, C.T., 2018. Late inception of a resiliently oxygenated upper ocean. Science, 361(6398), pp.174-177.

Lu, Z., Jenkyns, H.C. and Rickaby, R.E., 2010. Iodine to calcium ratios in marine carbonate as a paleo-redox proxy during oceanic anoxic events. Geology, 38(12), pp.1107-1110.
Männik, P. and Viira, V., 2005. Distribution of Ordovician conodonts. Mehikoorma (421) drill core, 6, pp.16-20.

Metzger, J.G., and Fike, D. A., 2013, Techniques for assessing spatial heterogeneity of carbonate $\delta^{13}C$ values: Implications for craton-wide isotope gradients: Sedimentology, v. 60, no. 6, p. 1405-1431.

McBride, E.F., 2012. Petrology of the Eureka Quartzite (Middle and Late Ordovician), Utah and Nevada, USA. Rocky Mountain Geology, 47(2), pp.81-111.
Monsen, S.A., Carr, M.D., Reheis, M.C. and Orkild, P.P., 1992. Geologic map of Bare Mountain. Nye County, Nevada: US Geological Survey Miscellaneous Investigations Map I-2201, scale, 1(24,000), p.6.

Munnecke, A., Zhang, Y., Liu, X., and Cheng, J., 2011, Stable carbon isotope stratigraphy in the Ordovician of South China: Palaeogeography, Palaeoclimatology, Palaeoecology, v. 307, no. 1–4, p. 17-43.

Nielsen, A.T., 2004. Ordovician sea level changes: a Baltoscandian perspective. The great Ordovician biodiversification event, 84, p.93.

Poole, F.G., Stewart, J.H., Palmer, A.R., Sandberg, C.A., Madrid, R.J., Ross Jr, R.J., Hintze, L., Miller, M.M. and Wrucke, C.T., 1992. Latest Precambrian to latest Devonian time; development of a continental margin. The Cordilleran Orogen: Conterminous US: Boulder, Colorado, Geological Society of America, The Geology of North America, 3, pp.9-56.

Rasmussen, C. M., Hansen, J., and Harper, D. A., 2007, Baltica: A mid Ordovician diversity hotspot: Historical Biology, v. 19, no. 3, p. 255-261.

Rau, G.H., Riebesell, U. and Wolf-Gladrow, D., 1997. CO_2aq-dependent photosynthetic 13C fractionation in the ocean: A model versus measurements. Global Biogeochemical Cycles, 11(2), pp.267-278.

Ross Jr, R.J., 1972. Fossils from the Ordovician bioherm at Meiklejohn Peak, Nevada (No. 685). US Govt. Print. Off.

Ross, R. J. Jr., Jaanusson, V., and Friedman , I., 1975. Lithology and origin of Middle Ordovician calcareous mudmound at Meiklejohn Peak, southern Nevada. U. S. Geol. Surv. Prof Paper 871, 1-48.

Ross, R.J., Ethington, R.L. and Mitchell, C.E., 1991. Stratotype of Ordovician Whiterock Series. Palaios, 6(2), pp.156-173.

Saltzman, M. R., Ripperdan, R. L., Brasier, M. D., Lohmann, K. C., Robison, R. A., Chang, W. T., Peng, S., Ergaliev, E. K., and Runnegar, B., 2000, A global carbon isotope excursion (SPICE) during the Late Cambrian: relation to trilobite extinctions, organic-matter burial and sea level: Palaeogeography, Palaeoclimatology, Palaeoecology, v. 162, no. 3–4, p. 211-223.

Saltzman, M. R., Runnegar, B., and Lohmann, K. C., 1998, Carbon isotope stratigraphy of Upper Cambrian (Steptoean Stage) sequences of the eastern Great Basin: Record of a global oceanographic event: Geological Society of America Bulletin, v. 110, no. 3, p. 285-297.

Schmitz, B., Bergström, S. M., and Xiaofeng, W., 2010, The middle Darriwilian (Ordovician) $\delta^{13}C$ excursion (MDICE) discovered in the Yangtze Platform succession in China: implications of its first recorded occurrences outside Baltoscandia: Journal of the Geological Society, v. 167, no. 2, p. 249-259.

Sepkoski Jr, J. J., 1981, A factor analytic description of the Phanerozoic marine fossil record: Paleobiology, p. 36-53.

Sepkoski Jr, J. J., 1995, The Ordovician radiations: diversification and extinction shown by global genus-level taxonomic data.

Sepkoski, J. J., Jablonski, D., and Foote, M., 2002, A compendium of fossil marine animal genera: Bulletins of American paleontology.

Sim, M.S., Bosak, T. and Ono, S., 2011. Large sulfur isotope fractionation does not require disproportionation. Science, 333(6038), pp.74-77.

Sperling, E.A., Frieder, C.A., Raman, A.V., Girguis, P.R., Levin, L.A. and Knoll, A.H., 2013. Oxygen, ecology, and the Cambrian radiation of animals. Proceedings of the National Academy of Sciences, 110(33), pp.13446-13451.

Stanley, S.M. and Hardie, L.A., 1998. Secular oscillations in the carbonate mineralogy of reef-building and sediment-producing organisms driven by tectonically forced shifts in

seawater chemistry. Palaeogeography, Palaeoclimatology, Palaeoecology, 144(1-2), pp.3-19.

Thompson, C.K. and Kah, L.C., 2012. Sulfur isotope evidence for widespread euxinia and a fluctuating oxycline in Early to Middle Ordovician greenhouse oceans. Palaeogeography, Palaeoclimatology, Palaeoecology, 313, pp.189-214.

Trotter, J. A., Williams, I. S., Barnes, C. R., Lécuyer, C., and Nicoll, R. S., 2008, Did cooling oceans trigger Ordovician biodiversification? Evidence from conodont thermometry: Science, v. 321, no. 5888, p. 550-554.

U.S. Geological Survey, 1987. Beatty Mtn. Quadrangle Nevada—Nye Co. 7.5 minute series (topographic). U.S. Department of the Interior.

Viira, V., Löfgren, A. and Sjöstrand, L., 2006. Distribution of Ordovician conodonts. Kerguta (565) Drill Core, 7, pp.11-13.

Webby, B. D., 2004, The great Ordovician biodiversification event, Columbia University Press.

Wing, B.A. and Halevy, I., 2014. Intracellular metabolite levels shape sulfur isotope fractionation during microbial sulfate respiration. Proceedings of the National Academy of Sciences, 111(51), pp.18116-18125.

Woulds, C., Cowie, G.L., Levin, L.A., Andersson, J.H., Middelburg, J.J., Vandewiele, S., Lamont, P.A., Larkin, K.E., Gooday, A.J., Schumacher, S. and Whitcraft, C., 2007. Oxygen as a control on sea floor biological communities and their roles in sedimentary carbon cycling. Limnology and Oceanography, 52(4), pp.1698-1709.

Young, S.A., Gill, B.C., Edwards, C.T., Saltzman, M.R. and Leslie, S.A., 2016. Middle–Late Ordovician (Darriwilian–Sandbian) decoupling of global sulfur and carbon cycles: Isotopic evidence from eastern and southern Laurentia. Palaeogeography, Palaeoclimatology, Palaeoecology, 458, pp.118-132.

Zhan, R., Rong, J., Cheng, J., and Chen, P., 2005, Early-Mid Ordovician brachiopod diversification in South China: Science in China Series D: Earth Sciences, v. 48, no. 5, p. 662-675.

Zhang, Y. and Munnecke, A., 2016. Ordovician stable carbon isotope stratigraphy in the Tarim Basin, NW China. Palaeogeography, Palaeoclimatology, Palaeoecology, 458, pp.154-175.

Chapter 7

Concluding Remarks

The body of work presented in this dissertation represents the progression of my thinking over many years and discoveries that my colleagues and I made together. While I have produced a considerable amount of high-resolution geochemical data and truly consider myself an expert on a handful of very specific topics, I hope it is clear from the contents of this volume that I have devoted an equal or greater amount of time thinking about the implications of integrating all available geochemical data over longer timescales. In addition to the projects highlighted here, during my time at UCR I have also had the privilege of working extensively on the Neoproterozoic and the Precambrian-Cambrian boundary. These projects have resulted in the publication of Evans, Diamond, Droser, and Lyons, 2018 and Chen, Diamond, et al., 2019, and several additional publications are in preperation.

Within the works selected for this document, an argument has been presented that because animals generally require a significant amount of oxygen, their initial evolution probably did also. This is by no means a new argument, but it is the overall theme of my dissertation. A healthy portion of the existing evidence in support of this hypothesis has been discussed, and in all honesty, I am not sure that an independent reader would draw the same conclusions that I have. That is, for better or worse, the nature of Precambrian Geology. It's a time period for dreamers.

The fact of the matter is that the Proterozoic records we have are painfully incomplete. While Paleozoic workers fill out the details of hundred-thousand-year timescales or less, we are at times left using a few thin formations to characterize a timeframe nearly as long as the Paleozoic itself (for non-geologists, the Paleozoic is essentially the time period since the initial appearance of animal fossils in the geological record, around five hundred and fifty million years). Given such a situation, it can be difficult to make definitive statements with confidence. Nonetheless, Precambrian workers continue to advance our knowledge. I began this work with a quote from Kurt Vonnegut's *Slaughterhouse Five*, and this reminds me of another. In the first chapter, as the narrator (Vonnegut) is giving the book to his publisher Sam, he describes it as follows…

> *It's so short and jumbled and jangled, Sam, because there is nothing intelligent to say about a massacre. Everybody is supposed to be dead, to never say anything or want anything ever again. Everything is supposed to be very quiet after a massacre, and it always is, except for the birds.*
>
> *And what do the birds say? All there is to say about a massacre, things like "Poo-tee-weet?"*

This is how I feel about the Proterozoic rock record, like there has been a massacre and we are just the birds flying around after, communicating the most intelligent things we can think of to say about it. Things like *"Poo-tee-weet?"*

It is clear enough to me at this point that no end-member arguments about deep-time Earth history are generally correct. Moving beyond these, however, will require the realization of significant improvements in both the quality, quantity, and resolution of geochemical data available and in the sophistication of mathematical modeling being applied. In many cases so far, the modeling efforts seem to be outpacing the geochemistry.

There are a limited number of rocks preserved from this time, that is a real problem. However, much work remains to be done.

I hope that the chapters presented herein make a cogent argument that the interpretations my colleagues and I have made about the specific geochemistry of individual formations and that of Earth's history in its entirety are correct. I certainly hold the opinion that they are a step in the right direction. Time will tell, and I genuinely hope that I live long enough and there are enough rocks preserved to find out the answers to some of the questions that this dissertation still leaves open. There is another argument pertaining to the role of O_2 in shaping the course of eukaryotic evolution, that to the best of my knowledge has not been made in the literature. It very recently occurred to me while reading work published by Miklós Müller M.D. Although I hope to explore this argument more completely in the near future, I will distill it down and state it here.

One role of oxygen in the evolution of animals is clear, it allowed them to build impressively complex structures using the large gross energy yields attainable with an aerobic lifestyle. However, aerobic lifestyles come at an enormous cost—cellular damage caused by a constant barrage of oxidizing agents. Eukaryotes attained a progression of evolutionary technologies to cope with this issue, inevitably leading to large, motile, apex predators. There is an implicit bias in both arguments described in this dissertation so far, though. That is, that it was a natural progression toward aerobic respiration because of the large increase in energy yield per unit of glucose oxidized. Few people stop to ask what the increased cost of operation in an aerobic environment is or how this compares to the

increased ATP yield. At least one study, Lever et al., 2015 *FEMS Micro. Bio. Rev.*, suggests that the costs outweigh the benefits from an energy balance standpoint.

That is not to say that there are not enormous other benefits conferred along with this transition, but if it is not energetically favorable in a net sense to move into oxygenated waters, evolution would not necessarily have done it unless other, greater, pressures were at play. The initial accumulation of O_2 in the surface ocean and atmosphere was the consequence of net photosynthetic production overrunning reductant delivery by geological processes, perhaps the progressive oxygenation of the whole system was mostly a product of this push-and-pull relationship as well. That is to say that the surface oceans became progressively more oxygenated as time went on and anoxic habitat space became smaller, particularly in the photic zone. This could have provided the evolutionary pressure to expand into the ecospace, even if it was energetically disadvantageous at the time.

This may sound like semantics, but it strikes at some core issues of the debate. Eukaryotes appear to have evolved early, but then played a minor role in ecosystems for roughly a billion years before rapidly developing and taking over the planet. This presents a paradox if the surface oceans were, for the most part, persistently oxygenated throughout this time. But, if we do not begin with the assumption that an aerobic lifestyle is a natural evolutionary progression, it is no longer a problem. The facts that evolution is a complicated and random process that takes time and in many cases we are talking about evolutionary events that happened only once in Earth's history, do not provide a satisfying explanation as to why it took so long for animals to appear, followed by such a rapid ascent to domination of the observable world. To me, it seems kind of like a Model-T and a horse.

The Model-T (internal combustion for that matter) was an amazing technological advancement. It allowed humans to go faster, do more work, etc. A Model-T can travel a mile significantly quicker than a horse, but to do so, it probably needs about a horse's worth of consolidated organic matter—the horse can do it on a few mouthfuls of grass.

I will close by again thanking you, the reader. The Forwards in each chapter, as well as the whole of the introduction and conclusion, generally lack rigorous explanation or extensive referencing. Instead, they offer some accounts of personal experience and professional interactions, along with generalized descriptions of the significance of each contribution as I see it. They tell a partial narrative of my time as a graduate student. While the inclusion of so much personal discourse in a STEM dissertation may be unconventional, it represents what I have come to feel science truly is—a series of iterative discussions and interactions between human beings, be they in person, over zoom, or through the literature. I felt that these sections would provide useful context for those who wish to read this with purely scientific motives and those reading it for personal reasons alike. Beyond that, it is fairly unlikely that *anyone* but me will read this dissertation after the next few months have passed. Given that, these will serve as a reminder of where I came from and the incredible adventure it has been.